STUDY OF A HEAT PIPE COOLED MICROWAVE WINDOW

A THESIS

Presented to

The Faculty of the Division of Graduate

Studies and Research

By

Julio A. Santander-Palmero

In Partial Fulfillment

of the Requirements for the Degree

Master of Science in Mechanical Engineering

Georgia Institute of Technology

March, 1975

STUDY OF A HEAT PIPE COOLED MICROWAVE WINDOW

Approved:

Gene T. Colwell, Chairman

Robert B. Evans

Harold L. Bassett

Date approved by Chairman: 2-28-75

ACKNOWLEDGEMENTS

The author wishes to express sincere appreciation to Dr. G. T. Colwell, his thesis advisor, for his constant patience, interest and guidance during this investigation.

Thanks are also extended to Dr. R. B. Evans and Mr. H. L. Bassett, members of the reading committee, for their careful review of this work.

A special note of thanks is also due to Mr. T. E. Clopton for his valuable help in setting up the experimental equipment.

The author further wishes to thank the Universidad de Carabobo in Venezuela, for providing financial assistance during his graduate work.

Finally, the author expresses his deepest gratitude to his wife and son, whose understanding, love and enccouragement made this work possible.

TABLE OF CONTENTS

Page

ACKNOWLEDGEMENTS ii

LIST OF TABLES v

LIST OF ILLUSTRATIONS vii

NOMENCLATURE ix

SUMMARY xiii

Chapter

I. INTRODUCTION 1

1. The Heat Pipe
2. Statement of the Problem
3. The Heat Pipe Cooled Microwave Window Concept
4. Literature Survey

II. EQUIPMENT 13

III. EXPERIMENTAL PROCEDURE 19

IV. THEORETICAL CONSIDERATIONS 23

1. Objective
2. Heat Pipe Limitations
3. Thermal Resistances
4. Selection of Working Fluid

V. PARAMETRIC STUDY 39

VI. EXPERIMENTAL RESULTS 50

1. Determination of the Working Fluid Volume
2. Heat Pipe Cooled Microwave Window Performance

VII. CONCLUSIONS AND RECOMMENDATIONS 62

1. Conclusions
2. Recommendations

Page

A. ESTIMATION OF THE CHOKING LIMIT 64

B. ESTIMATION OF THE ENTRAINMENT LIMIT 67

C. ESTIMATION OF THE BOILING HEAT FLUX LIMIT 69

D. DETERMINATION OF THE HEAT PIPE WICKING LIMIT 72

E. ESTIMATION OF INTERFACIAL INERTIAL FORCES 76

F. ESTIMATION OF THE VAPOR PRESSURE DROP 78

G. DETERMINATION OF THE PRESSURE DROP IN THE LIQUID PHASE 80

H. CALCULATION OF INVERSE PERMEABILITIES 84

I. CAPILLARY STRUCTURE DATA 91

J. EVALUATION OF THE EFFECTIVE THERMAL CONDUCTIVITY OF THE WICK-LIQUID MATRIX 92

K. EVALUATION OF THERMAL RESISTANCES 96

L. EXPERIMENTAL DATA 122

BIBLIOGRAPHY 129

LIST OF TABLES

Table		Page
1.	Capillary Structure Combinations Considered	40
2.	Test Model Choking Limit at Different Temperatures	65
3.	Test Model Entrainment Limit at Different Temperatures . .	68
4.	Test Model Heat Flux Limit at Different Temperatures . . .	71
5.	Test Model Wicking Limit at Different Temperatures Using Water as Working Fluid	73
6.	Test Model Wicking Limit at Different Temperatures Using Heptane as Working Fluid	74
7.	Inverse Permeability for Several Capillary Structures . . .	90
8.	Capillary Structure Data	91
9.	Effective Thermal Conductivity for Several Combinations of Capillary Structure and Working Fluid	94
10.	Window Thermal Resistances	97
11.	Wick-Liquid Resistance in Evaporator	99
12a.	Interfacial Resistance in Evaporator (Condenser Capillary Structure: 100 mesh copper screen)	100
12b.	Interfacial Resistnace in Evaporator (Condenser Capillary Structure: 200 mesh copper screen)	102
12c.	Interfacial Resistance in Evaporator (Condenser Capillary Structure: 400 mesh copper screen)	104
13a.	Thermal Resistance in Vapor (Condenser Capillary Structure: 100 mesh copper screen)	107
13b.	Thermal Resistance in Vapor (Condenser Capillary Structure: 200 mesh copper screen)	109
13c.	Thermal Resistance in Vapor (Condenser Capillary Structure: 400 mesh copper screen)	111

Page

14a. Interfacial Resistance at Condenser (Condenser Capillary Structure: 100 mesh copper screen) 113

14b. Interfacial Resistance at Condenser (Condenser Capillary Structure: 200 mesh copper screen) 115

14c. Interfacial Resistance at Condenser (Condenser Capillary Structure: 400 mesh copper screen) 117

15. Wick-Liquid Thermal Resistance in Condenser 120

16. Test Heat Pipe Temperature Distribution 123

17. Test Heat Pipe Operating Data 127

LIST OF ILLUSTRATIONS

Figure		Page
1.	The Basic Heat Pipe Configuration	2
2.	Approximate Range of Applicability of Some Working Fluids in the Various Temperature Regimes	4
3.	Typical Heat Flow of Thin Waveguide Window	7
4.	Preferred Direction of Heat Flow in Waveguide Window	7
5.	Longitudinal View of the Heat Pipe Cooled Microwave Window Arrangement	8
6.	Waveguide-Cooling Jacket Sub-Assembly	15
7.	Schematic of Test Section	16
8.	Block Diagram of Test Rig	17
9.	Heat Pipe Capillary Model	27
10.	Heat Pipe Model	30
11.	Schematic of Heat Pipe Potentials and Resistances	31
12.	Heat Pipe Number Vs. Temperature for Several Heat Pipe Working Fluids	37
13.	Wicking Limit Vs. Vapor Temperature for Various Capillary Structure Mesh Numbers Along the Waveguide	41
14.	Wicking Limit Vs. Vapor Temperature as a Function of the Number of Layers of Capillary Structure in the Condenser	42
15.	Wicking Limit Vs. Vapor Temperature as a Function of the Number of Layers of Capillary Structure in the Evaporator	44
16.	Wicking Limit Vs. Vapor Temperature as a Function of Heat Pipe Length (Window Spacing)	45
17.	Wicking Limit Vs. Vapor Temperature for Water and Heptane Used as Working Fluids	46

Page

18. Driving Potential Vs. Heat Transfer (Working Fluid: Water) 48

19. Driving Potential Vs. Heat Transfer (Working Fluid: Heptane) 49

20. Heat Transfer Vs. Vapor Temperature for Several Working Fluid Volumes 51

21. Heat Transfer Vs. Vapor Temperature for Various Cooling Water Flow Rates 53

22. Heat Transfer Vs. Vapor Pressure for Various Cooling Water Flow Rates 54

23. Ratio of Measured Vapor Pressure to the Saturation Vapor Pressure Corresponding to the Condenser Temperature Vs. Condenser Temperature 55

24. Heat Transfer Vs. Cooling Water Flow Rate for Various Vapor Temperatures 57

25. Heat Transfer Vs. Vapor Temperature for Water and Heptane Used as Working Fluids 58

26. Window Temperature Vs. Time 59

27. Comparison Between Theoretical and Experimental Performance of Test Heat Pipe 61

28. Wicking Limit Vs. Temperature for Test Model Using Water and Heptance as Working Fluids 75

29. Permeability of Screen Wicks 85

30. Liquid Annulus Model 89

NOMENCLATURE

Latin

A_N	area normal to the direction of flow
A_V	cross sectional area of vapor flow
b	circumference to mid-point of wick
$\vec{F}_{ext}$	external force
g	local acceleration due to gravity
g_c	constant that relates the units of force, mass, length, and time (32.2 lbm-ft/lbf-sec^2 or 4.17 x 10^8 lbm-ft/lbf-hr^2)
h_{fg}	latent heat of vaporization
J	mechanical equivalent of heat (778.26 ft-lbf/BTU)
K_1	inverse permeability based on approach velocity
K_1'	inverse permeability based on pore velocity
A^{K_1}	inverse permeability of material B (based on approach velocity)
B^{K_1}	inverse permeability of material A (based on approved velocity)
K_{eff}	effective thermal conductivity of the wick-liquid matrix
K_C	effective thermal conductivity of the wick-liquid matrix in the evaporator section
K_E	effective thermal conductivity of the wick-liquid matrix in the evaporator section
K_G	thermal conductivity of the waveguide material
K_ℓ	thermal conductivity of heat pipe working fluid
K_w	thermal conductivity of microwave window material
$A^{K_{ws}}$	thermal conductivity of solid in condenser

$_{B}K_{ws}$	thermal conductivity of solid in evaporator
l	straight line distance from mid-point of evaporator to mid-point of condenser
l_A	heat pipe length
l_e	evaporator length
l_{eff}	effective length of liquid flow
l_v	effective length of vapor flow
$\dot{m}$	working fluid flow rate through each evaporator surface ($\frac{1}{2}$ of total liquid flow rate)
$\dot{m}_l$	liquid flow rate in capillary structure
$\dot{m}_s$	rate of circulation of working fluid at choking
$\dot{m}_{wf}$	working fluid rate of circulation
N	heat pipe number
n	number of layers of capillary structure
$\vec{P}$	momentum
ΔP_c	pressure difference due to capillary pumping
ΔP_g	pressure difference due to gravity
ΔP_{vv}	pressure drop due to viscous losses in the vapor path
$\Delta P_{v\ell}$	pressure drop in the liquid phase
$\dot{q}_b$	boiling heat flux limit
$\dot{Q}$	heat transfer rate
$\dot{Q}_{max}$	maximum heat transfer capability of the heat pipe (wicking limit)
$\dot{Q}_s$	choking heat transfer limit
R	ideal gas constant
R_i	thermal resistance

r	effective radius of the critical nucleation cavity
r_b	radius of microwave window
r_v	vapor space radius from heat pipe centerline
A^rP	wick pore radius in condenser
B^rP	wick pore radius in evaporator
A^rws	radius of solid filament in condenser
B^rws	radius of solid filament in evaporator
T	temperature
t_w	microwave window thickness
T_{sat}	saturation temperature
$\Delta Tcrit$	critical superheat at the onset of nucleation
U_a	approach velocity
U_p	pore velocity
U_s	sonic velocity
U_v	vapor velocity

Greek

δ_A	thickness of capillary structure in condenser
δ_B	thickness of capillary structure in evaporator
ϵ	porosity
ϵ_A	porosity of capillary structure in condenser
ϵ_B	porosity of capillary structure in evaporator
ρ_ℓ	liquid density
ρ_v	vapor density
σ	surface tension

θ	angle of heat pipe with respect to the horizontal (positive when the evaporator is up)
μ_ℓ	liquid viscosity
μ_v	vapor viscosity

SUMMARY

The heat pipe is a self contained device capable of transferring large amounts of heat between a source and sink through a small temperature difference.

The design of a waveguide microwave window is difficult, at high average power, because dielectric materials have a low thermal conductivity and do not conduct easily the RF- generated heat to the walls of the waveguide. The materials that can be used for the construction of the windows must be restricted to those materials which possess a good thermal conductivity and very low dielectric loss. The heat dissipation problem is further aggravated if the window is thin, because the heat will be conducted in the radial direction, and thermal stresses will develop causing the window to fail. It would be better to conduct the heat in the axial direction, and this can be accomplished using the heat pipe principle. Bassett and Colwell (34) studied the feasibility of the design of a heat pipe cooled microwave window, and subsequently (35) an experimental heat pipe was constructed and tested. The test indicated that the heat pipe cooled windows could handle up to 2-3 MW of RF power at a frequency near 3.0 GH_z.

The purpose of this investigation was to optimize the design of a heat pipe cooled microwave window structure. Parametric studies were performed to determine the effects of changing window spacing, composition of capillary structure, thickness of capillary structure, window

thickness and window material.

An experimental program was carried out to determine the optimum amount of working fluid for the structure and the transient operating characteristics under a variety of conditions.

From the parametric study it was found that the heat pipe wicking limit decreases with increasing mesh size number. It was also observed that increasing the number of layers of capillary structure in the condenser from 1 to 2 produces a considerable increase in the wicking limit, while further increase in the number of layers raises the wicking limit only moderately. It was also determined that the wicking limit is strongly dependent on the number of layers of the capillary structure in the evaporator, but unfortunately, these should be kept to a minimum since the wick-liquid thermal resistance increases considerably with the number of layers. The effect of window spacing in the wicking limit was also studied, and it was found that it increased with decreasing window spacing. Regarding the effect of the window material on the performance of the heat pipe it was found that for the two window materials considered (aluminum oxide and beryllia) the performance was about the same if two or more layers of capillary structure are used in the evaporator.

From the experimental program the optimum amount of working fluid was found to be 30 ml. The heat pipe performance, for both heptane and water was observed to be very similar, but the burnout limit was much lower when heptane was used as working fluid.

CHAPTER I

INTRODUCTION

1. The Heat Pipe

The heat pipe is a self-contained device capable of transferring a large amount of heat between a source and sink through a small temperature difference. The basic heat pipe consists of a closed container of arbitrary shape, usually a long, right circular cylinder or parralelepiped, lined with a capillary structure along its inside wall as shown in Figure 1. To charge the device, the container is evacuated and a suitable working fluid is introduced in the container to saturate the the capillary structure (wick). Once this is done, the device is sealed. Under this condition, the liquid in the wick is in thermodynamic equilibrium with the vapor in the center portion or vapor space. An equilibrium condition is reached which corresponds with the surrounding temperature. The pressure inside the heat pipe will be equal to the saturation pressure for the working fluid at this temperature. The heat pipe operates on a closed vaporization-condensation cycle. Heat is added at one end (evaporator) causing the working fluid to evaporate; the vapor formed flows through the vapor space to the heat rejection section (condenser), where it condenses on the capillary structure as its latent heat is rejected to a coolant which is external to the container. During evaporation the liquid recedes somewhat into the pores of the wick forming a small radius of curvature at the liquid-vapor interface; while the

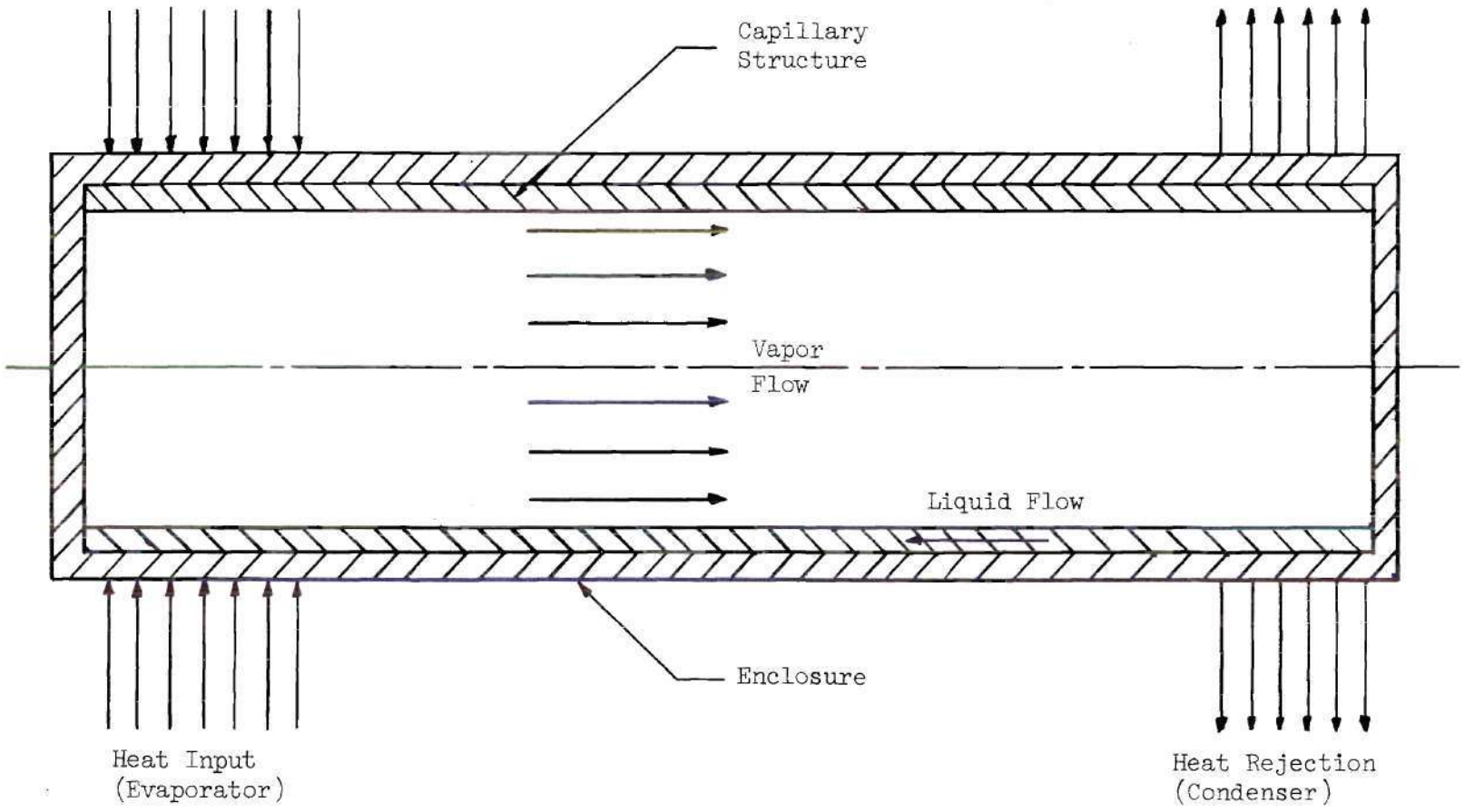

Figure 1. The Basic Heat Pipe Configuration

consensing vapor forms a large radius of curvature at the vapor-liquid interface. Since the curvature is different at the evaporator from that at the condenser, a net pressure difference exists within the system which causes the liquid to be pumped by capillary action from the condenser to the evaporator.

Heat pipes can be broadly classified in two general types - "conventional" and "variable conductance"(1). The conventional heat pipe is a device which operates at no fixed temperature (i.e., its temperature rises or falls according to variations in the heat source or heat sink) and possesses an effective thermal conductivity much larger than any known material. The variable conductance heat pipe permits a control on its effective thermal conductivity, allowing the device to be operated at a fixed temperature independently of the source and sink conditions.

According to its operating temperature, heat pipes can be classified, rather arbitrarily, as "cryogenic" (0 - 150K) (459 - 189°F), "low temperature" (150 - 750K) (189 - 890°F), and "high temperature" (750 - 3000K) (890 - 5432°F)(1). The vapor pressure characteristics of the working fluid used determines the temperature range of applicability. Figure 2 shows the approximate range of applicability of various working fluids in various temperature regimes.

The heat transfer capability of a heat pipe may be limited by a number of considerations. First, if the capillary pumping is not sufficient to replenish the liquid being evaporated, a local dryout of the wick occurs at the evaporator. Second, if boiling of the liquid occurs, a vapor film forms at the wick-pipe interface, which considerably decreases the heat transfer coefficient of the device. Rapid

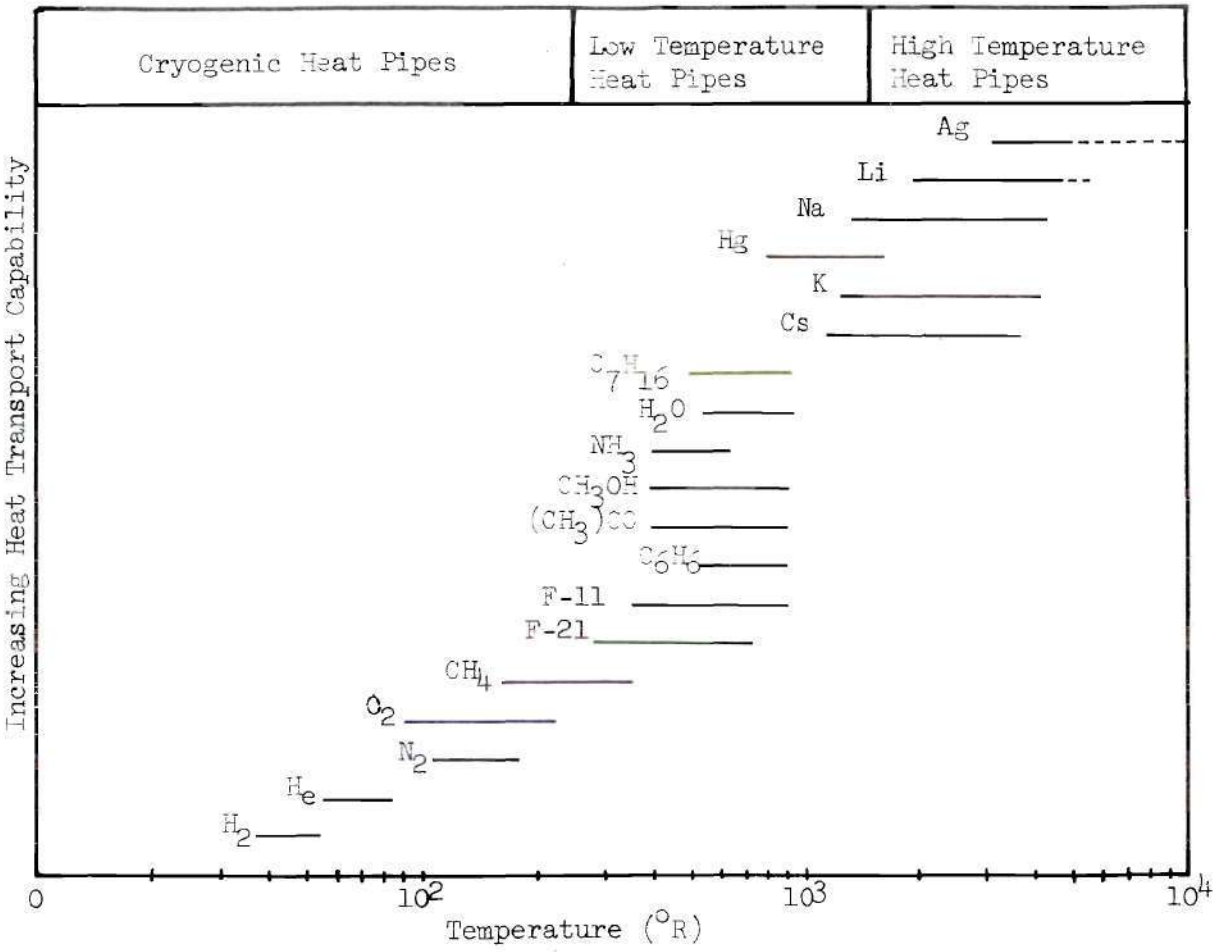

Figure 2. Approximate Range of Applicability of Some Working Fluids in the Various Temperature Regimes. (1)

increase in temperature occurs and burn out of the wick will result. Third, if the vapor velocity reaches the sonic velocity, further increase in mass flow rate is not possible without raising the saturation vapor pressure and therefore the temperature in the evaporator. Finally, the high velocity vapor may also interfere with the recirculating liquid causing liquid droplets to be entrained in the vapor and preventing sufficient liquid from returning to the evaporator.

2. Statement of the Problem

The purpose of this project was to optimize the design of a heat pipe cooled microwave window structure. Parametric studies were performed to determine the effects of changing window spacing, composition of capillary structure, thickness of capillary structure, window thickness and window material.

An experimental program was carried out to determine the optimum amount of working fluid for the structure and the transient operating characteristics under a variety of conditions.

3. The Heat Pipe Cooled Microwave Concept

The construction of a waveguide microwave window is difficult, at high average power, because the dielectric material has a low thermal conductivity and does not conduct easily the RF- generated heat to the walls of the waveguide. The materials that can be used for the construction of the windows must be restricted to those materials which possess a good thermal conductivity and very low dielectric loss. The heat dissipation problem is further aggravated if the window is thin, because the heat will be conducted in the radial direction as shown in

Figure 3, and thermal stresses will develop causing the window to fail. It would be better to conduct the heat in the axial direction as shown in Figure 4. This can be accomplished using the heat pipe principle.

The heat pipe action takes place between the two waveguide windows of Figure 5. This figure shows the location of the heat pipe wick, the window elements and the waveguide walls. The wick along the waveguide walls is made of 100 mesh copper screen, while the wick across the window is a dielectric. The window material is either alumina or beryllium oxide, which possess a low RF loss. The air-tight dielectric window elements, because of dielectric losses, are heated by the incident RF power. The dielectric wick and the copper wick are saturated by a fluid whose boiling point is near the desired operating temperature of the window. The waveguide walls are cooled externally by conventional means (i.e., fan, water cooling, fins, etc.). When the windows become warm, the liquid in the dielectric wick evaporates, absorbing the windows' heat. This vapor condenses on the "cold" vapor wick along the waveguide walls releasing its heat, which is then absorbed by the external cooling system. The wick returns the condensate to the window area (evaporator) by capillary action, completing the cooling cycle. The heat transfer is by mass transfer and not by conduction.

4. Literature Survey

The first patent issued for a device operating on the principle of the heat pipe was awarded to R. S. Gaugler (U. S. Patent 2350348) in 1944[2]. However, the pioneer work in this field is due to Grover, et. al.[3] at the University of California, Los Alamos Scientific Laboratory,

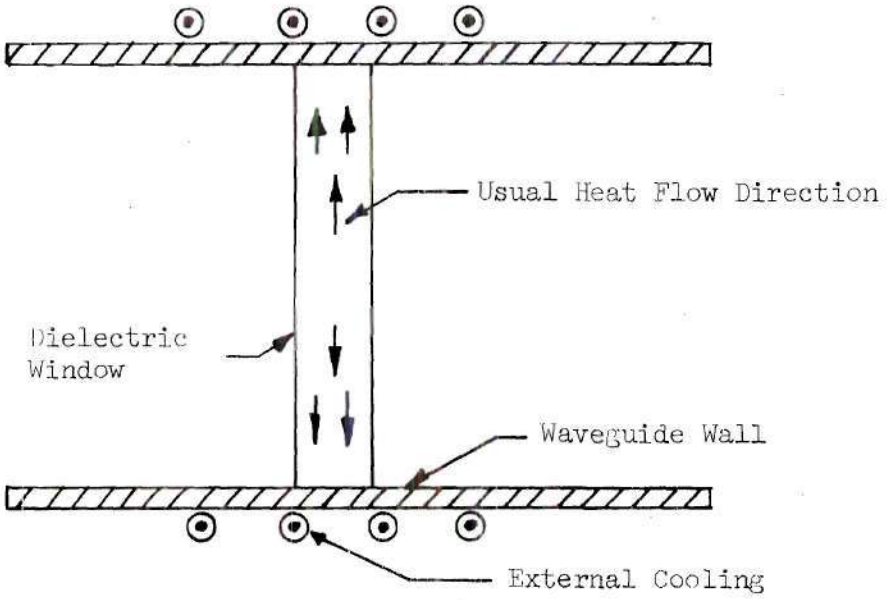

Figure 3. Typical Heat Flow of Thin Waveguide Window

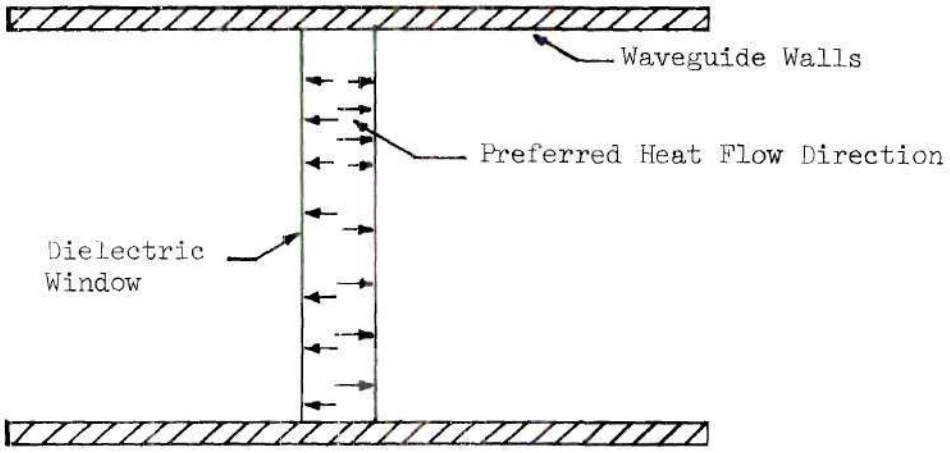

Figure 4. Preferred Direction of Heat Flow in Waveguide Window

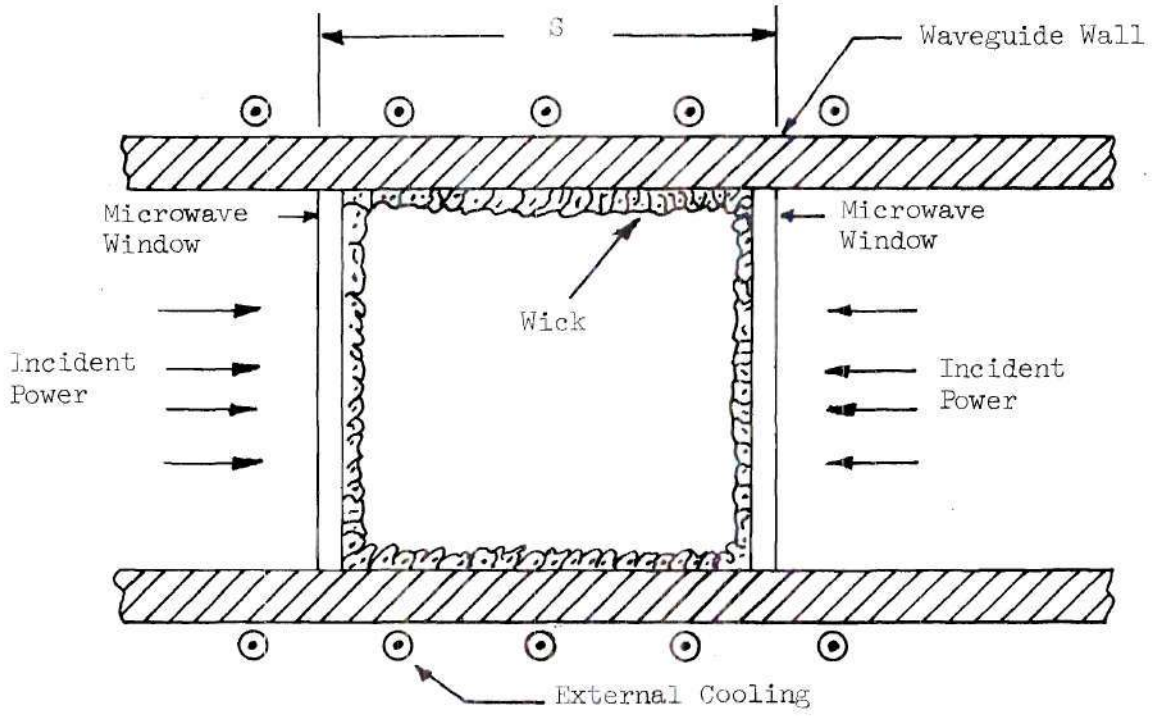

Figure 5. Longitudinal View of the Heat Pipe Cooled Microwave Window Arrangement

who independently rediscovered in 1964, a device similar to Gaugler's and coined the name "heat pipe" to describe it. Grover and his co-workers were working in the area of spacecraft power generation at the time, but immediately recognized the potential of the heat pipe in other areas.

In 1965, Cotter(4) presented the first quantitative engineering theory for the design and performance analysis of heat pipes. He concluded that the heat transfer capability of the device is limited by the ability of the wick to sustain the required circulation of liquid to the evaporator zone. He also pointed out that boiling of the liquid in the evaporator could also decrease the heat transfer characteristics of heat pipes.

Cosgrove(5) in 1967, made an analytical study of heat pipe operation. His model was based on heat, mass and momentum balance in the wick, assuming that capillary action was the controlling factor in heat pipe performance. He concluded that the maximum heat transfer is a function of the working fluid, wick characteristics and the angle of inclination of the heat pipe with respect to gravity. An experimental program using water as the working fluid was performed and there was a good correlation between the analytical model and the experimental results.

Winters and Barsch(6) and Marcus(7) have published up-to-date refinements and extensions to Cotter's original presentation. These publications also treat other topics such as heat pipe design, heat transfer, and variable conductance techniques. Winters and Barsch present a detailed survey of many theoretical models, while Marcus

summarizes well accepted features of the basic theory which are of interest to heat pipe designers.

Strabeck and Bienert[1] have prepared a heat pipe design handbook. This work is divided in two parts. Part one covers theory, design, performance curves, wick data, fluid properties and materials compatibility. An extensive bibliography is also included. Part two presents computer codes which include heat pipe analysis and design code, data acquisition code, and variable conductance heat pipe analysis code.

Williams[8] presented an analytical and experimental study for the purpose of identifying and correlating heat pipe parameters. Using dimensional analysis, twenty-four potentially important dimensionless groups were listed. An experimental program was carried out in order to evaluate the parameters required for correlation. Agreement between the experimental data and the correlation theory developed was found to be good.

Large numbers of heat pipes of many different shapes have been built and tested. The most common heat pipe is the long thin pipe[4]. Heat pipes having a small length to diameter ratio, known as "Vapor Chambers" or "Vapor Chamber Fins", have also been used[9]. Gray[10] has introducted a heat pipe that rotates about its longitudinal centerline and utilizes centrifugal acceleration instead of capillaries for return-pumping of the condensate to the evaporator. Katzoff[1] and Conway and Kelly[12] have considered a doughnut shaped heat pipe. Several investigators[13], [14], [15] have proposed and designed

flexible heat pipes. The effect of the working fluid on the performance of the heat pipe has also been studied (16), (17), (18). Wick characteristic and their performance have been studied by several authors (19), (20), (21), (22), (23). Considerable work has been done in the area of heat transfer limitation of heat pipes by Neal (16), Cosgrove et. al. (24), Kuntz et. al. (19) and Busse (23), to name but a few. Leyman and Huang (26) as well as Fox et. al. (27) have studied the temperature distribution in a heat pipe. The vapor flow in cylindrical heat pipes has been considered by Bankston and Smith (28). Colwell et. al. (29) studied the effect of noncondensables in a heat pipe and concluded that at low heat transfer rates, the presence of noncondensables in a heat pipe greatly affects its thermal conductance, while at higher levels of heat transfer rates the effect is not as marked.

Regarding the practical applications of heat pipes, it can only be said that they are innumerable, they range from domestic uses to space applications. Corman and McLaughlin (30), (31) have used heat pipes to cool integrated circuits as well as A-C motors. Sparrow et. al. (32) have suggested the use of heat pipes for solar collector modules. Katzoff (11) has considered a doughnut shaped heat pipe for the external control of a spacecraft. Kirkpatrick (33) has presented the progress achieved at NASA's Ames Research Center using heat pipes as (1) a variable conductance link between a heat source and sink to provide temperature stability; (2) a feedback control mechanism that acts to directly maintain the source at constant temperature; (3) or as a thermal diode that allows heat to be transferred in one direction only.

Bassett and Colwell[34] studies the feasibility of the design of a heat pipe cooled microwave window, and subsequently[35] an experimental heat pipe was constructed and tested. The test indicated that the heat pipe cooled windows could handle up to 2 - 3 megawatts of RF power at a frequency near 3.0 GHz.

CHAPTER II

EQUIPMENT

The heat pipe used in this investigation was designed with future experimental testing in mind. The device provides great flexibility since several of its components can be exchanged fairly easily; for instance, different wicks, microwave windows, heaters and working fluids can be used.

The heat pipe shell (waveguide) was made of a 2.5 in. inside diameter by 7.20 in. long copper tube. The capillary structure along the waveguide (condenser) consisted of four layers of 100 mesh copper screen. The capillary structure on the windows (evaporator) was also made of four layers of 100 mesh copper screen for reasons of simplicity, and due to the fact that only the thermal characteristics of the device were being evaluated. In the real model the capillary structure in the evaporator region would be made of a dielectric material with low dielectric loss (such as fiberglass cloth). It should be mentioned that some preliminary testing has been done by Colwell et. al.(35) using fiberglass cloth as the capillary structures in the evaporator, and a satisfactory performance was obtained.

The working fluid cavity was sealed by an O-ring between the waveguide wall and the window on each end. A retaining collar was used to apply a force on each end of the heat pipe assembly. Three separate ports of access to the heat pipe were provided, one for injecting the

working fluid, another for connecting a pressure transducer, and a third to connect a vacuum system. The waveguide was surrounded by a cooling jacket to remove the heat generated during operation. Figures 6, 7 and 8, show the waveguide-cooling jacket sub-assembly, a schematic of the test section and a block diagram of the test rig respectively. The heating elements at each end, as shown in Figure 8, were arranged to provide a tapering of power per unit area in order to stimulate the $TE_{1,1}$ mode power distribution which concentrates the heating energy in the central region of the microwave window. The notation $TE_{1,1}$ identifies the particular mode of transmission. For any mode of transmission in a circular waveguide, the transverse fiels may be resolved into two components, tangential and radial. Both of these components vary periodically along a circular path concentric with the wall and vary in a manner related to a Bassel function of order m along the radius. Any particular mode is identified by the notation $TE_{m,n}$ or $TM_{m,n}$, where m is the total number of full period variations of either component of field along a circular path concentric with the wall and n is one more than the total number of reversals of sign of either component of field along a radial path (36). Due to the fragility of the ceramic microwave windows (aluminum oxide and beryllia), aluminum windows were used in the experimental testing. Colwell et. al.(35) used aluminum oxide windows in a preliminary testing and good results were obtained.

There were fourteen Chromel-Alumel thermocouples mounted on the test heat pipe. Ten were located along the waveguide, and two were installed on each end of the heat pipe, in the evaporator region. Three

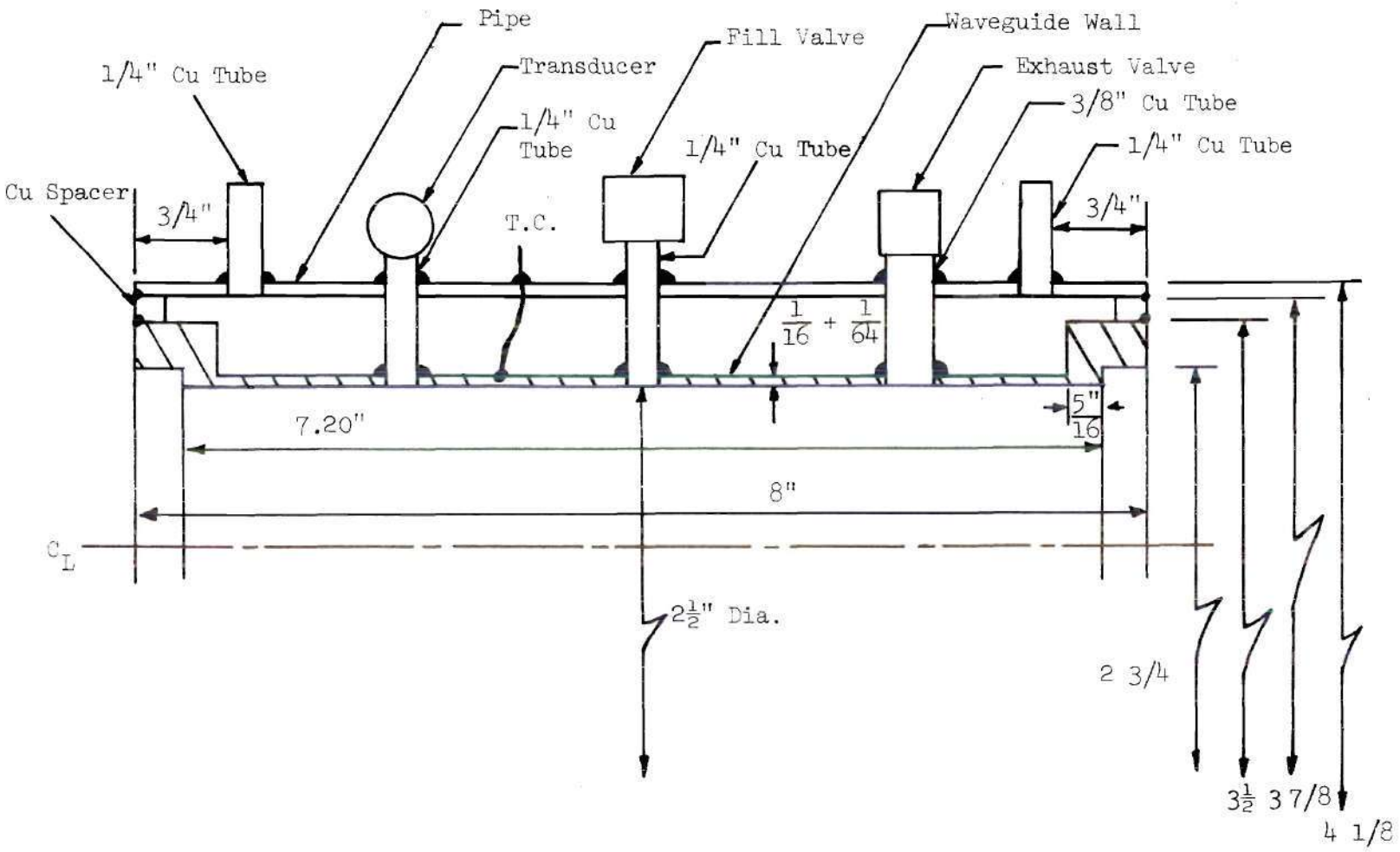

Figure 6. Waveguide - Cooling Jacket Sub-Assembly

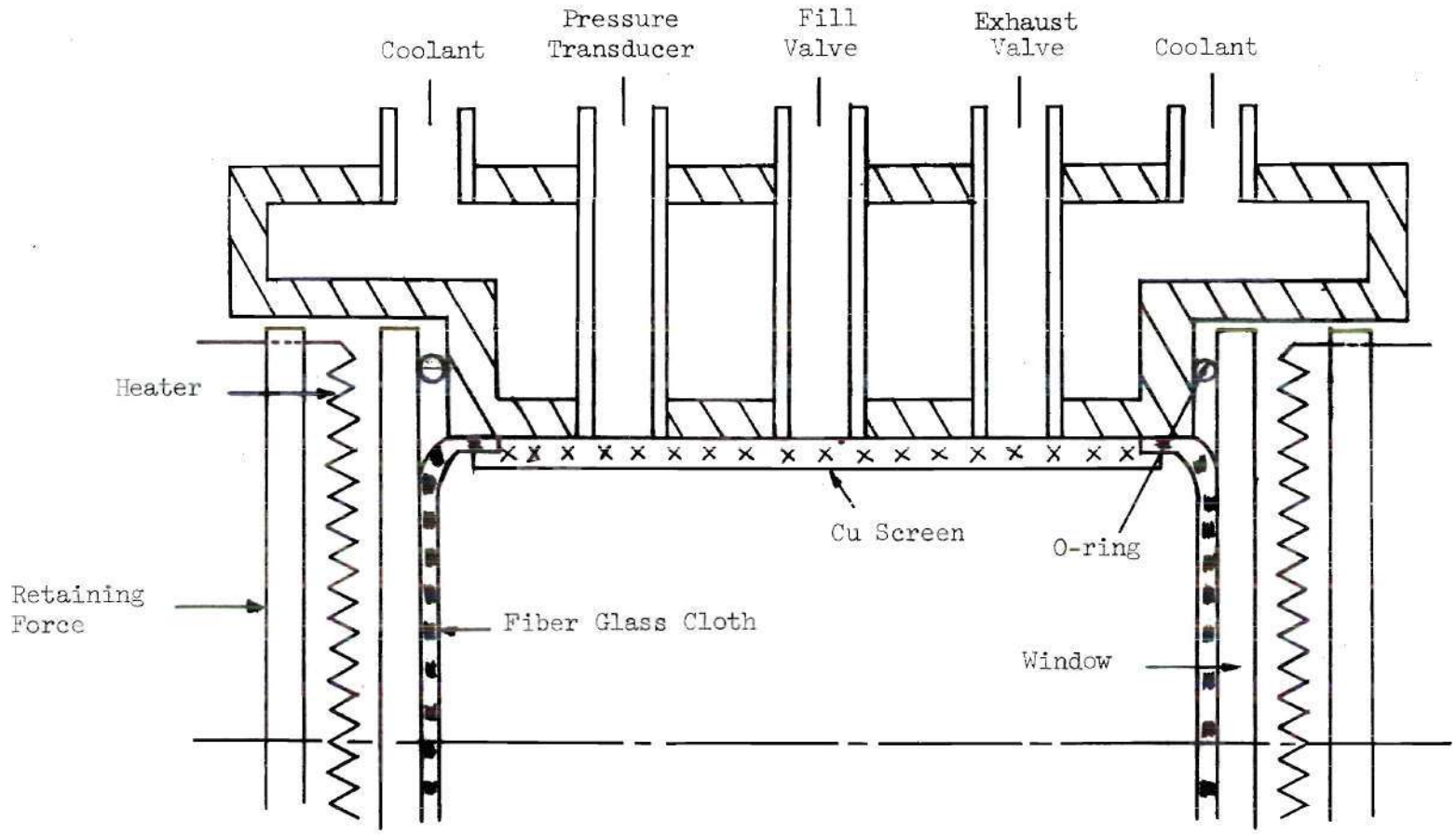

Figure 7. Schematic of Test Section

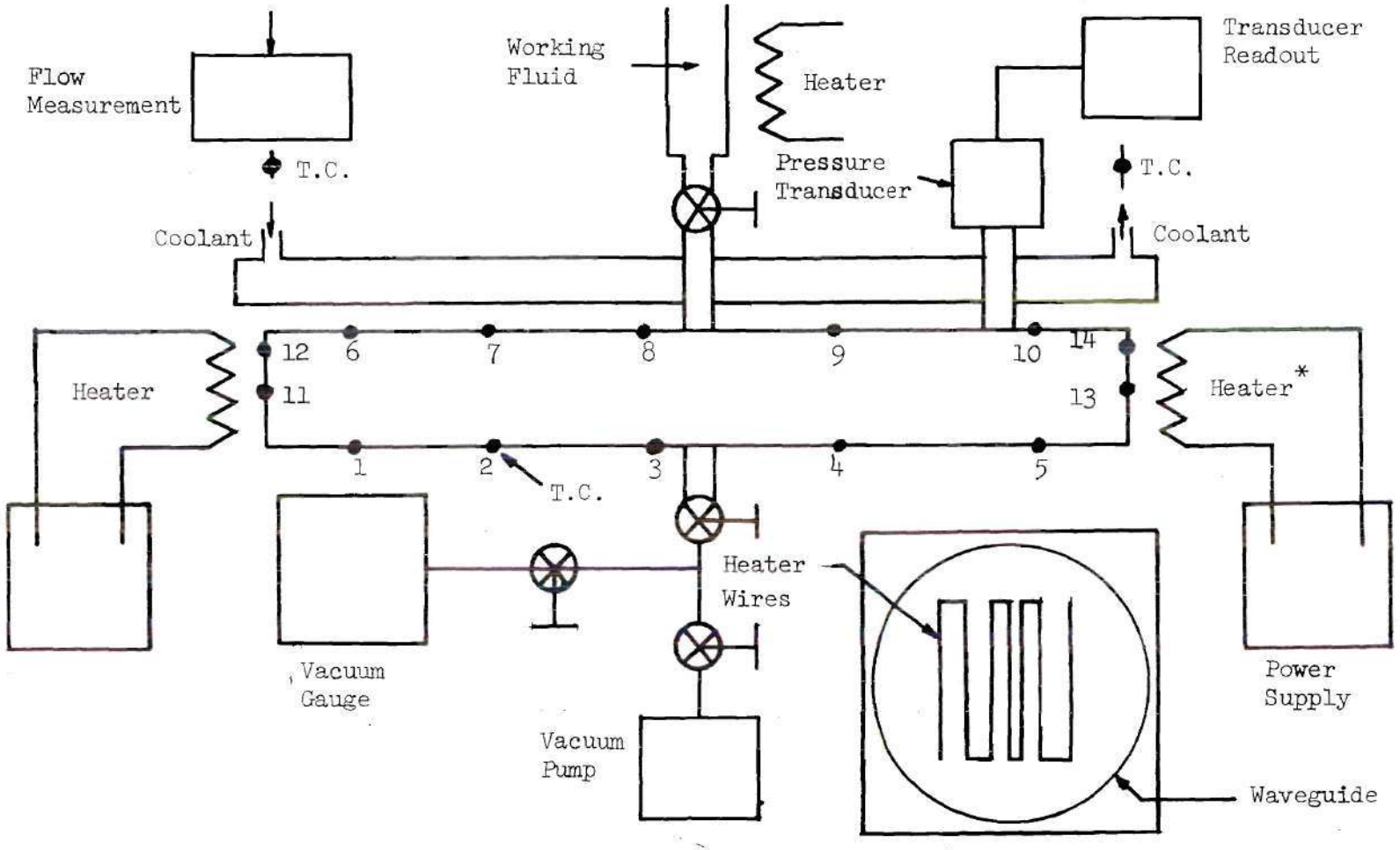

* Heater Wires Simulate TE_{11} Waveguide Model

Figure 8. Block Diagram of Test Rig

Copper-Constantan thermocouples were also installed in the device, two at the inlet port and one at the exit port of the cooling jacket. One thermocouple measured the temperature of the cooling water at the inlet port, while the other two measured the increase in water temperature from the inlet to the exit of the cooling jacket. See Figure 8.

The power supply system to the heating elements consisted of an alternating current voltage regulator, volt meter, and ammeter. The excitation voltage for the pressure transducer was provided by a D.C. power supply. The vacuum system comprised the vacuum pump, connecting copper tubing, vacuum needle valves, and a thermocouple vacuum gage. The condenser cooling water system, on the other hand, was composed of a constant head tank supplied with building water, cooling jacket inlet control valve, water cllection beaker, and connecting tubing. Lastly, the working fluid injection system consisted of a 50 ml. graduated burette wrapped with an electric heating element which allowed pre-heating of the working fluid in order to drive out air dissolved in it before injection. A needle valve was used to aid in accurately metering the amount of working fluid used.

The readings of the Chromel-Alumel thermocouples were recorded on a 16-channel Honeywell recorder, while the difference in readings between the cooling water inlet and outlet, as well as the pressure transducer outputs were registered directly on a Leeds and Northrup 2-channel continuous recorder. The water temperature at the cooling jacket inlet was monitored with a Leeds and Northrup potentiometer. Finally, a vacuum gage control was used to determine the initial pressure inside the heat pipe.

CHAPTER III

EXPERIMENTAL PROCEDURE

The experimental program carried out during the present investigation consisted of two parts. First, the amount of working fluid needed to saturate the heat pipe capillary structure had to be determined. Once this was done, the second step in the program was to evaluate the performance of the heat pipe cooled microwave window model for both water and heptane.

The following steps were taken in order to determine the amount of working fluid needed to saturate the capillary structure.

a. The heat pipe was thoroughly cleaned with acetone and then assembled.

b. The heat pipe was positioned horizontally on the test bench, and the pressure transducer, vacuum system and calibrated burette were connected to it.

c. The system was pumped down until the pressure inside the heat pipe was about 30μHg.

d. All valves were closed and the system was monitored for leaks with a thermocouple vacuum gage. If the leak rate was about five micron of Hg per hour, the system was assumed to be leak tight for the purpose of this investigation.

e. The working fluid to be used (distilled water), was heated in the calibrated burette to remove absorbed gases and then slowly bled

into the heat pipe.

f. The cooling water was then allowed to flow from the constant head tank thrcugh the cooling jacket. The cooling water flow rate was adjusted by means of a valve and it was measured by collecting the flow in a graduated cylinder over a certain time interval. This flow rate was checked periodically during each run in order to maintain as constant a flow rate as possible.

g. Next, the evaporator heaters were turned on with an initial power setting of about 15 watts. The temperatures along the waveguide, at the windows, the pressure inside the heat pipe and the temperature increase of the cooling water were continuously monitored and recorded, until steady state operation was attained.

h. The power setting was then increased to the next desired level and again, all temperatures and the pressure inside the heat pipe were recorded. This step was repeated for several power settings until the maximum power input desired was reached.

i. Then an additional 10 ml. of working fluid was bled into the heat pipe and steps g and h were repeated.

j. The previous step was repeated until the total amount of working fluid inside the heat pipe reached 50 ml.

Once the amount of working fluid needed to wet the capillary structure was determined (see Chapter VI), the following steps were taken in order to evaluate the heat pipe performance.

1. The system was pumped down until the pressure inside the heat pipe was about 30μHg.

2. The system was then monitored for leaks.

3. Next, 30 ml. of distilled water previously heated in the calibrated burette were slowly bled into the device.

4. The cooling water was set at a small flow rate (about 4.80 lbm/hr.).

5. The evaporator heaters were turned on with an initial power setting of about 15 watts. The temperatures along the waveguide, at the windows, the pressure inside the heat pipe and the temperatures increase of the cooling water were continuously monitored and recorded, until steady state operation was attained.

6. The power setting was then increased to the next desired level and again, all temperatures and the pressure inside the heat pipe were recorded. This step was repeated for various power settings until a maximum power input of about 430 watts was reached.

7. Steps 5 and 6 were repeated for medium (about 10.15 lbm/hr.) and high (about 23.02 lbm/hr.) cooling water flow rate.

8. When the testing program described above had been completed the power was set at 280 watts and the cooling water flow rate was set at about 5.82 lbm/hr. After the system had stabilized, the vacuum pump was turned on and the working fluid (water) was removed from the heat pipe. This was done in order to monitor the microwave window temperatures when they were heat pipe cooled and when the heat was transferred by conduction.

9. When the testing program described above was finished the system was evacuated again and heptane was injected in the heat pipe to use it as working fluid.

10. The cooling water was set at a high flow rate (about 23.02 lbm/hr.).

11. Steps 5 and 6 were repeated in order to evaluate the performance of the device.

12. Step 8 was repeated.

It should be mentioned that special care was taken when working with heptane due to its volatility, flamability and toxious effects.

CHAPTER IV

THEORETICAL CONSIDERATIONS

1. Objective

The purpose of this chapter is to study the general relations which describe the performance of a heat pipe. These relations are applied to the model of the heat pipe cooled microwave window in order to determine its theoretical performance under a variety of conditions.

2. Heat Pipe Limitations

It was pointed out in Chapter I that there are several factors which may limit the heat transport through a heat pipe. These include choking in the vapor region, vapor entrainment of the liquid from the capillary structure, boiling in the evaporator and dryout of the wick at the evaporator region, due to insufficient capillary pumping (maximum capillary flow or wicking limit). This last type of limitation is the most important mode of failure in the present application. (See Appendices A, B, C, D,)

A. Choking

A heat pipe is said to be "choked" when flow of its working fluid is restricted due to sonic velocity occurring at some point in the flow path. When this happens the circulation rate is limited to:

$$\dot{m}_s = \rho_v U_s \pi r_v^2 \qquad (4.1)$$

and the maximum axial rate of heat transfer is given by:

$$\dot{Q}_s = \dot{m}_s \, h_{fg} \tag{4.2}$$

B. Entrainment

Entrainment is associated with high axial vapor velocities. Since the vapor and liquid flows are in opposite directions inside the heat pipe, it is possible for the vapor to pick up liquid from the capillary structure.

Entrainment takes place when the Weber number (ratio of the inertial forces in the vapor and tension forces in the liquid) is unity[1]. The Weber number is defined as:

$$We = \frac{Z \rho_v \bar{v}^2}{\sigma} \tag{4.3}$$

where $\bar{v}$ is the average vapor velocity and Z is a characteristic dimension for the surface. The axial heat flux is given by:

$$\frac{\dot{Q}}{A_v} = \bar{v} \, \rho_v \, h_{fg} \tag{4.4}$$

substitution of $\bar{v}$, from equation (4.3) with We = 1 into equation (4.4) yields:

$$\frac{\dot{Q}}{A_v} = \left(\frac{\rho_v \, \sigma \, h_{fg}^2}{Z} \right) \tag{4.5}$$

which represents the axial heat flux at the onset of entrainment.

At the present time, it is not possible to predict theoretically the value of the characteristic dimension Z. Experimental data seem to indicate that at the onset of entrainment the Weber number is unity,

if Z is approximately equal to the mesh size of the wick. Furthermore, there is not sufficient quantitative information to decide whether Z is related to the wire diameter or the wire spacing(1).

Entrainment increases the circulation losses in the heat pipe and consequently reduces its heat transfer capability. Of all the heat transfer limitations of heat pipes, the entrainment limit is the least severe.

C. Boiling in the Evaporator

This type of limitation has received so far very little attention. Cotter(4) was the first to point out the possibility of nucleate boiling in the evaporator and stated that:

> The onset of boiling may be characterized by a critical bubble radius of curvature r, which depends on the nature and geometry of the interface where bubbles nucleate. If the difference between the pressure of the vapor in the bubble and the pressure in the surrounding liquid is less than 2 σ/r, then the bubble will collapse.

Boiling within the evaporator is believed to decrease the heat transfer capability of the heat pipe due to vapor blockage in the evaporator. So far, there is no consistent theory which has been tested experimentally.

It is a common design practice to define the heat flux limit at the onset of nucleate boiling(1) as:

$$\dot{q}_b = \frac{K_{eff}}{\delta_B} \Delta T_{crit}. \qquad (4.6)$$

this boiling heat flux limit corresponds to the conduction heat flux, which yields a critical super heat ΔT_{crit}. The amount of super heat at nucleate boiling is, according to Davis(37), and Silverstein(38):

$$\Delta T_{crit} = \frac{2\sigma T_{sat}}{h_{fg} \rho_v r} \tag{4.7}$$

where r is the effective radius of the critical nucleation cavity. Typical values for smooth surfaces are between 10^{-4} and 10^{-3} inches. For a wick, little is known about the value of r, but the pore radius of the wick can be used for practical purposes (1).

D. Capillary Limitation

The most important limitation in the present investigation is the maximum capillary flow that the wick structure can sustain. As liquid flows in the capillary structure, pressure losses develop and at maximum flow rate the pressure loss is equal to the maximum pressure rise furnished by the wick.

In order to determine the capillary limited heat flux, consider the model shown in Figure 9.

From the momentum equation:

$$\sum \vec{F}_{ext} = \frac{d\vec{P}}{dt} \tag{4.8}$$

Assuming steady operation and that the velocities are small, the changes in momentum can be neglected and equation (4.8) reduces to:

$$\sum \vec{F}_{ext} = 0 \tag{4.9}$$

The momentum equation, can then be written (neglecting interfacial pressure drops (see Appendix E) as:

$$\Delta P_c = \Delta P_{v\ell} + \Delta P_{vv} \pm \Delta P_g \tag{4.10}$$

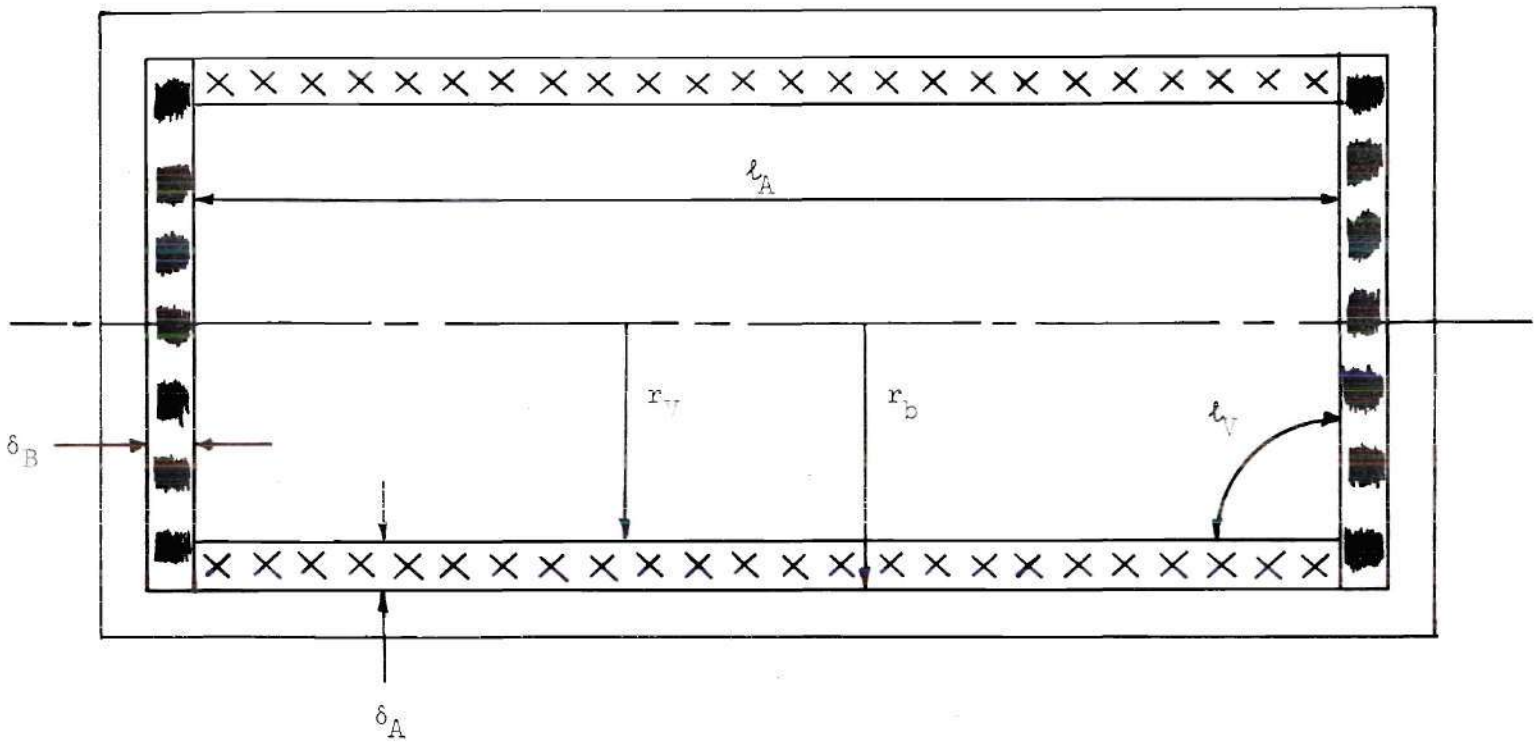

Figure 9. Heat Pipe Capillary Model

The maximum capillary pumping is given by (39) as:

$$\Delta P_c = \frac{2\sigma}{B r_P} \tag{4.11}$$

The pressure difference due to gravity is determined from (39),

$$\Delta P_g = g \rho_\ell \sin \theta \tag{4.12}$$

but since the heat pipe in this investigation is in the horizontal position, the effect of the gravitational field is neglected.

The pressure drop due to viscous losses in the vapor path, has been estimated in the heat pipe literature (39) to be given fairly accurately by:

$$\Delta P_w = \frac{8 \mu_v \dot{m} \ell_v}{\pi \rho_v r_v^4} \tag{4.13}$$

This pressure drop is very small (see Appendix E) in the present application, and therefore, may be neglected.

The pressure drop in the liquid phase can be determined from (see Appendix G):

$$\Delta P_{v\ell} = \frac{\mu_\ell \dot{m}}{P_\ell} \left[\frac{0.055 \, B K_1}{\epsilon_B \delta_B} + \frac{\ell_A A K_1}{4 \epsilon_A \delta_A b} \right] \tag{4.14}$$

Therefore, substitution of (4.11) and (4.14) into (4.10) yields:

$$\frac{2\sigma}{B r_P} = \frac{\mu_\ell \dot{m}}{\rho_\ell} \left[\frac{0.055 B K_1}{\epsilon_B \delta_B} + \frac{\ell_A A K_1}{4 \epsilon_A \delta_A b} \right] \tag{4.15}$$

the heat transfer rate for the heat pipe is given by:

$$\dot{Q} = \dot{m} h_{fg}$$

or

$$\dot{m} = \frac{\dot{Q}}{h_{fg}} \tag{4.16}$$

Substituting (4.16) into (4.15) and solving for $\dot{Q}$, gives the maximum heat transfer capability, or wicking limit of the heat pipe.

$$\dot{Q}_{max} = \frac{2\sigma\rho_\ell h_{fg}}{\mu_\ell B r_P}\left[\frac{1}{\frac{0.055_B K_1}{\epsilon_B \delta_B} + \frac{\ell_A A K_1}{4\epsilon_A \delta_A b}}\right] \tag{4.17}$$

or in terms of the heat pipe number N,

$$\dot{Q} = \frac{2N}{B r_P}\left[\frac{1}{\frac{0.055\ B K_1}{\epsilon_B\ \delta_B} + \frac{\ell_A\ A K_1}{4\epsilon_A \delta_A b}}\right] \tag{4.18}$$

where

$$N = \frac{P_\ell\ \sigma\ h_{fg}}{\mu_\ell} \tag{4.19}$$

3. Thermal Resistances

In order to determine the overall thermal resistance of the heat pipe structure, consider the model shown in Figure 10. Symmetry about the centerline and about the mid plane of the pipe is assumed. Under these assumptions the total energy transported by the device will be twice that of the computed for the model. Figure 11 shows schematically the potentials and resistances of the heat pipe model. The heat transfer

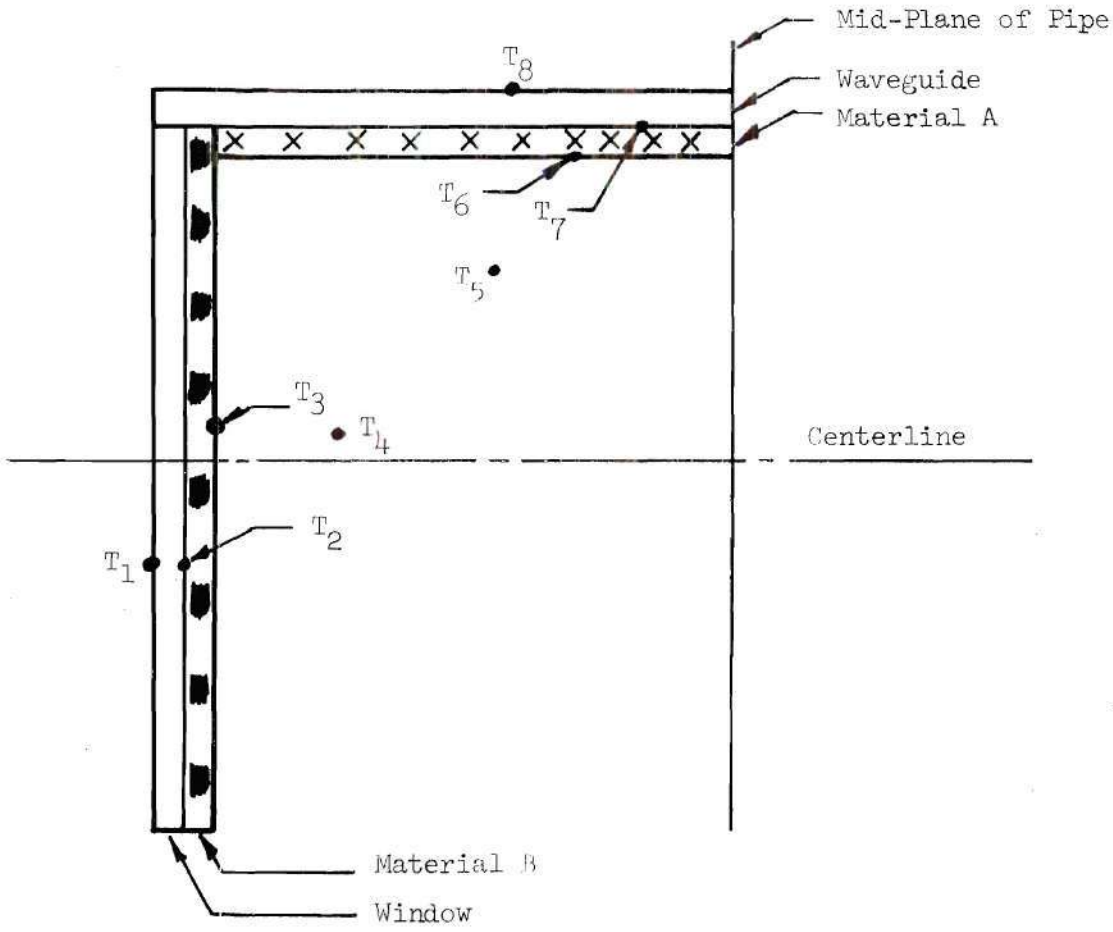

Figure 10. Heat Pipe Model

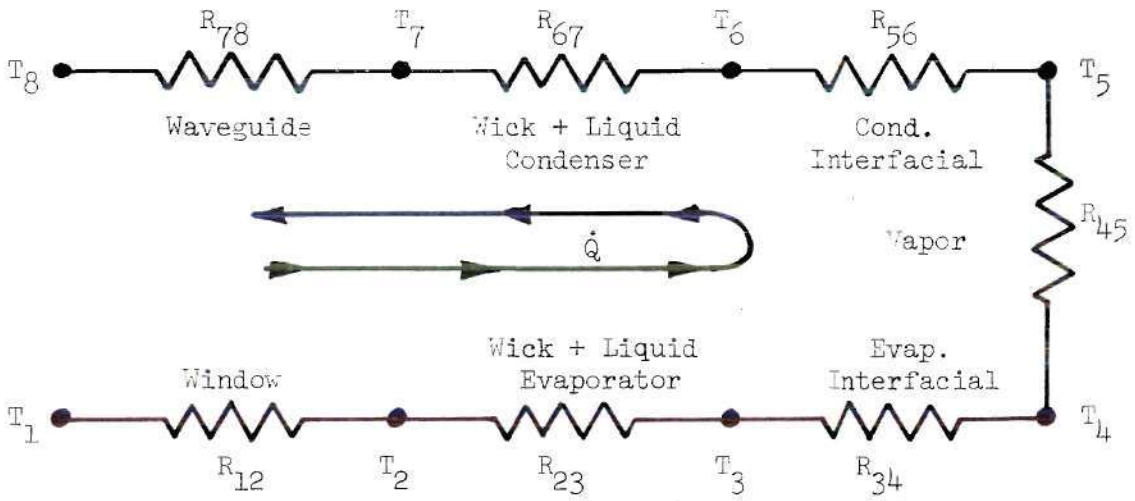

Figure 11. Schematic of Heat Pipe Potentials and Resistance

of the device is given then by:

$$\dot{Q} = \frac{T_1 - T_8}{\sum_i R_i} \tag{4.20}$$

It is now necessary to determine each one of the thermal resistances of the device.

A. Microwave Window Resistance

The thermal resistance of the microwave window is given by (40)

$$R_{12} = \frac{t_w}{\pi K_w r_b^2} \tag{4.21}$$

B. Wick-Liquid Resistance in Evaporator

The composite wick-liquid matrix in the evaporator has a thermal resistance given by:

$$R_{23} = \frac{\delta_B}{K_E \pi r_b^2} \tag{4.22}$$

The effective thermal conductivity of the wick liquid in the evaporator can be determined according to Williams (8) from:

$$\frac{K_E}{K_\ell} = \frac{1}{\left[\frac{B^r P}{B^r ws} + 1\right]\left[\frac{2K_\ell}{B^K ws} + \left(\frac{B^r P}{B^r ws} - 1\right)\right]}$$

$$+ \frac{2}{\left[\frac{B^r P}{B^r ws} + 1\right]\left[\frac{K_\ell}{B^K ws}\left(\frac{B^r ws}{B^r P} + 1\right)\right]} + \frac{1}{\left[\frac{B^r ws}{B^r P} + 1\right]^2} \tag{4.23}$$

C. Interfacial Resistance at Evaporator

The interfacial thermal resistance is given, according to Wilcox and Rohsenow(41), by:

$$R_{34} = \frac{(2\pi)^{\frac{1}{2}} R^{3/2} T_3^{5/2}}{2\pi r_v^2 P_3 h_{fg}^2 (g_c)^{\frac{1}{2}} J} \qquad (4.24)$$

Where P_3 is the saturation pressure corresponding to T_3. This expression was derived from kinetic theory assuming that the accumulation coefficient is unity (the probability of condensation of an impinging vapor molecule).

D. Thermal Resistance in Vapor

The thermal resistance in the vapor can be determined in the following way.

Since the total vapor pressure ΔP_v is relatively small for the heat pipe, the vapor may be treated as an ideal gas, and the Clausius-Clapeyron equation may be used to determine the corresponding temperature difference:

$$T_4 - T_5 = \frac{\Delta P_v T_4 \left(\frac{1}{\rho_v} - \frac{1}{\rho_\ell} \right)}{h_{fg}} \qquad (4.25)$$

Where ΔP_v is given by equation (4.13).

The heat flux is given by:

$$\dot{Q} = \frac{T_4 - T_5}{R_{45}} \qquad (4.26)$$

or

$$R_{45} = \frac{T_4 - T_5}{\dot{Q}} \qquad (4.27)$$

Since

$$\dot{Q} = \dot{m}\, h_{fg} \tag{4.28}$$

Then

$$R_{45} = \frac{8\mu_v \ell_v T_4 \left(\frac{1}{\rho_v} - \frac{1}{\rho_\ell} \right)}{\pi \rho_v r_v^4 h_{fg}^2 (g_c)\, J} \tag{4.29}$$

E. Interfacial Resistance at Condenser

The interfacial thermal resistance in the condenser is given by (39).

$$R_{56} = \frac{(2)\ (2\pi)^{\frac{1}{2}}\ R^{3/2}\ T_6^{5/2}}{(2)\ 2\pi\ T_v\ \ell_A P_6 h_{fg}^2 (g_c)^{\frac{1}{2}}\ J} \tag{4.30}$$

Where P_6 is the saturation pressure corresponding to T_6.

F. Wick-liquid Resistance in Condenser

The wick-liquid thermal resistance in the condenser is determined from:

$$R_{67} = \frac{\ln \frac{r_b}{r_v}}{\pi K_C \ell_A} \tag{4.31}$$

The effective thermal conductivity of the wick-liquid matrix in the condenser, K_C, is given by (8),

$$\frac{K_C}{K_\ell} = \frac{1}{\left[\frac{A^r P}{A^r ws} + 1 \right] \left[\frac{2K_\ell}{A^K ws} + \left(\frac{A^r P}{A^r ws} - 1 \right) \right]}$$

$$+ \frac{2}{\left[\frac{A^{r}P}{A^{r}ws} + 1\right]\left[\frac{K_{\ell}}{A^{K}ws}\left(\frac{A^{r}ws}{A^{r}P} + 1\right)\right]} + \frac{1}{\left[\frac{A^{r}ws}{A^{r}P} + 1\right]^{2}} \quad (4.32)$$

G. Waveguide Resistance

The waveguide thermal resistance is given by,

$$R_{78} = \frac{\ell n \frac{r_a}{r_b}}{\pi K_G \ell_A} \quad (4.33)$$

the overall thermal resistance of the heat pipe is therefore given by:

$$\sum Ri = \frac{tw}{\pi K_w r_b^2} + \frac{\delta_B}{K_E \pi r_b^2} + \frac{(2\pi)^{\frac{1}{2}} R^{2/3} T_3^{5/2}}{2\pi r_v^2 P_3 h_{fg}^2 (g_c)^{\frac{1}{2}} J}$$

$$+ \frac{8\mu_v \ell_v T_4 \left(\frac{1}{\rho_v} - \frac{1}{\rho_\ell}\right)}{\pi \rho_v r_v^4 h_{fg}^2} + \frac{(2\pi)^{\frac{1}{2}} R^{3/2} T_6^{5/2}}{2\pi r_v \ell_A P_6 h_{fg}^2 (g_c)^{\frac{1}{2}} J}$$

$$+ \frac{\ell n \frac{r_b}{r_v}}{\pi K_C \ell_A} + \frac{\ell n \frac{r_a}{r_b}}{\pi K_G \ell_A} \quad (4.34)$$

The heat flux can now be computed using equation (4.20). The values of T_3, T_4, and T_6 have to be assumed before the overall thermal resistance can be computed. It should be noted that partial wick dry out and retreat of the liquid into the pores have not been accounted

for in these resistances. Under certain conditions these effects may be significant. For a discussion in this area, see Reference (42). Once $\dot{Q}$ has been determined, all unknown temperatures can be computed.

4. Selection of Working Fluid

The selection of the heat pipe working fluid is extremely important for the proper performance of the device. In general the working fluid must have (a) high surface tension to provide satisfactory capillary pumping, (b) good wetting characteristic, for the same reason as in (a), (c) low viscosity, to aid pumping, (d) high latent heat of vaporization to aid axial heat transfer, (e) high thermal conductivity to aid heat transfer between fluid, wall and wick, (f) freezing and boiling points compatible with the range of operation, (g) large density to reduce flow resistance, (h) compatibility with the wick and container in relation to corrosion and (i) chemical stability. In addition to these properties, the working fluid used in the present application must possess a good microwave transmission characteristic, i.e., low dielectric loss.

In equation (4.19), the heat pipe number, N, was defined as,

$$N = \frac{\rho_\ell \sigma h_{fg}}{\mu_\ell}$$

This number, also known as the liquid transport factor, depends only on the fluid properties and gives an indication of how suitable a given fluid is for heat pipe applications. The higher the value of this factor, the higher the circulation rate in the heat pipe. Figure 12 shows the heat pipe number as a function of temperature for a number

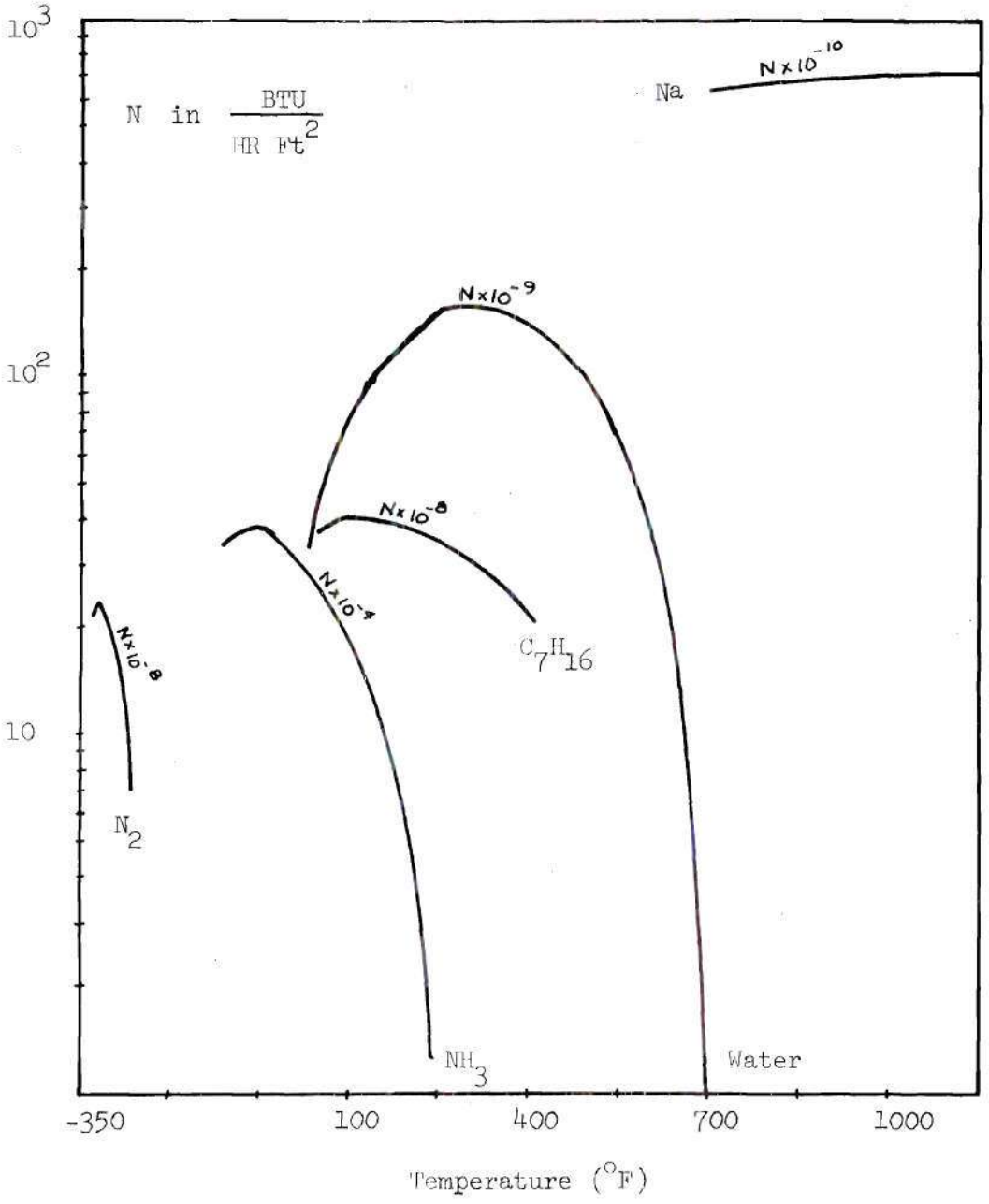

Figure 12. Heat Pipe Number Vs. Temperature For Several Heat Pipe Working Fluids

of heat pipe working fluids.

A number of working fluids were considered by Colwell et. al.[35], and several were found to have desirable properties (both thermal and microwave). Two of these, heptane and carbon tetrachloride, were found to be particularly suitable. The decision to use heptane in the present investigation was due to its' higher heat pipe number, and better microwave characteristics.

CHAPTER V

PARAMETRIC STUDY

The purpose of this chapter is to discuss the effects of changing different design parameters of the heat pipe colled microwave window on its performance.

The first step in this parametric study was to determine the wicking limit of the heat pipe model using first water and then heptane as working fluids for several capillary structure arrangements. Table 1 shows the different capillary structure combinations considered in the present investigation.

Figure 13 shows the variation of the wicking limit with the mesh size of the capillary structure in the condenser. This variation is illustrated for a capillary structure consisting of 2 layers of fiberglass cloth in the evaporator, 2 screen layers in the condenser and water used as working fluid, but the results follow the same pattern for other combinations shown in Table 1. From Figure 13, it can be seen that the wicking limit decreases with increasing mesh size number. As indicated in Chapter IV, the heat pipe under consideration is assumed to be symmetrical about its centerline and mid plane. Under this condition the total energy transported by the device will be twice that of the computed for the model shown in Figure 10. Therefore, in Figure 13, one half $\dot{Q}_{max}$ refers to one window, while $\dot{Q}_{max}$ refers to both windows.

Figure 14 shows the effect that the number of layers in the

Table 1. Capillary Structure Combinations Considered

Evaporator Capillary Structure	Number of Layers in Evaporator				Number of Layers in Condenser	Condenser Capillary Structure
	1	2	3	4		
	X	X	X	X	1	100 mesh copper screen
	X	X	X	X	2	
	X	X	X	X	3	
	X	X	X	X	4	
Fiberglass Cloth	X	X	X	X	1	200 mesh copper screen
	X	X	X	X	2	
	X	X	X	X	3	
	X	X	X	X	4	
	X	X	X	X	1	400 mesh copper screen
	X	X	X	X	2	
	X	X	X	X	3	
	X	X	X	X	4	

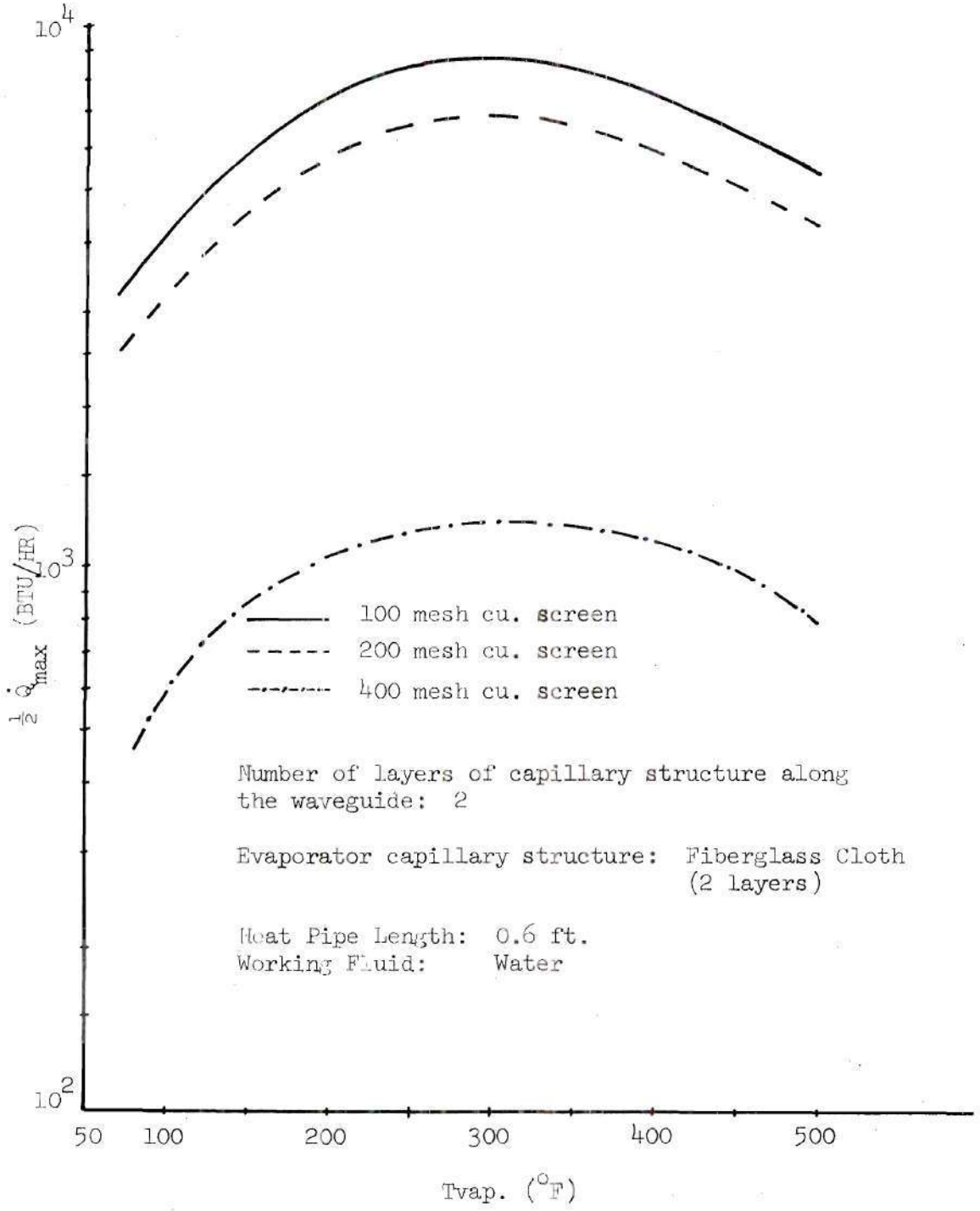

Figure 13. Wicking Limit Vs. Vapor Temperature for Various Capillary Structure Mesh Number Along the Wavequide

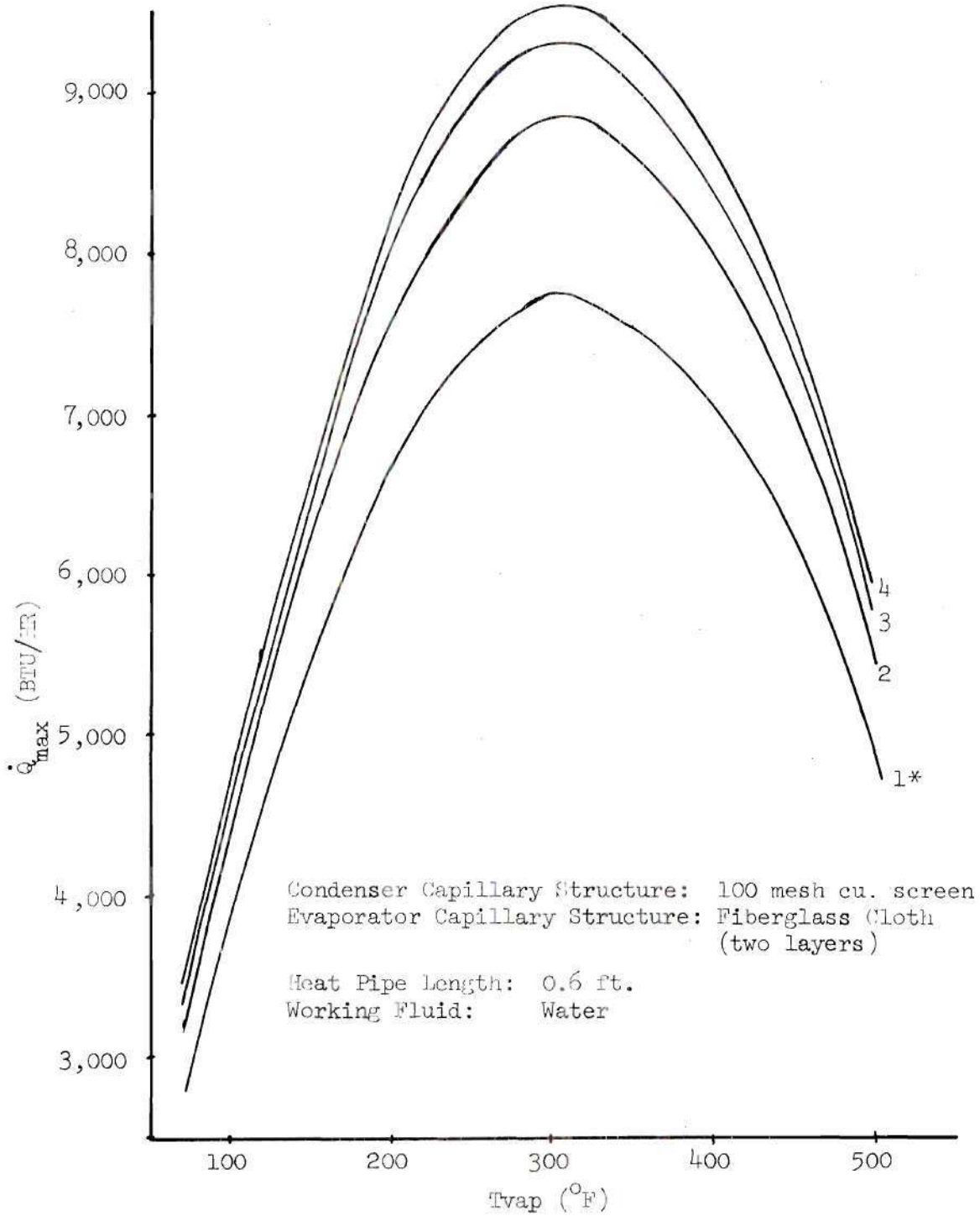

* Numbers indicate number of layers of capillary structure in the condenser

Figure 14. Wicking Limit Vs. Vapor Temperature as a Function of Capillary Structure in the Condenser

condenser have on the wicking limit of the device. From the Figure, it can be observed that increasing the number of layers of capillary structure in the condenser from 1 to 2 produces a considerable increase in the wicking limit, while further increase in the number of layers raises the wicking limit only moderately.

Figure 15 shows the variation of the wicking limit with the number of layers of capillary structure in the evaporator. It is obvious from this plot that the wicking limit is strongly dependent on the number of layers of the capillary structure in the evaporator. Unfortunately, the number of layers in the evaporator should be kept to a minimum since the wick-liquid thermal resistance increases considerably with the number of layers, as can be seen from Appendix K.

Figure 16 shows how the window spacing affects the wicking limit of the device. It should be mentioned that the window spacing was varied arbitrarily in order to show its effect upon the heat pipe capillary limitation. In a real application, the windows have to be separated a specific distance in order to offer a good impedance match to the incident RF signal. From the Figure it is observed that the wicking limit increases with decreasing window spacing.

Figure 17 depicts the heat pipe wicking limit for the two working fluids considered in this investigation.

It should be pointed out that even though a capillary structure consisting of 2 layers of 100 mesh copper screen in the condenser, two layers of fiberglass cloth in the evaporator and water as working fluid was used to arrive at the conclusions derived from the previous Figures (13 through 17), the same general pattern in each case was observed

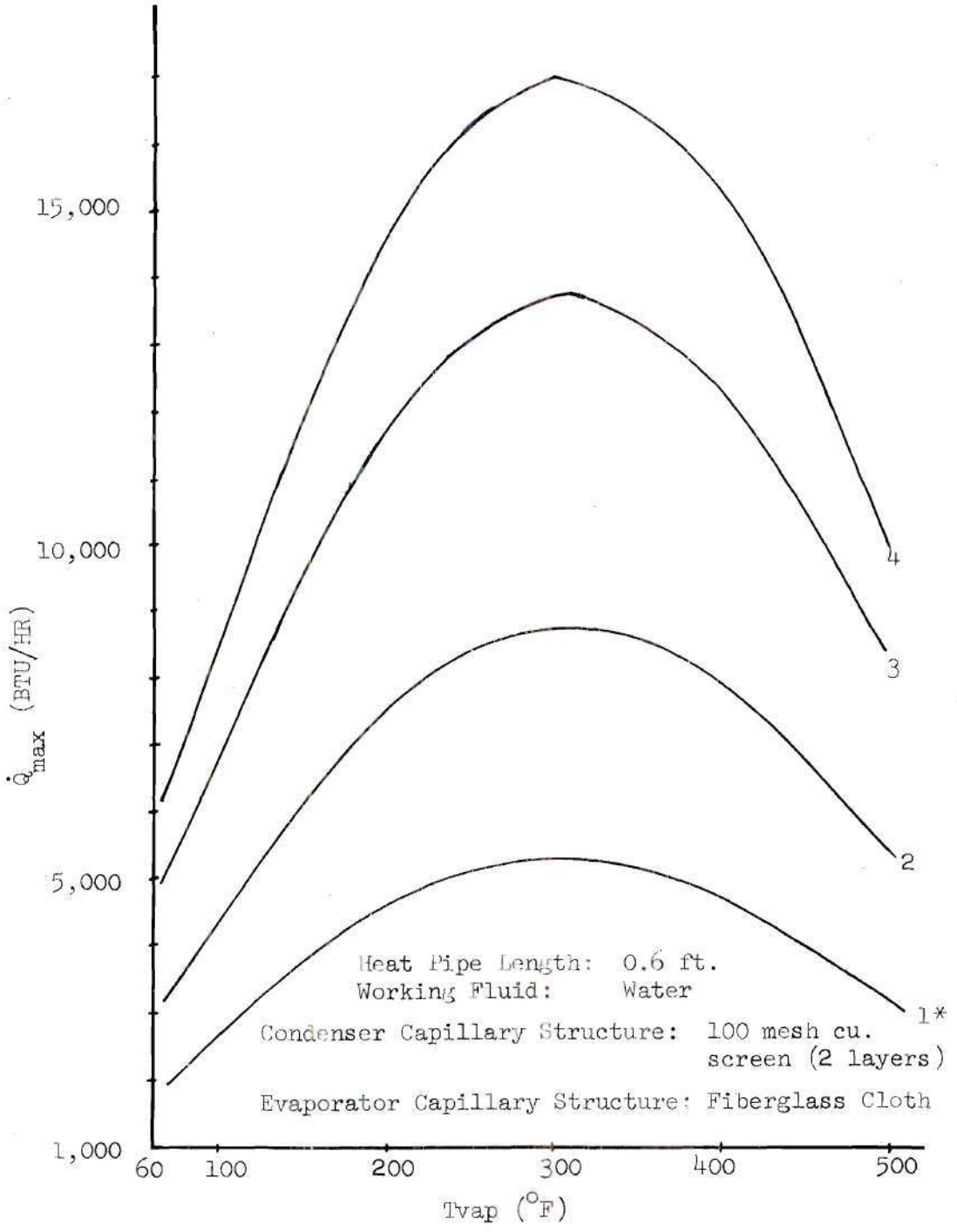

* Numbers indicate number of layers of capillary structure in the evaporator

Figure 15. Wicking Limit Vs. Vapor Temperature as a Function of the Number of Layers of Capillary Structure in the Evaporator

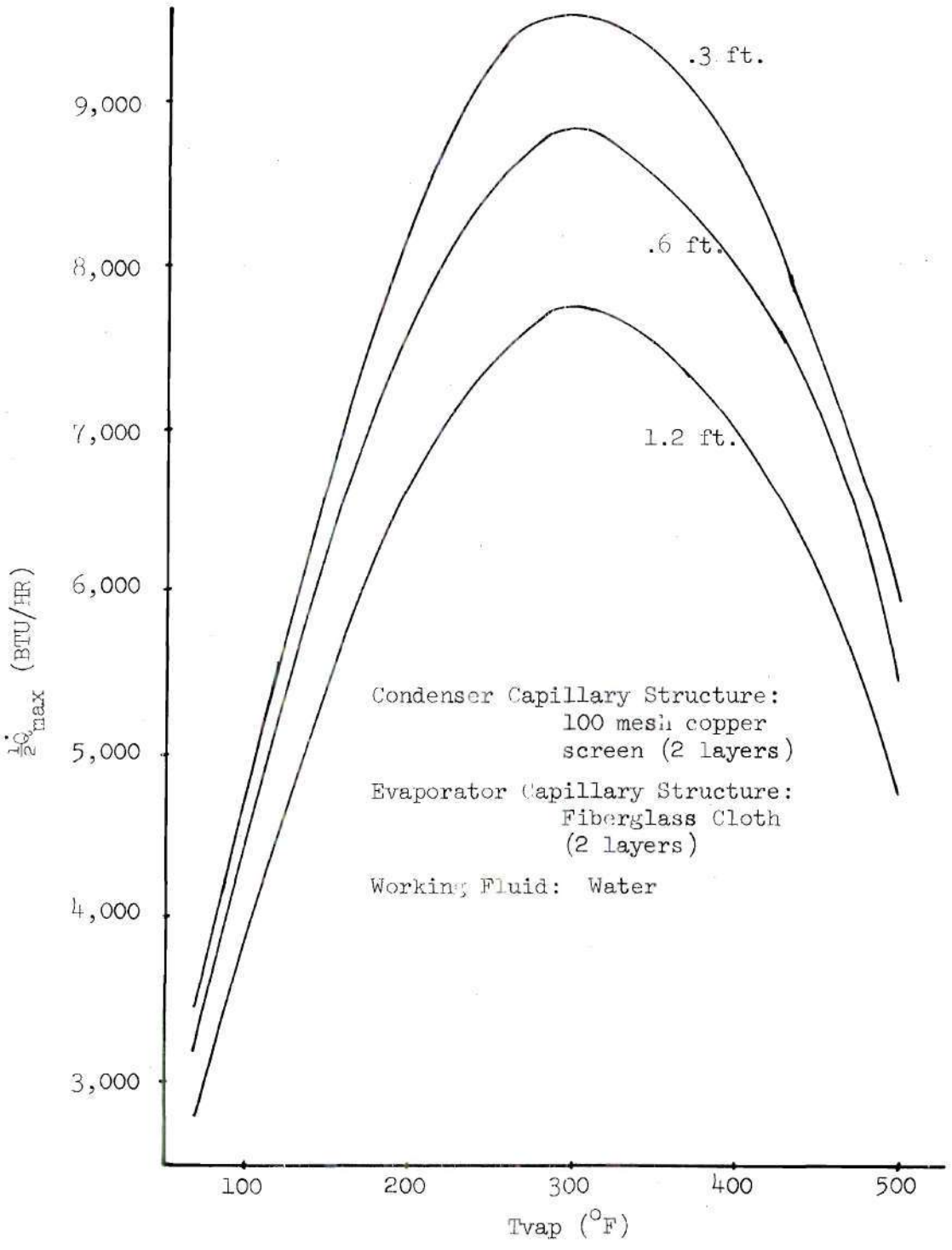

Figure 16. Wicking Limit Vs. Vapor Temperature as a Function of Heat Pipe Length (Window Spacing)

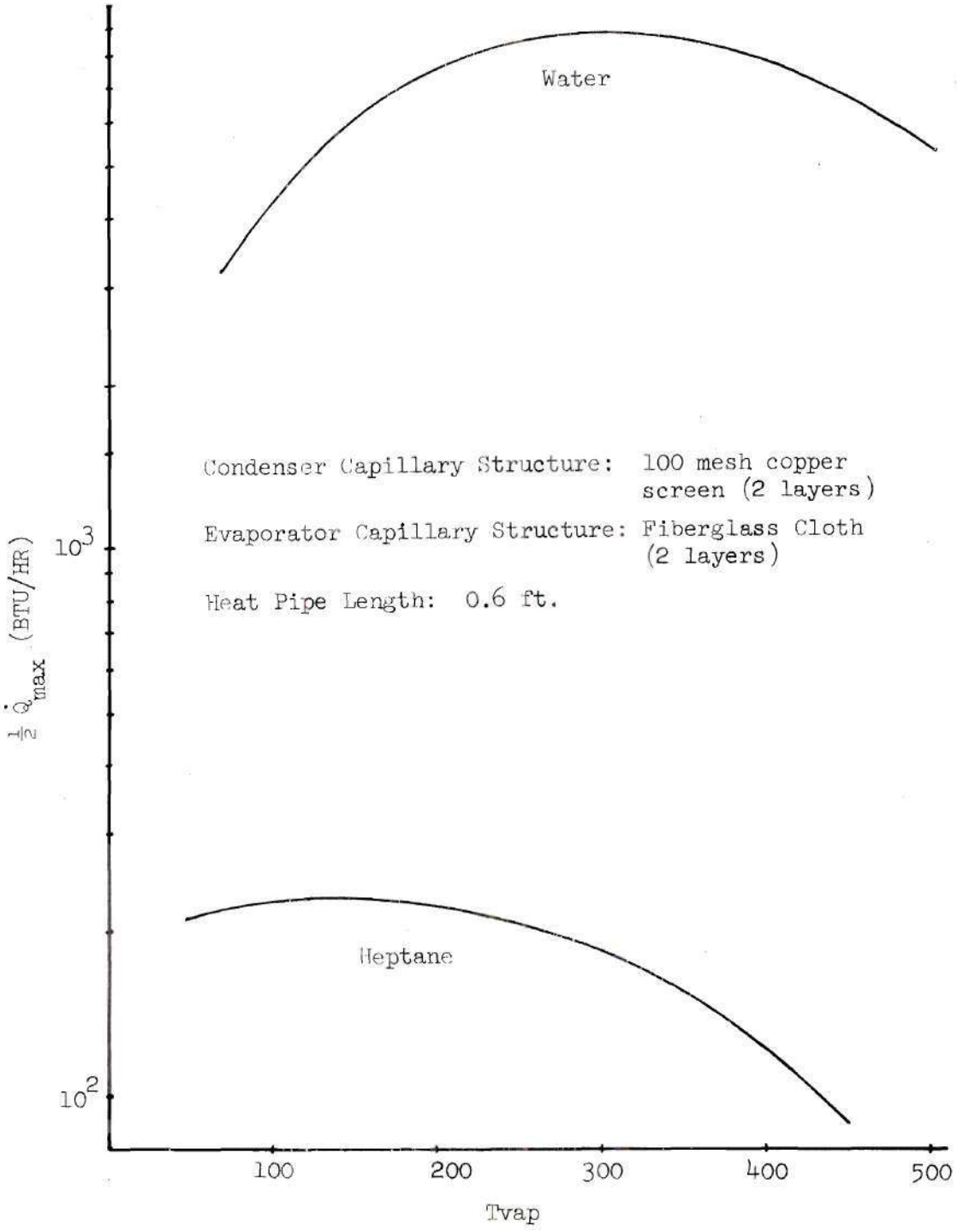

Figure 17. Wicking Limit Vs. Vapor Temperature for Water and Heptane Used as Working Fluids

for other combinations considered in the present investigation.

Figures 18 and 19 show the calculated performance for a heat pipe cooled microwave window. In Figure 18 two different types of microwave window materials were considered, and water was assumed to be the working fluid. Furthermore, in both figures, the effect that the number of layers of capillary structure in the evaporator have on performance can be appreciated.

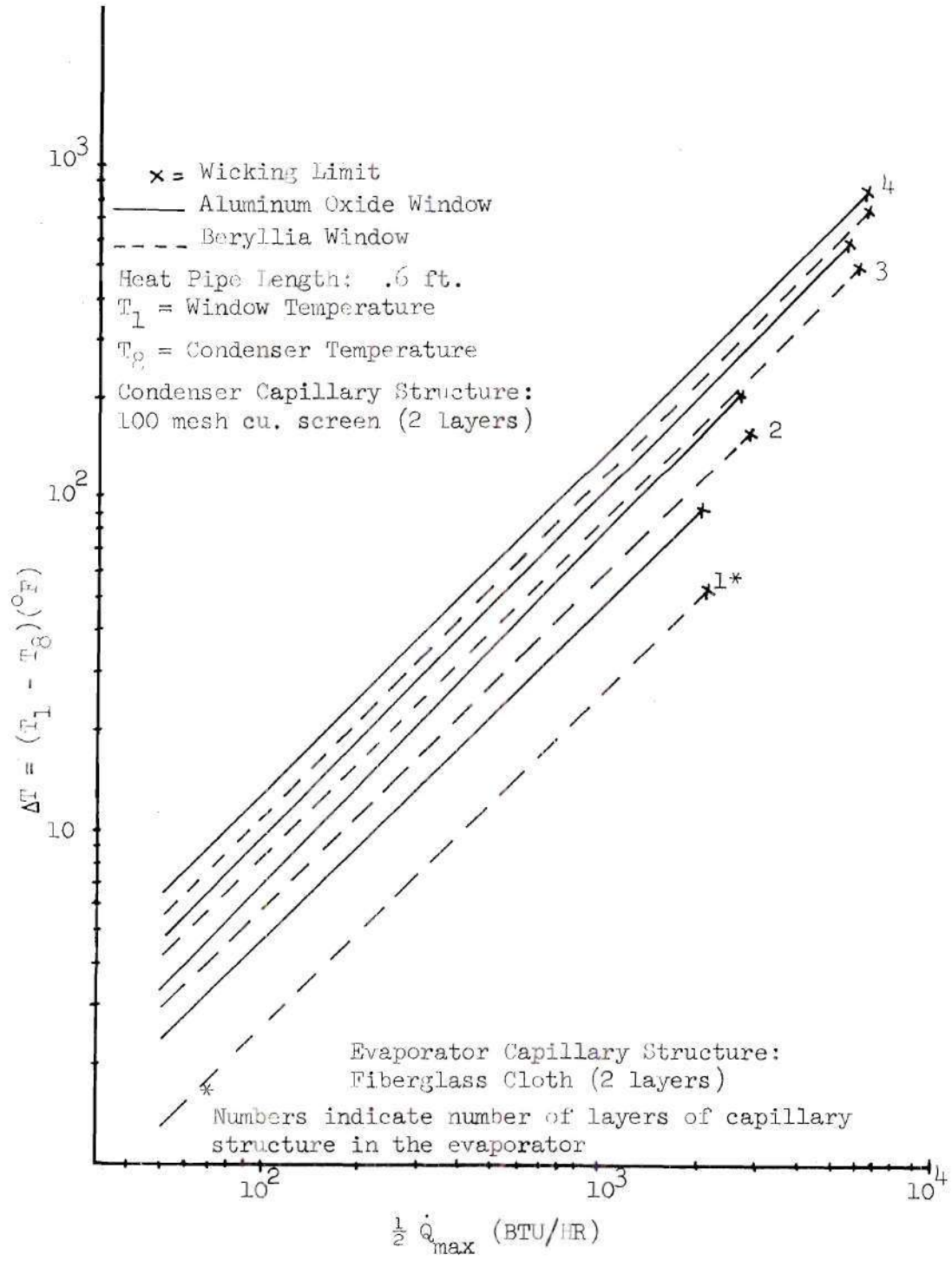

Figure 18. Driving Potential Vs. Heat Transfer (Working Fluid: Water)

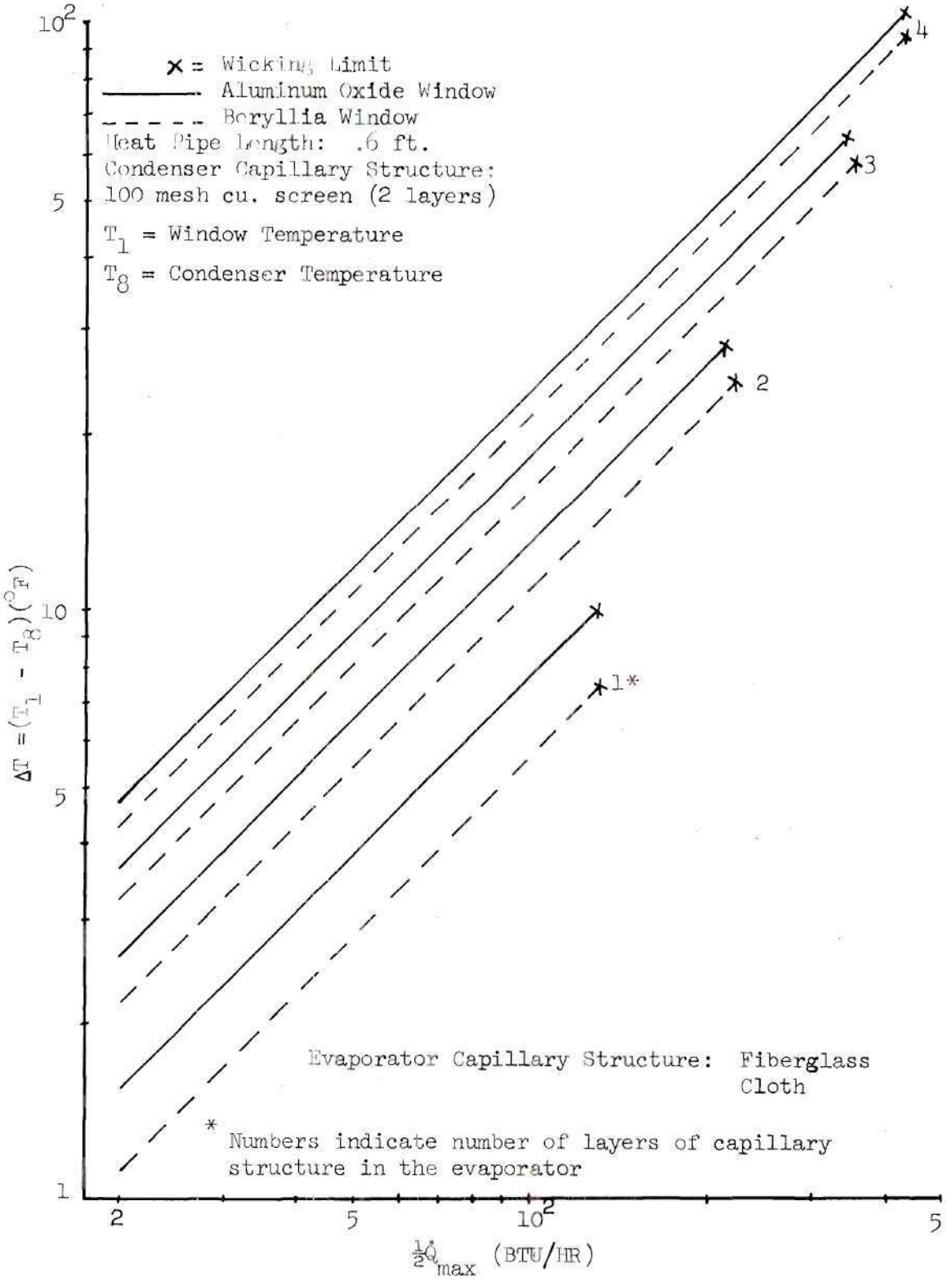

Figure 19. Driving Potential Vs. Heat Transfer (Working Fluid: Heptane)

CHAPTER VI

EXPERIMENTAL RESULTS

1. Determination of the Working Fluid Volume

The first part of the experimental program carried out, consisted of determining the optimum amount of working fluid needed for proper operation of the heat pipe cooled microwave window. It was decided to experimentally determine the working fluid volume of the device, due to the various connections that were made on it. The connections made theoretical estimation somewhat uncertain, since the working fluid partially filled them.

The procedure followed was outlined in Chapter III, and the results obtained are shown in Figure 20. This Figure shows the heat pipe performance for several volumes of working fluid. It can be observed that the rate of heat transferred increased when the volume of working fluid was augmented from 20 to 30 ml. When the working fluid volume was again increased, this time to 40 ml., the amount of heat transferred decreased. The working fluid was further increased, to 50 ml., and the heat transferred increased again in this case. It was believed however, that this last increase in the amount of heat transferred was probably due to convective effects from the excess amount of working fluid and not to heat piping. Consequently, in evaluating the heat pipe performance, it was assumed that the ideal volume of working fluid for the proper functioning of the heat pipe

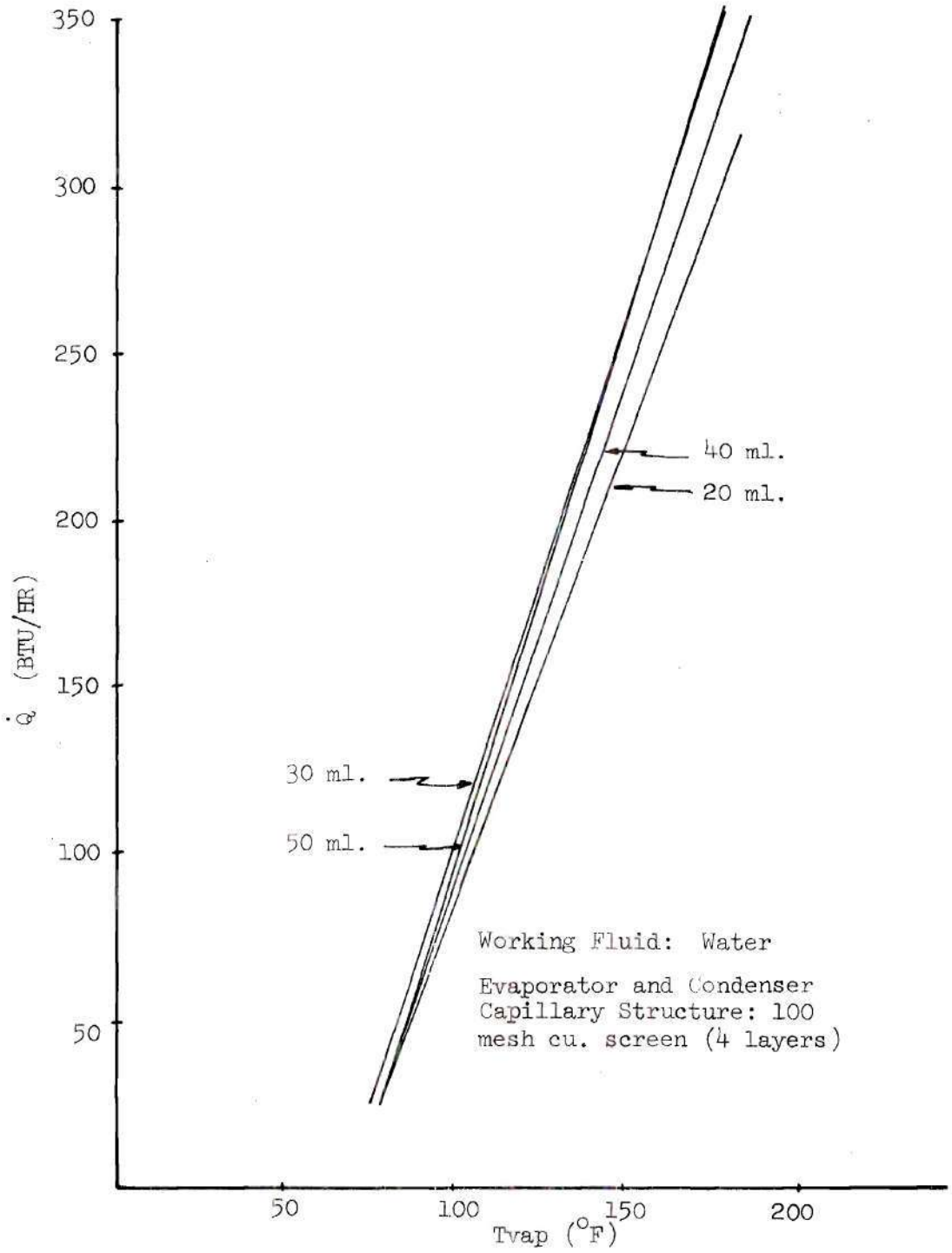

Figure 20. Heat Transfer Vs. Vapor Temperature for Various Working Fluid Volumes

cooled microwave window was 30 ml.

2. Heat Pipe Cooled Microwave Window Performance

The performance of the device was evaluated first using water and then heptane as working fluids.

Figure 21 shows the heat transferred vs. vapor temperature for various cooling water flow rates. It was found that for high flow rates (23.06 lbm/hr) it was possible to maintain the vapor temperature at about 100°F for a heat flux of 435 watts. It should be mentioned that about 35 percent of this heat input was lost to the surroundings, since the system was not insulated. None-the-less, it is expected that considerably higher power levels could be handled when vapor temperatures are allowed to increase to the 300 to 400°F range. At this point, it should also be pointed out that the heat pipe condenser section must be redesigned in order to obtain higher vapor temperatures. At the present time, the highest vapor temperature attainable is about 213°F, at which point the water in the cooling jacket starts boiling.

Figure 22 is a plot of the heat transferred vs. vapor pressure for various cooling water flow rates. It can be observed that the vapor pressures were very small (especially for high cooling water flow rate), the reason for these being, as explained above, the inadequacy of the condenser.

Figure 23 shows a plot of the ratio of the measured vapor pressure, to the vapor pressure corresponding to the measured condenser temperature vs. the temperature in the condenser. The shape of the curve seems to indicate that at low operating temperatures the liquid

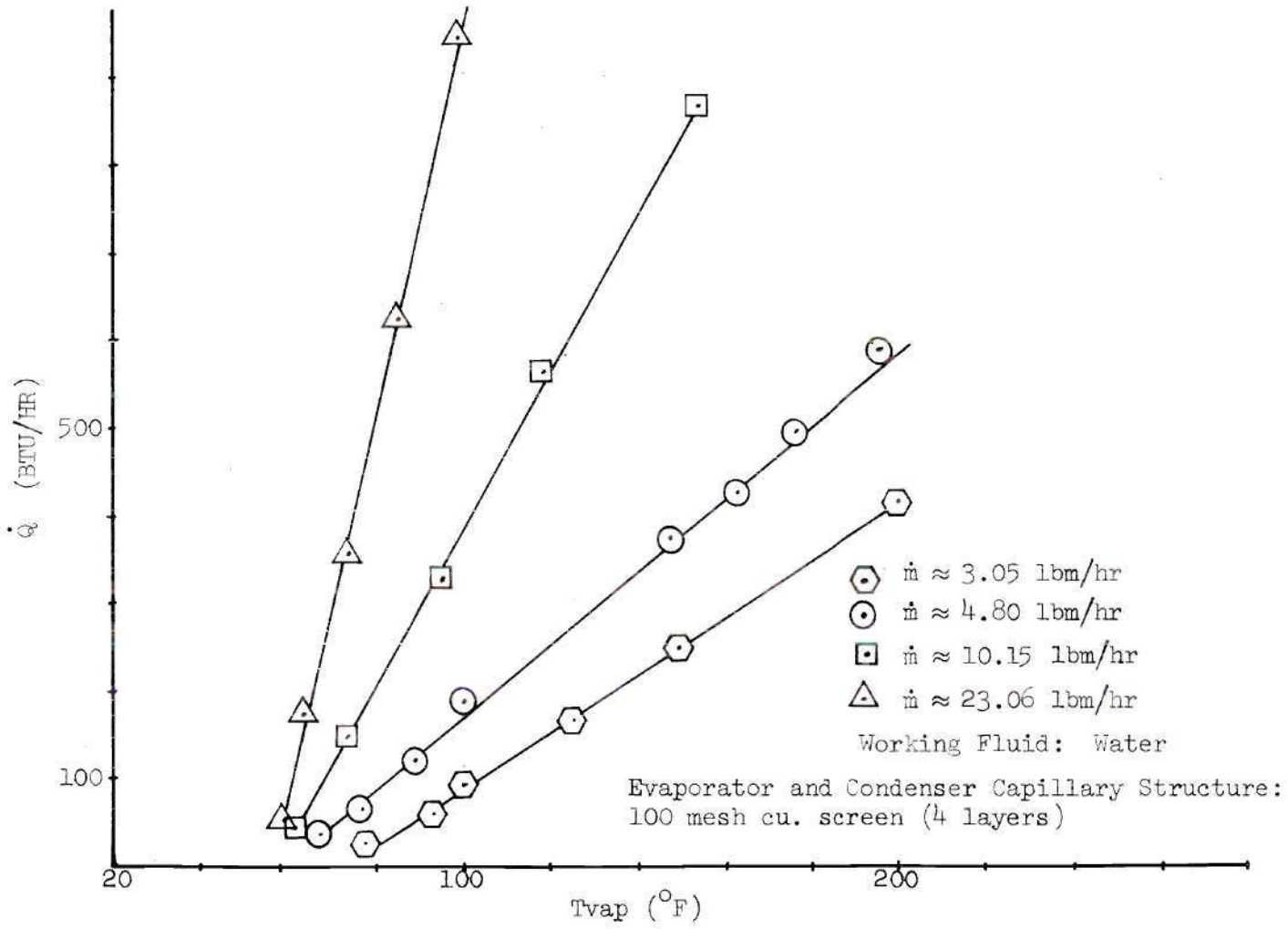

Figure 21. Heat Transfer Vs. Vapor Temperature for Various Cooling Water Flow Rates

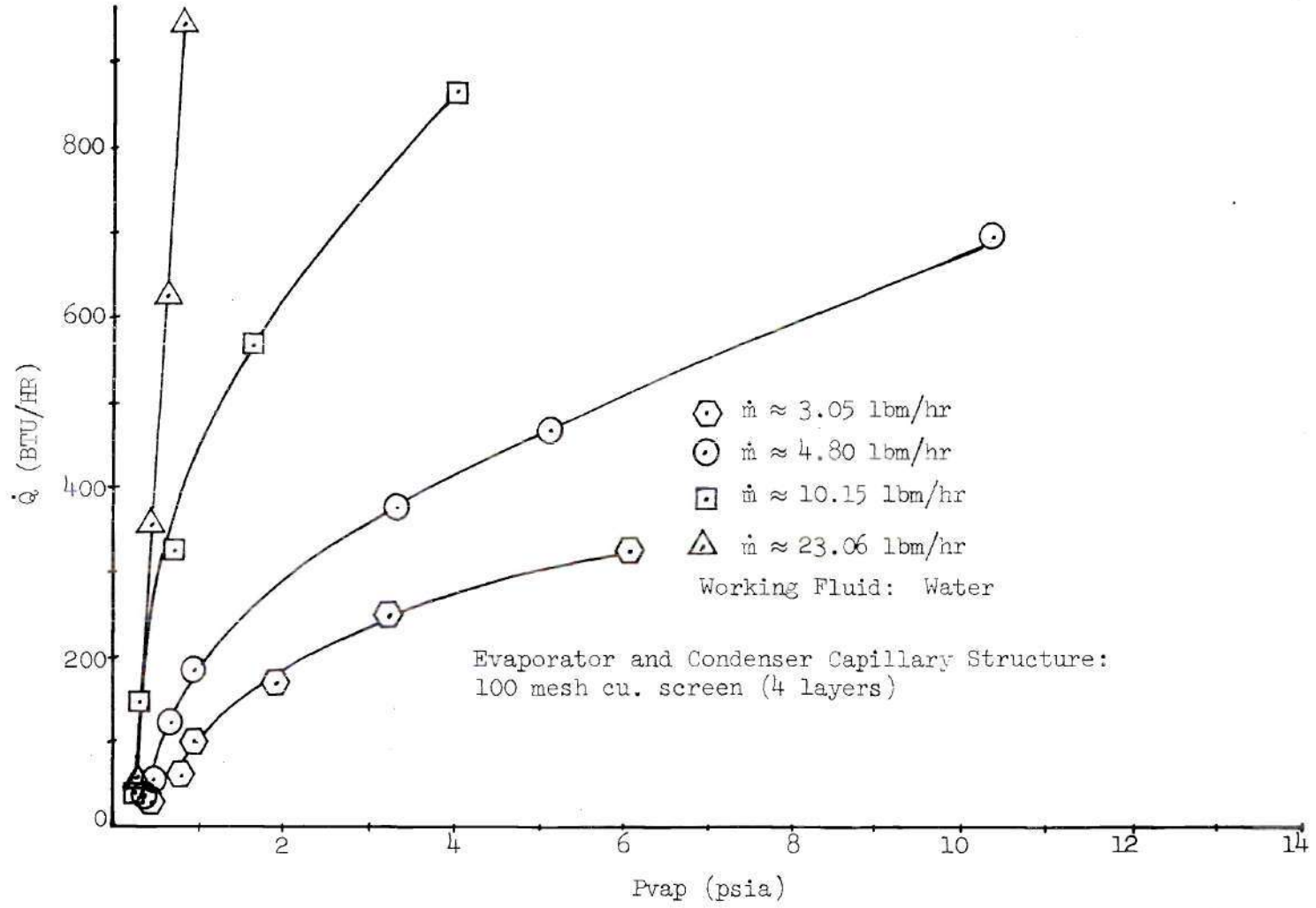

Figure 22. Heat Transfer Vs. Vapor Pressure for Various Cooling Water Flow Rates

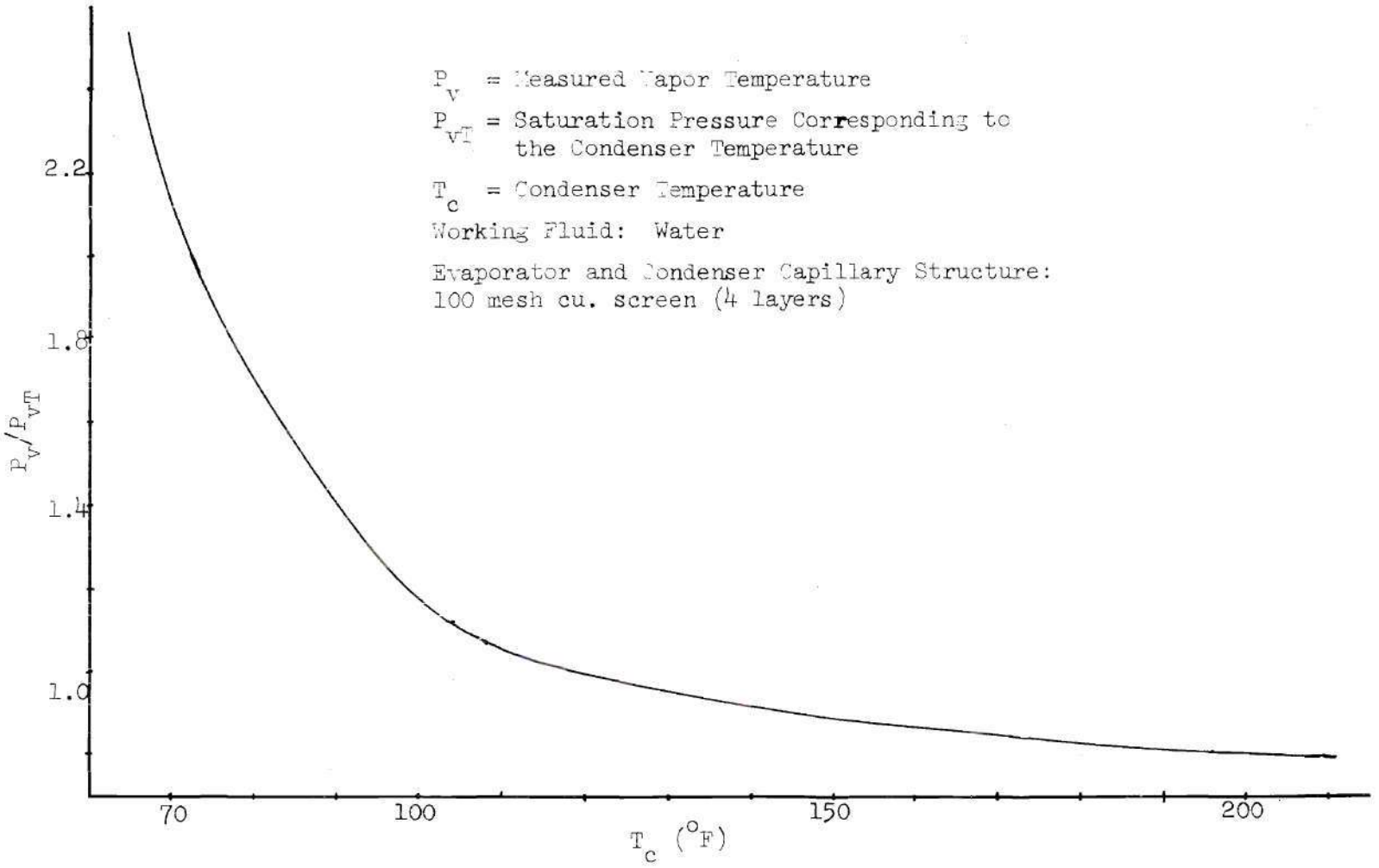

Figure 23. P_v/P_{vT} Vs T_c

inside the heat pipe may not be in saturated condition and that higher thermal resistance exists at low density.

Figure 24 is a cross plot obtained from Figure 21. It shows the heat transferred vs. cooling water flow rate for various vapor temperatures. It can be observed that higher heat transfer rates are obtained with increasing vapor temperature.

Figure 25 compares the heat pipe performance when water and heptane are used as working fluids. The heat pipe behaves in a very similar manner with both fluids, but of course the burnout limit is much lower when heptane is used as a working fluid (see Chapter V).

Figure 26 compares the temperature in the microwave windows when they were being heat pipe cooled and when the heat was being removed by pure conduction. As can be seen from this figure, the window temperatures were considerably lower when being heat pipe cooled as opposed to the case when the heat pipe was not in operation. This figure was obtained by setting the power level at 280 watts, the cooling water flow rate at 5.82 lbm/hr. and waiting for the system to stabilize. Once this was accomplished the vacuum pump was turned on and the valves connecting it to the heat pipe were opened and the working fluid removed from the heat pipe.

It can also be observed from the above mentioned figure that the window temperature increases faster when heptane rather than water is being removed from the heat pipe. This is due to the fact that heptane has a higher vapor pressure than water and consequently can be pumped out faster.

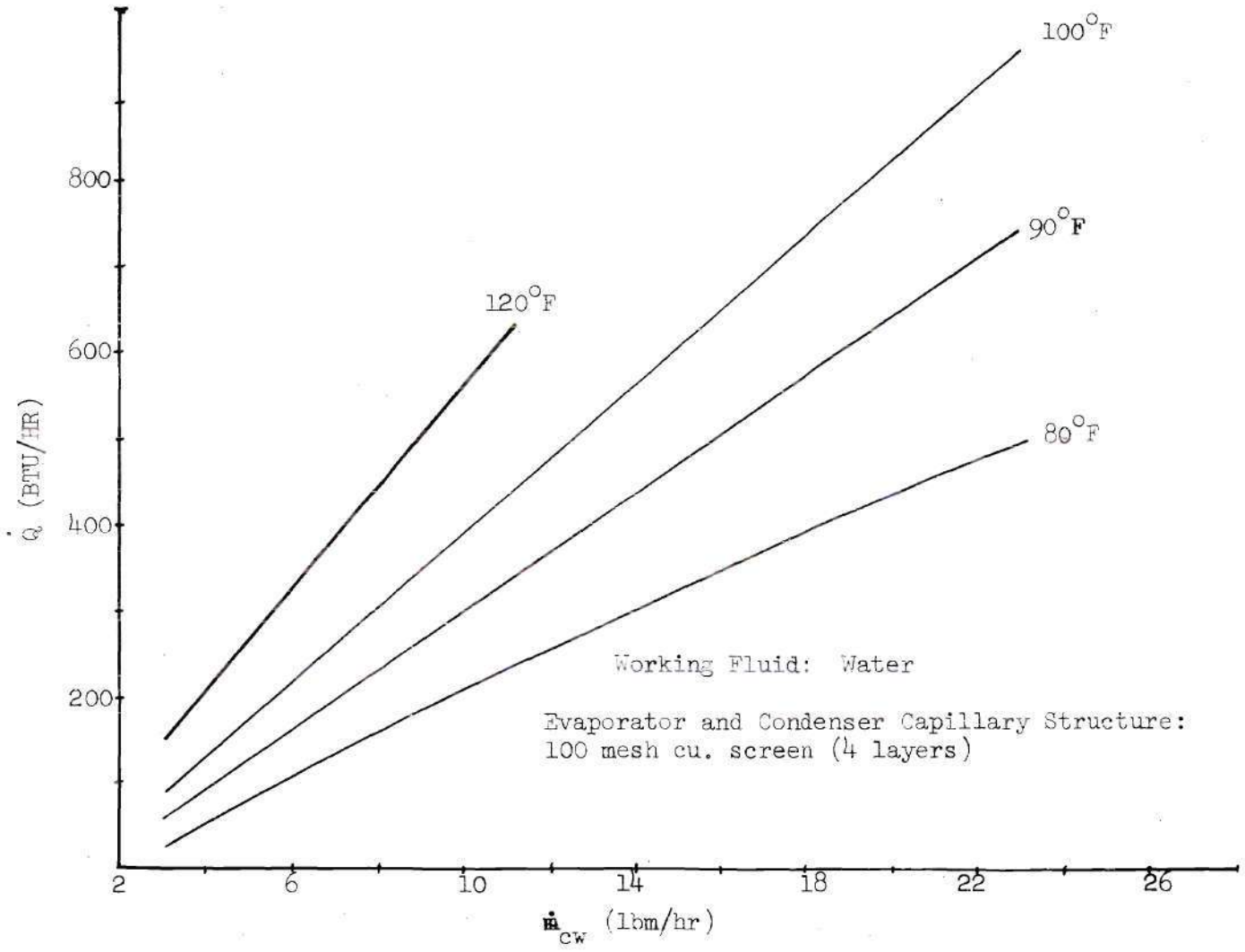

Figure 24. Heat Transfer Vs. Cooling Water Flow Rate for Various Vapor Temperatures

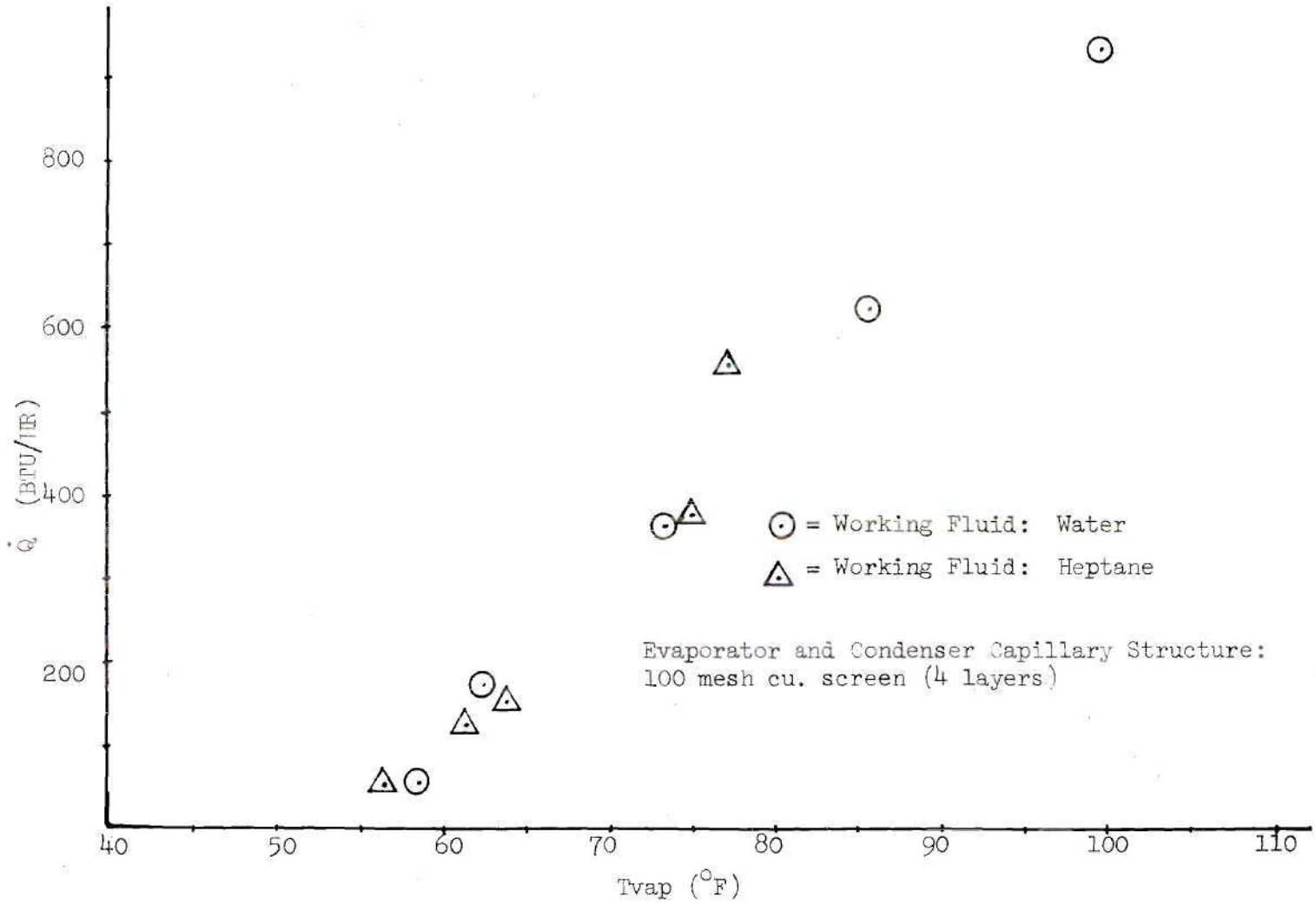

Figure 25. Heat Transfer Vs. Vapor Temperature for Water and Heptane Used as Working Fluids

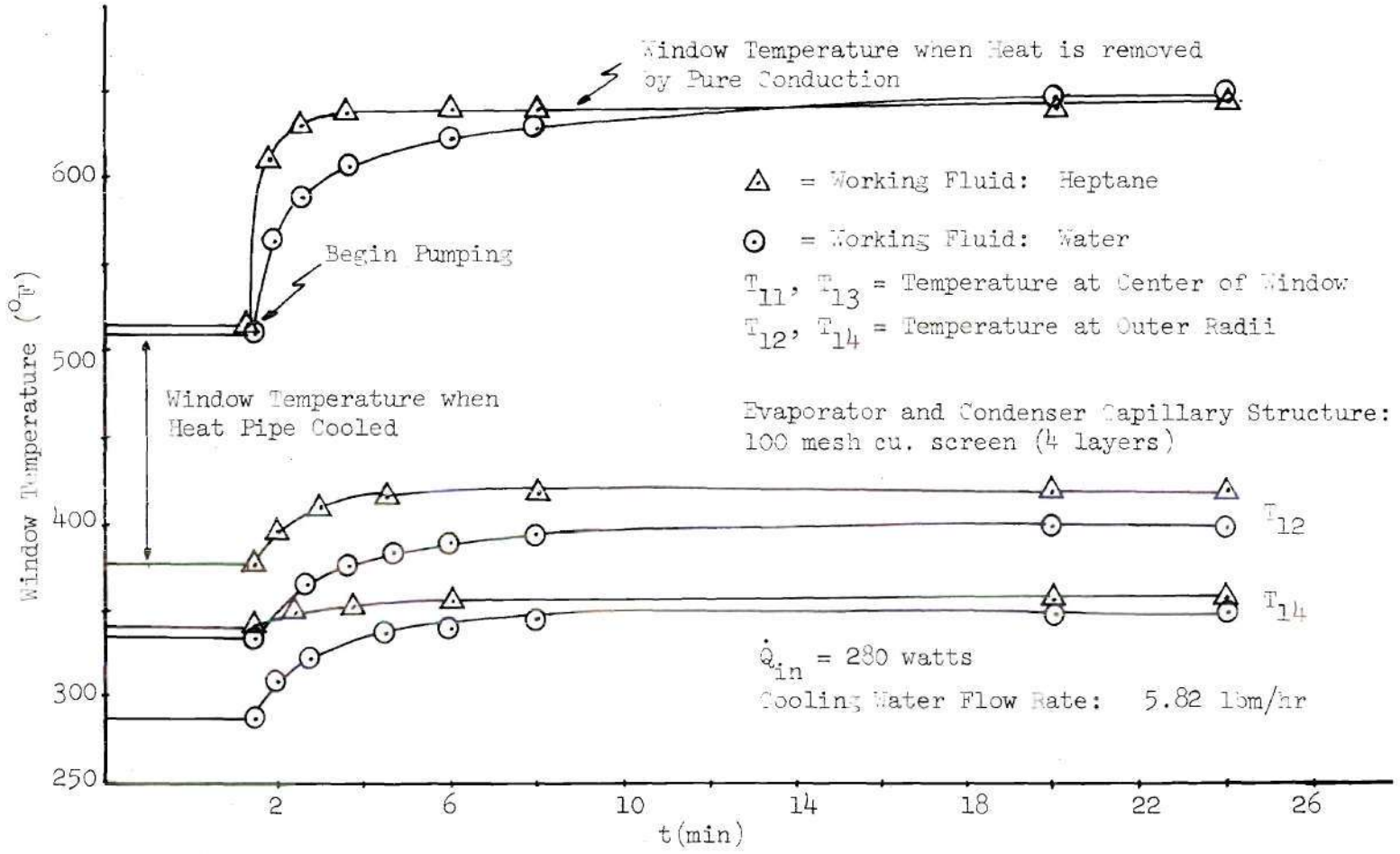

Figure 26. Window Temperature Vs. Time

Figure 27 allows a comparison between the theoretical and experimental performance of the heat pipe tested. It is obvious that theoretically large amounts of heat can be transferred for relatively small temperature gradients. Experimentally, this was not the case. For example, according to calculations, it is possible to transfer about 1000 BTU/HR. for a ΔT of $1^{\circ}F$, while from the experiment it is required a ΔT of about $500^{\circ}F$. The explanation for this is that any gap filled with water between the window and the evaporator capillary structure, as well as similar gaps between the various capillary layers will produce large temperature gradients. For instance, at 1000 BTU/HR., a gap of 1/16 in. between the window and the evaporator capillary structure, as well as between each of the evaporator layers, would produce about $500^{\circ}F$ temperature drop. These gaps actually existed in the experimental setup, and in the future, care must be taken to tightly pack the layers next to the windows. It should also be pointed out that in the theoretical calculations performed the window was assumed to have a uniform temperature, while this was not actually the case.

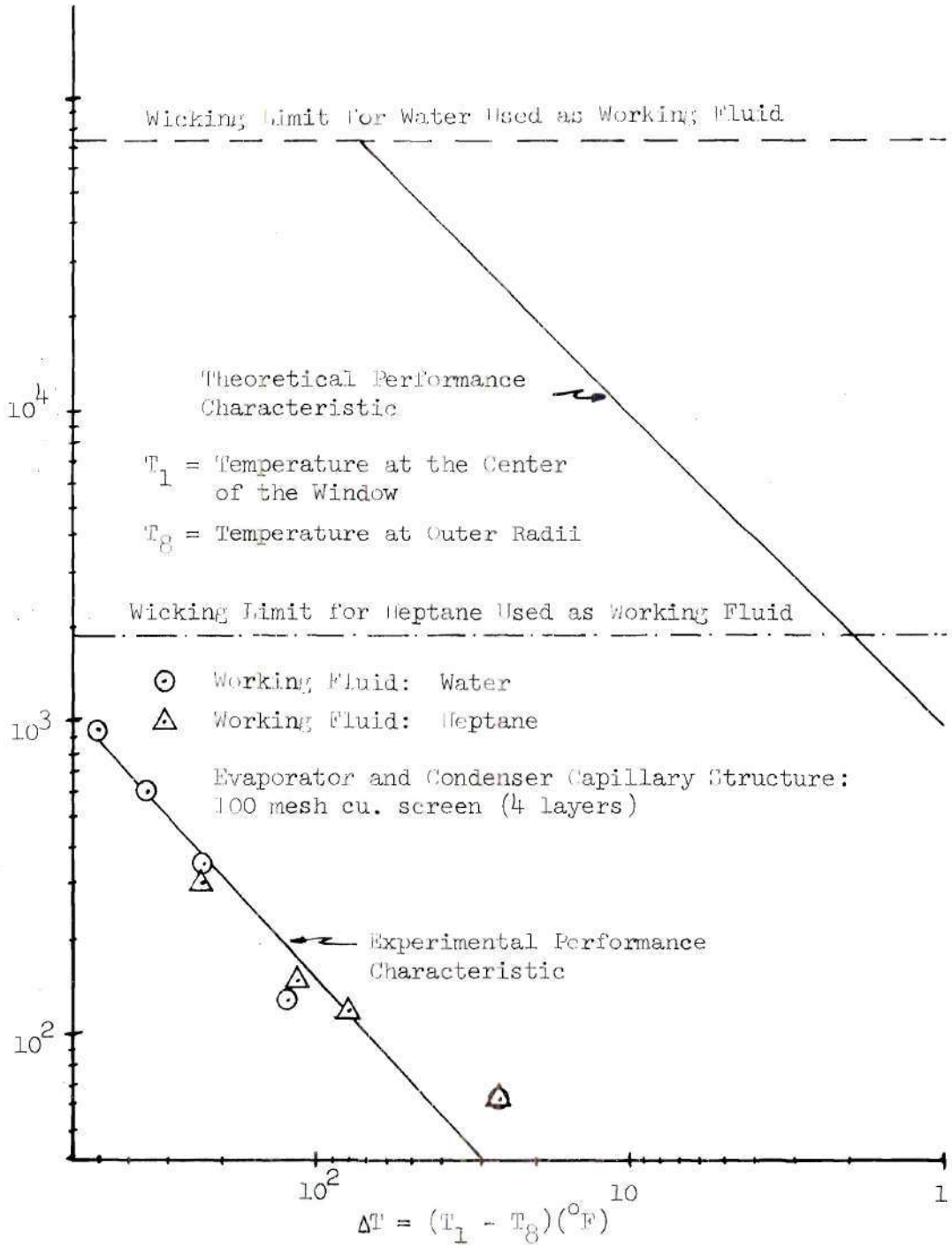

Figure 27. Comparison Between Theoretical and Experimental Performance of Test Heat Pipe

CHAPTER VII

CONCLUSIONS AND RECOMMENDATIONS

1. Conclusions

From the experimental program, as well as from the theoretical calculations performed, the following conclusions can be drawn.

1. The heat pipe cooled microwave window arrangement is feasible to conduct RF-generated heat to the walls of the waveguide.

2. Water is a better working fluid for the heat pipe than heptane, but it does not have good microwave characteristics.

3. Heptane is a suitable working fluid for the heat pipe, but modifications in the capillary structure will have to be made in order to increase the burnout limit, i.e., have open channels (annuli) between the wick layers along the waveguide.

2. Recommendations

The following recommendations are made in order to improve the actual testing facility, as well as to obtain a better understanding of the operating characteristics of the device.

1. A better way to seal the heat pipe is needed.

2. The evaporator capillary structure has to be modified in order to insure that no gaps exist neither between the window and the capillary structure, nor between the various layers of the wick.

3. The heat pipe condenser has to be redesigned in order to attain higher vapor temperature.

4. Additional thermocouples have to be installed, especially in the evaporator region, in order to better determine the temperature distribution in the windows.

APPENDIX A

ESTIMATION OF THE CHOKING LIMIT

The maximum axial rate of heat transfer under choking condition is given by equation (4.2) as:

$$\dot{Q}_s = \dot{m}_s \, h_{fg} \tag{A.1}$$

where

$$\dot{m}_s = \rho_v U_s \pi r_v^2 \tag{A.2}$$

and

$$U_s = \sqrt{k g_c R T} \tag{A.3}$$

Assuming an operating temperature of $80^{\circ}F$, and water as the working fluid, it follows that:

$k = 1.329$ $\qquad$ $\rho_v = 1.58 \times 10^{-3}$ lbm/ft^3

$g_c = 32.2$ lbm-ft/lbf-sec^2 $\qquad$ $r_v = 0.101$ ft

$R = 85.76$ ft-lbf/lbm$^{\circ}$R

$T = 540^{\circ}$R

Substitution of these values in equation (A.1) through (A.3) yields:

$$\dot{Q}_s = 2.69 \times 10^5 \ \frac{\text{BTU}}{\text{HR}}$$

Table 2 shows the choking limit at different temperatures for the heat pipe under consideration.

Table 2. Test Model Choking Limit at Different Temperatures

Temperature (°F)	Working Fluid	$Q_s \times 10^{-6}$ (BTU/HR)
70	Water	.193
	Heptane*	.124
100	Water	.489
	Heptane	.256
150	Water	1.79
	Heptane	.738
200	Water	5.21
	Heptane	1.56
250	Water	12.7
	Heptane	3.11
300	Water	27.2
	Heptane	5.99
350	Water	51.8
	Heptane	9.46
400	Water	90.9
	Heptane	15.65
450	Water	149.0
	Heptane	20.27
500	Water	229.0
	Heptane	20.99

* Physical properties for Heptane can be found in Reference 42.

From Table 2 it is obvious that the choking limit will not be reached with the present design.

APPENDIX B

ESTIMATION OF THE ENTRAINMENT LIMIT

The entrainment limit is given by equation (4.5) as:

$$\dot{Q} = A_v \left(\frac{\rho_v \sigma h_{fg}^2 g_c}{Z} \right) \qquad (B.1)$$

For an operating temperature of $80^{\circ}F$ and using water as the working fluid, it follows that,

$\rho_v = 1.5 \times 10^{-3}$ lbm/ft^3 $\qquad Z = 5.83 \times 10^{-4}$ ft.

$\sigma = 5 \times 10^{-3}$ lbf/ft. $\qquad A_v = \pi(.101)^2$ ft^2

$h_{fg} = 1048.6$ BTU/lbm

therefore

$$\dot{Q} = 7.94 \times 10^4 \frac{\text{BTU}}{\text{HR}}$$

Table 3 gives the entrainment limit for the heat pipe under study for various temperatures.

Comparing these values with those of the wicking limit (see Appendix D), it can be concluded that the entrainment limit will not be reached with the present design.

Table 3. Test Model Entrainment Limit at Different Temperatures

Temperature (^{o}F)	Working Fluid	$\dot{Q} \times 10^{-4}$ (BTU/HR)
70	Water	6.82
	Heptane	1.81
100	Water	10.4
	Heptane	2.42
150	Water	18.6
	Heptane	3.57
200	Water	29.3
	Heptane	4.44
250	Water	42.2
	Heptane	5.56
300	Water	56.6
	Heptane	6.68
350	Water	70.7
	Heptane	6.89
400	Water	83.7
	Heptane	7.23
450	Water	94.0
	Heptane	6.48
500	Water	97.1
	Heptane	4.26

APPENDIX C

ESTIMATION OF THE HEAT PIPE LIMITATION DUE TO BOILING IN THE EVAPORATOR

The heat flux limit at the onset of nucleate boiling in the evaporator is given by equation (4.6) as:

$$\dot{q}_b = \frac{K_{eff}}{\delta_B} \Delta Tcrit \qquad (C.1)$$

or

$$\dot{Q}_b = \dot{q}_b A_e = \frac{A_e K_{eff}}{\delta_B} \Delta Tcrit$$

where

$$\Delta Tcrit = \frac{2\sigma\, Tsat}{h_{fg}\, \rho_v\, r\, J} \qquad (C.2)$$

and A_e is the evaporator area.

For the 100 mesh capillary structure, water as the working fluid and a saturation temperature of 200°F, it follows that:

K_{eff} = 111.32 BTU/HR-ft-°F h_{fg} = 977.9 $\frac{BTU}{lbm}$

δ_B = 4(10.43 x 10^{-4} ft) = 4.172 x 10^{-4} ft ρ_v = 2.97 x 10^{-2} $\frac{lbm}{ft3}$

σ = 4.1 x 10^{-3} lbf/ft r = $B^r P$ = 2.24 x 10^{-4} ft

Tsat = 660°R A_e = 3.41 x 10^{-2} ft^2

and

$$\dot{q}_b = 2.85 \times 10^5 \text{ BTU/HR. ft}^2$$

Table 4 gives the values of the heat flux limit at the onset of nucleate boiling for the heat pipe under consideration at different temperatures.

Table 4. Test Model Heat Flux Limit at Different Temperatures

Temperature ($^{\circ}F$)	Working Fluid	$\dot{q}_b \times 10^{-4}$ (BTU/HR ft^2)
70	Water	1350
	Heptane	218
100	Water	556
	Heptane	105
150	Water	162
	Heptane	34.6
200	Water	57.0
	Heptane	15.6
250	Water	23.8
	Heptane	7.28
300	Water	11.2
	Heptane	3.51
350	Water	5.74
	Heptane	2.00
400	Water	3.08
	Heptane	.952
450	Water	1.74
	Heptane	.667
500	Water	.946
	Heptane	.562

APPENDIX D

DETERMINATION OF THE HEAT PIPE WICKING LIMIT

The wicking limit of the heat pipe under consideration is given by equation (4.17) as:

$$\dot{Q}_{max} = \frac{2\sigma h_{fg}}{\mu_{\ell} B r_P} \left[\frac{1}{\frac{.055\ B K_1}{\epsilon_B\ \delta_B} + \frac{\ell_{AA} K_1}{4\epsilon_A \delta_{Ab}}} \right] \qquad (D.1)$$

Tables 5 and 6 give the wicking limit of the heat pipe under consideration for various temperatures using water and heptane respectively as working fluids. The same information is plotted in Figure 28.

From these tables and from calculations in Appendices A, B, and C, it is obvious that the wicking limit is the most important limitation for the heat pipe under study.

Table 5. Test Model Wicking Limit at Different Temperatures Using Water as Working Fluid

Temperature ($^{\circ}F$)	$\dot{Q}_{max} \times 10^{-3}$ (BTU/HR)
70	26.94
100	37.16
150	51.10
200	64.10
250	72.00
300	74.78
350	73.84
400	67.34
450	58.06
500	46.44

Table 6. Test Model Wicking Limit at Different Temperatures Using Heptane as Working Fluid

Temperature (°F)	$\dot{Q}_{max}$ (BTU/HR)
50	1732.40
100	1881.00
150	1857.80
200	1746.40
250	1723.20
300	1588.40
350	1300.40
400	1040.40
450	766.40

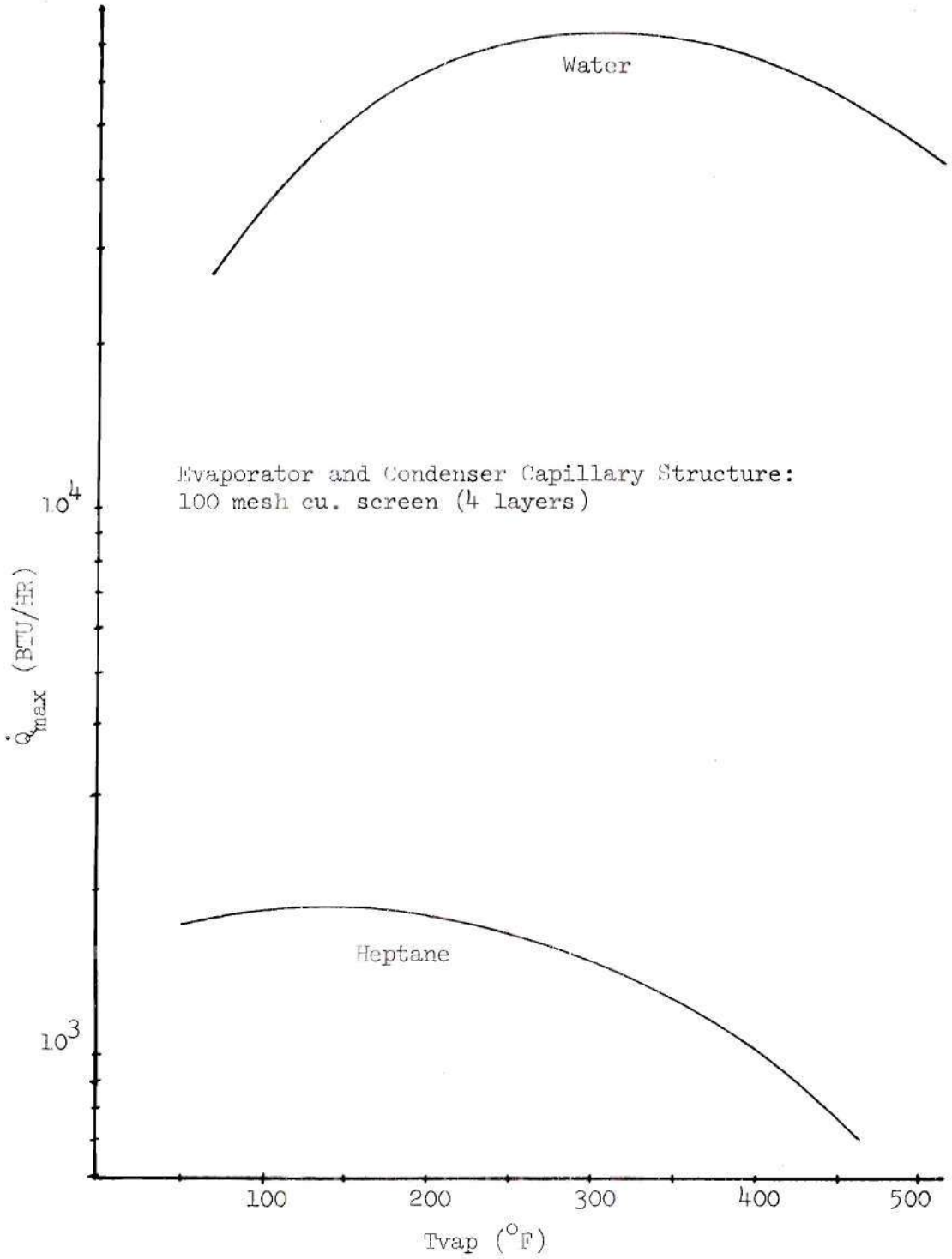

Figure 28. Wicking Limit Vs. Temperature for Test Model Using Water and Heptane as Working Fluid

APPENDIX E

ESTIMATION OF INTERFACIAL INERTIAL FORCES

The pressure change across an evaporative interface, including inertial forces, is given by (8) as:

$$P_v - P_\ell = \frac{2\sigma}{B^r P} - \frac{(\rho_v U_v)^2}{\rho_v}\left(1 - \frac{\rho_v}{\rho_\ell}\right) \qquad (E.1)$$

or

$$P_v - P_\ell = \frac{2\sigma}{B^r P}\left[1 - \frac{B^r P}{2\sigma}\frac{(\rho_v U_v)^2}{\rho_v}\left(1 - \frac{\rho_v}{\rho_\ell}\right)\right] \qquad (E.2)$$

From experimental data, it is found that for

$$\dot{Q}_{out} = 358.50 \text{ BTU/HR}, \quad T = 190^{\circ}F$$

therefore

$$\rho_v U_v = \frac{\dot{Q}_{out}}{2\pi r_v \ell_e h_{fg}} = \frac{358.50}{(2\pi)(.101)(.116)(948.1)}\left(\frac{1}{3600}\right)$$

$$\rho_v U_v = 1.43 \times 10^{-3} \text{ lbm/ft}^2\text{-sec}$$

and

$$\frac{B^r P}{2\sigma}\frac{(\rho_v U_v)^2}{\rho_v}\left(1 - \frac{\rho_v}{\rho_\ell}\right) = \frac{2.24 \times 10^{-4}(1.43 \times 10^{-3})^2}{2(4.2 \times 10^{-3})(2.7 \times 10^{-2})(32.2)}\left(1 - \frac{2.7 \times 10^{-2}}{61}\right)$$

$$= 6.27 \times 10^{-8}$$

Consequently, the magnitude of the inertial term is negligible compared with unity.

APPENDIX F

ESTIMATION OF THE VAPOR PRESSURE DROP

The magnitude of the vapor axial pressure drop is determined from equation (4.13) as indicated by Chisholm[39]:

$$\Delta P_{vv} = \frac{8\mu_v \dot{m} \ell_v}{\pi \rho_v r_v^4 g_c} \tag{F.1}$$

where

$$\dot{m} = \frac{\dot{Q}_{out}}{h_{fg}} \tag{F.2}$$

or

$$\frac{\Delta P_{vv}}{\ell_v} = \frac{8\mu_v \dot{Q}_{out}}{\pi \rho_v r_v^4 h_{fg} g_c} \tag{F.3}$$

From experimental data for $\dot{Q}_{out}$ = 358.50 BTU/HR, T = 190°F, therefore

$$\frac{\Delta P_{vv}}{\ell_v} = \frac{8(3.05 \times 10^{-1})(358.50)}{\pi(27 \times 10^{-2})(.101)^4(948.1)(32.2)(3600)^2(12)^3}$$

$$= 1.45 \times 10^{-7} \text{ psi/in}$$

the magnitude of ΔP_c is determined by equation (4.11) as:

$$\Delta P_c = \frac{2\sigma}{B^r P} = \frac{2(4.2 \times 10^{-3})}{2.24 \times 10^{-4}\ 144} = 2.60 \times 10^{-1} \text{ psi}$$

Comparing ΔP_c with $\Delta P_{vv}/\ell_v$ and considering the dimensions of the heat pipe it can be seen that the vapor pressure drop is negligible.

APPENDIX G

DETERMINATION OF THE PRESSURE DROP IN THE LIQUID PHASE

In order to determine the pressure drop in the liquid phase, it is necessary to first define an inverse permeability (or friction factor) as (35):

$$\Delta P = K_1 \frac{\mu_\ell}{\rho_\ell} \frac{\dot{m}_\ell \ell_{eff}}{A_N} \tag{G.1}$$

It should be noted that the inverse permeability K_1 is based on approach velocity and not pore velocity. An inverse permeability based on pore velocity is defined in the same way except that the porosity is included. Equation (G.1) can also be written as:

$$\Delta P = K_1 \mu_\ell \ell_{eff} U_a \tag{G.2}$$

If pore velocity is used, the pressure drop in the liquid face is given by

$$\Delta P = K_1' \mu_\ell \ell_{eff} U_P \tag{G.3}$$

from equations (G.2) and (G.3)

$$K_1 U_a = K_1' U_p \tag{G.4}$$

or

$$K_1 = K_1' \frac{U_p}{U_a} \tag{G.5}$$

But since by definition

$$U_p = \frac{U_a}{\epsilon} \tag{G.6}$$

The inverse permeabilities based on pore and approach velocities are related by:

$$K_l = \frac{K_l'}{\epsilon} \tag{G.7}$$

Since the evaporator and condenser have different geometries, as well as different capillary structure the pressure drop in the liquid region is determined separately for each section.

Consider first the liquid pressure drop in the evaporator. It is assumed that the liquid evaporates uniformly over the evaporator surface.

The liquid flow rate entering each evaporator surface is:

$$\frac{\dot{m}}{2} = \tfrac{1}{2}\ \Phi\ \pi\ r_b^{\,2} = \int_{r_m}^{r_b} \Phi\ 2\pi r\ dr \tag{G.8}$$

where

Φ = rate of evaporation per unit area

r_m = radius to mid-point of evaporator area

r = radius of evaporator at a particular location

therefore

$$\tfrac{1}{2}\ r_b^{\,2} = 2 \int_{r_m}^{r_b} r dr \tag{G.9}$$

Integration yields

$$r_m = \frac{r_b}{\sqrt{2}} = .707\ r_b \tag{G.10}$$

The effective length that an average element of fluid travels in the evaporator is

$$\ell_{\substack{\text{eff} \\ \text{Evap}}} = r_b - r_m = r_b - .707\ r_b = .293\ r_b \tag{G.11}$$

Substitution of this value in equation (G.1) gives the liquid pressure drop experienced by an average element of fluid in the evaporator section. As the fluid flows an elemental distance in the radial direction, the pressure loss is

$$dP = B^{K_1} \frac{\mu_\ell}{\rho_\ell} \frac{\dot{m}\ dr}{2\pi r \delta_B} \tag{G.12}$$

If it is assumed that liquid evaporates at the mean location

$$dP = B^{K_1} \frac{\mu_\ell}{\rho_\ell} \frac{\dot{m}}{2\pi r \delta_B} \int_{r_m}^{r_b} \frac{dr}{r} \tag{G.13}$$

which upon integration gives

$$\Delta P = B^{K_1} \frac{\mu_\ell}{\rho_\ell} \frac{\dot{m}}{2\pi\delta_B} \ln \frac{r_b}{r_m} \tag{G.14}$$

substitution of (G.10) into the above expression gives

$$\Delta P = 0.0552 \frac{B^{K_1}\ \mu_\ell\ \dot{m}}{\rho_\ell \delta_B} \tag{G.15}$$

The liquid pressure drop in the condenser can be determined in a similar fashion. If it is assumed that the heat transfer and fluid flow are symmetrical, the effective length of liquid flow in the condenser is one fourth of the total heat pipe length.

$$\ell_{\substack{\text{eff} \\ \text{Cond}}} = \frac{\ell_A}{4} \tag{G.16}$$

Consequently the liquid pressure drop in this section is given by:

$$\Delta P = A^{K_1} \frac{\mu_\ell}{\rho_\ell} \frac{\dot{m}\ \ell_A}{4\delta_A{}^b} \tag{G.17}$$

Combining the liquid pressure drop in the evaporator and condenser gives the total liquid viscous loss as:

$$\Delta P_{v\ell} = 0.0552 \frac{B^{K_1}\ \mu_\ell\ \dot{m}}{\rho_\ell \delta_B} + \frac{A^{K_1}\ \mu_\ell\ \dot{m}\ \ell_A}{4\rho_\ell \delta_A{}^b} \tag{G.18}$$

or

$$\Delta P_{v\ell} = \frac{\mu_\ell\ \dot{m}}{\rho_\ell} \left[\frac{0.0552\ B^{K_1}}{\delta_B} \frac{A^{K_1}\ \ell_A}{4\delta_A{}^b} \right] \tag{G.19}$$

APPENDIX H

CALCULATION OF INVERSE PERMEABILITIES

According to Marcus[7], the permeability of screen wicks can be calculated by

$$K_1 = \frac{d^2 \varepsilon^3}{122 (1 - \varepsilon)^2} \qquad (H.1)$$

where d is the wire diameter and the screen porosity ε, is given by

$$\varepsilon = 1 - \frac{\pi F M d}{4} \qquad (H.2)$$

Where F is the crimping factor, usually equal to 1.05, and M is the numbers of wires per inch of the capillary structure.

Figure 29 shows a comparison between data collected from several researchers by Marcus[7] and equation (H.1). It should be noted that Marcus used pore velocities in his investigation instead of approach velocities as is the case in the present investigation. Therefore equation (G.7) is used to relate the permeabilities based on these two types of velocities.

A sample calculation for the evaluation of the inverse permeability, K_1, of a 100 mesh screen is now illustrated.

From Figure 29, the permeability K, for the 100 mesh screen is found to be approximately 4.5×10^{-9} ft^2 and the inverse permeability based on pore velocity is then

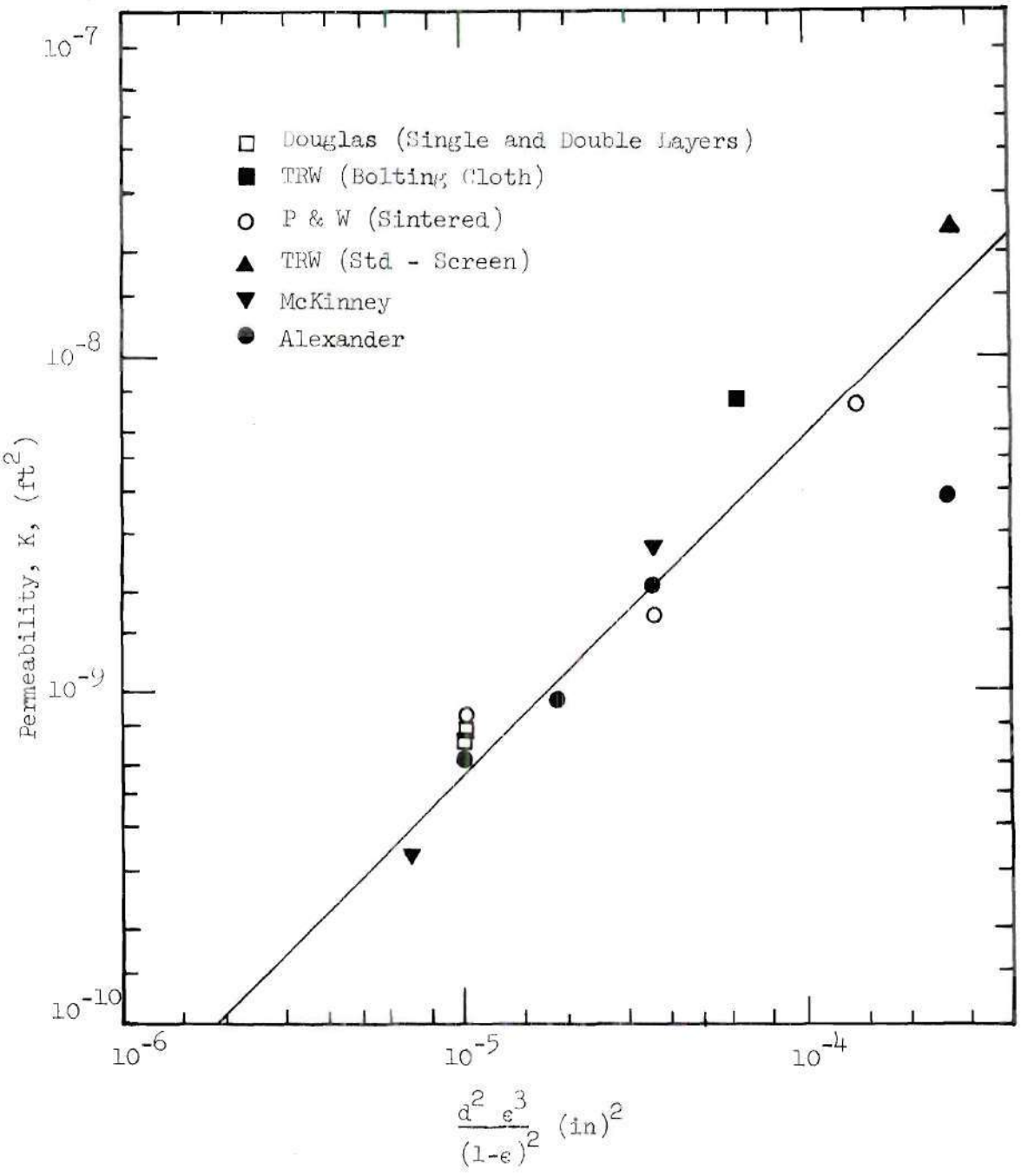

Figure 29. Permeability of Screen Wicks[20]

$$K_1' = \frac{1}{K} = 2.22 \times 10^8 \ 1/ft^2$$

Therefore, the inverse permeability based on approach velocity is then

$$K_1 = \frac{K_1'}{\epsilon} = \frac{2.22 \times 10^8}{0.632} = 3.52 \times 10^8 \ 1/ft^2$$

where the value of the porosity, ϵ, is obtained from published data such as (21). (See also Appendix I).

It is also interesting to investigate the inverse permeability associated with flow in an annulus bounded by solid material (or screen) on both radii, in order to establish a lower limit on inverse permeability and to determine the effects of using annular channels between layers of screen or other porous materials.

In order to determine the inverse permeability, K_1, for an annulus consider the model shown in Figure 30.

Assuming that the flow is laminar, steady, incompressible and fully developed, a force balance or the fluid elements yields:

$$\Delta P(2\pi \ r_c \ dy) = d\tau(2\pi \ r_c) \ dz \qquad (H.3)$$

where $d\tau$ is the difference in shear stress on the two faces on the element. From (H.3) it follows that

$$\frac{\Delta P}{\Delta z} = \frac{d\tau}{dy} \qquad (H.4)$$

since

$$\tau = \mu \frac{dV_z}{dy} \qquad (H.5)$$

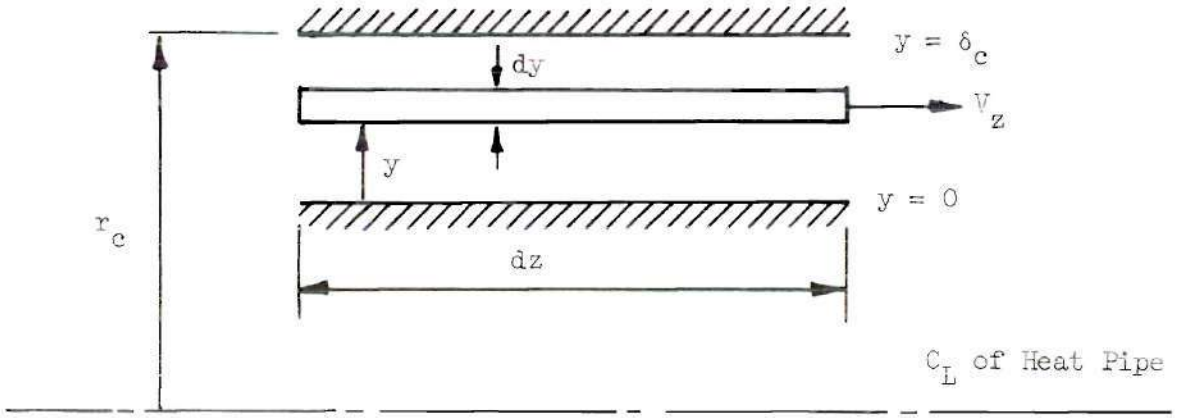

Figure 30. Liquid Annulus Model

substitution on (H.4) gives:

$$\frac{\Delta P}{\Delta z} = \mu \frac{d^2 V_z}{dy^2} \tag{H.6}$$

Integrating twice, and using the following boundary conditions

$$V_z = 0 \text{ @ } y = 0 \text{ and at } y = \delta_c$$

$$V_z = \frac{\delta_c^2}{2\mu} \frac{\Delta P}{\Delta z} \left[\left(\frac{y}{\delta_c} \right)^2 - \left(\frac{y}{\delta_c} \right) \right] \tag{H.7}$$

The mass flow rate in the channels can be evaluated from:

$$\dot{m} = 2\pi r_c \rho \int_{y=0}^{\delta_c} V_z \, dy \tag{H.8}$$

and it is found to be

$$\dot{m} = \frac{\rho \delta_c^3}{12\mu} \frac{\Delta P}{\Delta z} (2\pi r_c) \tag{H.9}$$

From the definition of inverse permeability, K_1, it is known that

$$\frac{\Delta P}{\Delta z} = K_1 \frac{\mu_\ell}{\rho_\ell} \frac{\dot{m}}{A_A \epsilon} \tag{H.10}$$

where $\epsilon = 1$ and $A_A = 2\pi r_c \delta_c$.

Combining equations (H.9) and (H.10) gives

$$K_1 \frac{\mu_\ell}{\rho_\ell} \frac{\dot{m}}{2\pi r_c \delta_c} = \frac{12 \mu_\ell \dot{m}}{\rho \delta_c^3 (2\pi r_c)} \tag{H.11}$$

or

$$K_{\perp} = \frac{12}{\delta_c^2} \qquad \text{(H.12)}$$

Table 7 summarizes the value of inverse permeabilities for several capillary structures, as well as for .005 in annulus.

Table 7. Inverse Permeability for Several Capillary Structures

Capillary Structure	K $(1/ft.^2)$
100 mesh screen	3.52×10^8
200 mesh screen	5.23×10^8
400 mesh screen	4.01×10^9
Fiber Glass Cloth	2.48×10^9
0.005 in. Annulus	6.67×10^7

APPENDIX I

CAPILLARY STRUCTURE DATA

The following Table summarizes some wick data useful for heat pipe calculations.

Table 8. Capillary Structure Data (21), (44)

Capillary Structure	$D_p \times 10^4$ (ft)	$D_w \times 10^4$ (ft)	$\delta \times 10^4$ (ft)	ϵ
100 mesh copper screen	4.47	5.83	10.43	.632
200 mesh copper screen	2.89	2.42	4.43	.736
400 mesh copper screen	1.25	1.02	2.44	.712
Fiberglass cloth	3.33	1.67	4.17	.50

where D_p : Pore diameter

D_w : Wire diameter

δ : Thickness

ϵ : Porosity

APPENDIX J

EVALUATION OF THE EFFECTIVE THERMAL CONDUCTIVITY OF THE WICK-LIQUID MATRIX

The effective thermal conductivity of the wick-liquid matrix is given by equation (4.23). A sample calculation follows.

Consider the capillary structure to be made up of 100 mesh copper screen and the working fluid to be water at 200°F.

For the above combination it is known that

$$B^r P = 2.24 \times 10^{-4} \text{ ft}$$

$$B^r ws = 2.92 \times 10^{-4} \text{ ft}$$

$$K_\ell = .394 \text{ BTU/HR ft } ^\circ\text{F}$$

Substitution of these values into equation (4.23) yields

$$\frac{K_E}{K_\ell} = \frac{1}{\left(\frac{2.24}{2.92} + 1\right)\left[\frac{2(.394)}{228.39} + \left(\frac{2.24}{2.92} - 1\right)\right]}$$

$$+ \frac{2}{\left(\frac{2.24}{2.92} + 1\right)\left[\frac{.394}{228.39}\left(\frac{2.92}{2.24} + 1\right)\right]} + \frac{1}{\left(\frac{2.92}{2.24} + 1\right)^2}$$

or

$$K_E = 111.35 \frac{\text{BTU}}{\text{HR Ft } ^\circ\text{F}}$$

Table 9 gives values of the effective thermal conductivity of the wick-liquid matrix for various combinations of capillary structure

and working fluid.

Table 9. Effective Thermal Conductivity for Several Combinations of Capillary Structure and Working Fluid

Capillary Structure	Working Fluid	Temperature (°F)	K (BTU/HR ft °F)
100 mesh copper screen	Water	70	111.39
		100	111.35
		200	111.28
		300	111.28
		400	111.31
		500	111.38
	Heptane	70	112.00
		100	112.00
		200	112.01
		300	112.01
		400	112.02
		500	112.02
200 mesh copper screen	Water	70	114.13
		100	114.20
		200	114.27
		300	114.27
		400	114.24
		500	114.16
	Heptane	70	113.47
		100	113.47
		200	113.46
		300	113.46
		400	113.45
		500	113.44

Table 9. (Continued)

Capillary Structure	Working Fluid	Temperature (°F)	K (BTU/HR ft °F)
400 mesh copper screen	Water	70	113.81
		100	113.85
		200	113.92
		300	113.92
		400	113.89
		500	113.81
	Heptane	70	113.20
		100	113.20
		200	113.20
		300	113.19
		400	113.19
		500	113.18
Fiberglass Cloth	Water	70	.425
		100	.433
		200	.448
		300	.449
		400	.442
		500	.426
	Heptane	70	.399
		100	.398
		200	.396
		300	.394
		400	.393
		500	.391

APPENDIX K

EVALUATION OF THERMAL RESISTANCES

In this appendix, sample calculations of the different thermal resistances of the device are presented. Several tables are given which give the value of these thermal resistances for various conditions.

In the following sample calculations, it was assumed that the window was made of aluminum oxide and the capillary structure in the evaporator consisted of one layer of fiberglass cloth, while the capillary structure along the waveguide was made of 100 mesh copper screen. The working fluid was assumed to be water and the operating temperature 100°F.

Window Resistance (R_{12})

Consider an aluminum oxide window .1178 thick. From equation (4.21) it is known that

$$R_{12} = \frac{t_w}{\pi K_w r_b^2}$$

therefore:

$$R_{12} = \frac{0.0098}{\pi(12.1)(.1042)^2}$$

$$R_{12} = 2.38 \times 10^{-2} \frac{Hr\text{-}^{\circ}F}{BTU}$$

Table 10 lists the values of R_{12} for several window materials.

Table 10. Window Thermal Resistance (R_{12})

Window Material	Thickness (in)	R x 10^3 (Hr-^{o}F/BTU)
Aluminum Oxide	.1178	28.3
Beryllia	.0635	1.28
Aluminum	.1178	2.18

Wick-Liquid Resistance in Evaporator (R_{23})

The effective thermal conductivity of the fiberglass water combination varies very little in the range of possible operating temperatures of the device (see Appendix J). An average value of the effective thermal conductivity was therefore used in evaluating the wick-liquid resistance in the evaporator. From equation (4.22)

$$R_{23} = \frac{\delta_B}{K_E \pi r_b^2}$$

therefore

$$R_{23} = \frac{10.43 \times 10^{-4}}{(.441)\pi(.1042)^2}$$

$$R_{23} = 2.77 \times 10^{-2} \frac{Hr\text{-}^{\circ}F}{BTU}$$

Values of R_{23} are listed in Table 11.

Interfacial Resistance in Evaporator (R_{34})

The interfacial resistance in the evaporator is given by equation (4.24). Therefore, for the model being considered:

$$R_{34} = \frac{(2\pi)^{\frac{1}{2}} (85.76)^{3/2}(560)^{5/2}}{(2\pi)(4.17 \times 10^{8})(778)(1037.2)^2(136.68)(1.0 \times 10^{-1})^2}$$

$$R_{34} = 10.07 \times 10^{-5} \frac{Hr\text{-}^{\circ}F}{BTU}$$

Tables 12a, 12b, and 12c list the values of R_{34} for several types of capillary structures and working fluids.

Table 11. Wick-Liquid Resistance in the Evaporator (R_{23})

Capillary Structure	Number of Layers	Working Fluid	$R_{23} \times 10^4$ (Hr-°F/BTU)
100 mesh copper screen	1	Water	2.75
	2	Water	5.49
	3	Water	8.24
	4	Water	11.00
	1	Heptane	2.73
	2	Heptane	5.46
	3	Heptane	8.19
	4	Heptane	10.90
Fiberglass Cloth	1	Water	277
	2	Water	554
	3	Water	832
	4	Water	1110
	1	Heptane	529
	2	Heptane	1060
	3	Heptane	1590
	4	Heptane	2120

Table 12a. Interfacial Resistance in Evaporator (R_{34}) (Condenser Capillary Structure: 100 Mesh Copper Screen)

Number of Layers	Working Fluid	Temperature (°F)	$R_{34} \times 10^5$ (Hr-°F/BTU)
1	Water	70	20.87
2			21.29
3			21.71
4			22.19
1	Heptane	70	35.00
2			35.68
3			36.39
4			37.20
1	Water	100	9.47
2			9.66
3			9.85
4			10.07
1	Heptane	100	19.41
2			19.79
3			20.19
4			20.63
1	Water	200	1.32
2			1.35
3			1.38
4			1.41
1	Heptane	200	5.22
2			5.32
3			5.43
4			5.55
1	Water	300	.374
2			.381
3			.389
4			.397

Table 12a. (Continued)

Number of Layers	Working Fluid	Temperature (°F)	$R_{34} \times 10^5$ (Hr-°F/BTU)
1	Heptane	300	2.21
2			2.25
3			2.30
4			2.35
1	Water	400	.168
2			.171
3			.174
4			.178
1	Heptane	400	1.52
2			1.55
3			1.58
4			1.62
1	Water	500	.107
2			.109
3			.112
4			.114
1	Heptane	500	5.28
2			5.38
3			5.49
4			5.61

Table 12b. Interfacial Resistance in Evaporator (R_{34}) (Condenser Capillary Structure: 200 Mesh Copper Screen)

Number of Layers	Working Fluid	Temperature (°F)	$R_{34} \times 10^5$ (Hr-°F/BTU)
1	Water	70	20.59
2			20.79
3			20.96
4			21.16
1	Heptane	70	34.52
2			34.86
3			35.13
4			35.48
1	Water	100	9.34
2			9.43
3			9.51
4			9.60
1	Heptane	100	19.15
2			19.34
3			19.49
4			19.68
1	Water	200	1.31
2			1.32
3			1.33
4			1.34
1	Heptane	200	5.15
2			5.20
3			5.24
4			5.29
1	Water	300	.369
2			.372
3			.375
4			.379

Table 12b. (Continued)

Number of Layers	Working Fluid	Temperature (°F)	$R_{34} \times 10^5$ (Hr-°F/BTU)
1	Heptane	300	2.18
2			2.20
3			2.22
4			2.24
1	Water	400	.165
2			.167
3			.168
4			.170
1	Heptane	400	1.50
2			1.51
3			1.52
4			1.54
1	Water	500	.106
2			.107
3			.108
4			.109
1	Heptane	500	5.21
2			5.26
3			5.30
4			5.35

Table 12c. Interfacial Resistance in Evaporation (R_{34}) (Condenser Capillary Structure: 400 Mesh Copper Screen)

Number of Layers	Working Fluid	Temperature (^{o}F)	$R_{34} \times 10^{5}$ ($Hr-^{o}F/BTU$)
1	Water	70	20.51
2			20.63
3			20.71
4			20.83
1	Heptane	70	34.39
2			34.59
3			34.73
4			34.93
1	Water	100	9.60
2			9.31
3			9.36
4			9.40
1	Heptane	100	19.08
2			19.19
3			19.26
4			19.37
1	Water	200	1.30
2			1.31
3			1.31
4			1.32
1	Heptane	200	5.13
2			5.16
3			5.18
4			5.21
1	Water	300	.367
2			.369
3			.371
4			.373

Table 12c. (Continued)

Number of Layers	Working Fluid	Temperature (°F)	$R_{34} \times 10^5$ (Hr-°F/BTU)
1	Heptane	300	2.17
2			2.18
3			2.19
4			2.20
1	Water	400	.165
2			.166
3			.166
4			.167
1	Heptane	400	1.49
2			1.50
3			1.51
4			1.52
1	Water	500	.105
2			.106
3			.106
4			.107
1	Heptane	500	5.19
2			5.22
3			5.24
4			5.27

Thermal Resistance in Vapor (R_{45})

The vapor thermal resistance is found to be from equation (4.29)

$$R_{45} = \frac{8(3.052 \times 10^{-2})(560)(2.6 \times 10^{-2})(876.9 - 0.01606)}{\pi(4.17 \times 10^{8})(778)(1.140 \times 10^{-3})(1037.2)^2(1.0 \times 10^{-1})^4}$$

$$R_{45} = 1.256 \times 10^{-9} \frac{\text{Hr-}^{\circ}\text{F}}{\text{BTU}}$$

Typical values of R_{45} for the cases considered in this investigation appear in Tables 13a, 13b, and 13c.

Interfacial Resistance at Condenser (R_{56})

Applying equation (4.30) to the case being considered, the interfacial resistance in the condenser is found to be:

$$R_{56} = \frac{2(2\pi)^{\frac{1}{2}}(85.76)^{3/2}(560)^{5/2}}{4\pi(.6)(4.17 \times 10^{8})^{\frac{1}{2}}(778)(136.68)(1037.2)^2(1.0 \times 10^{-1})}$$

$$R_{56} = 1.678 \times 10^{-5} \frac{\text{Hr-}^{\circ}\text{F}}{\text{BTU}}$$

Tables 14a, 14b, and 14c give typical values of R_{56} for the different heat pipe configurations considered in the present investigation.

Wick-Liquid Resistance in Condenser (R_{67})

The thermal resistance of the wick-liquid combination at the condenser is from equation (4.31)

$$R_{67} = \frac{\ell n \quad \frac{.1042}{.100}}{\pi(111.32)(.6)}$$

Table 13a. Thermal Resistance in Vapor (R_{45}) (Condenser Capillary Structure: 100 Mesh Copper Screen)

Number of Layers	Working Fluid	Temperature (°F)	$R_{45} \times 10^{11}$ (Hr-°F/BTU)
1	Water	70	1904
2			1979
3			2059
4			2151
1	Heptane	70	411.5
2			427.9
3			445.1
4			465.0
1	Water	100	352.3
2			366.3
3			381.0
4			398.1
1	Heptane	100	111.1
2			115.6
3			120.2
4			125.6
1	Water	200	5.131
2			5.335
3			5.549
4			5.797
1	Heptane	200	4.756
2			4.946
3			5.144
4			5.374
1	Water	300	.304
2			.316
3			.329
4			.344

Table 13a. (Continued)

Number of Layers	Working Fluid	Temperature (°F)	$R_{45} \times 10^{11}$ (Hr-°F/BTU)
1	Heptane	300	.490
2			.509
3			.530
4			.534
1	Water	400	.0422
2			.0439
3			.0457
4			.0477
1	Heptane	400	.103
2			.107
3			.112
4			.116
1	Water	500	.0106
2			.0110
3			.0115
4			.0120
1	Heptane	500	.131
2			.136
3			.142
4			.148

Table 13b. Thermal Resistance in Vapor (R_{45})
(Condenser Capillary Structure:
200 Mesh Copper Screen)

Number of Layers	Working Fluid	Temperature (^{o}F)	$R_{45} \times 10^{11}$ (Hr.-^{o}F/BTU)
1	Water	70	1853
2			1889
3			1919
4			1956
1	Heptane	70	400.6
2			408.4
3			414.8
4			422.9
1	Water	100	342.9
2			349.6
3			355.1
4			362.0
1	Heptane	100	108.2
2			110.3
3			112.0
4			114.2
1	Water	200	4.994
2			5.091
3			5.171
4			5.273
1	Heptane	200	4.629
2			4.720
3			4.793
4			4.888
1	Water	300	.304
2			.316
3			.329
4			.344

Table 13b. (Continued)

Number of Layers	Working Fluid	Temperature (^{o}F)	$R_{45} \times 10^{11}$ ($Hr-^{o}F/BTU$)
1	Heptane	300	.477
2			.486
3			.494
4			.503
1	Water	400	.0411
2			.0419
3			.0426
4			.0434
1	Heptane	400	.100
2			.102
3			.104
4			.106
1	Water	500	.0106
2			.0110
3			.0115
4			.0120
1	Heptane	500	.128
2			.130
3			.132
4			.135

Table 13c. Thermal Resistance in Vapor (R_{45})
(Condenser Capillary Structure:
400 Mesh Copper Screen)

Number of Layers	Working Fluid	Temperature (°F)	$R_{45} \times 10^{11}$ (Hr - °F/BTU)
1	Water	70	1839
2			1860
3			1874
4			1896
1	Heptane	70	397.5
2			402.1
3			405.2
4			409.9
1	Water	100	340.3
2			344.2
3			346.9
4			350.9
1	Heptane	100	107.3
2			108.6
3			109.4
4			110.7
1	Water	200	4.956
2			5.013
3			5.052
4			5.111
1	Heptane	200	4.594
2			4.647
3			4.683
4			4.738
1	Water	300	.294
2			.297
3			.300
4			.303

Table 13c. (Continued)

Number of Layers	Working Fluid	Temperature (°F)	$R_{45} \times 10^{11}$ (Hr - °F/BTU)
1	Heptane	300	.473
2			.479
3			.482
4			.488
1	Water	400	.0408
2			.0413
3			.0416
4			.0421
1	Heptane	400	.095
2			.101
3			.102
4			.103
1	Water	500	.0102
2			.0103
3			.0104
4			.0106
1	Heptane	500	.127
2			.128
3			.129
4			.131

Table 14a. Interfacial Resistance at Condenser (R_{56}) (Condenser Capillary Structure: 100 Mesh Copper Screen)

Number of Layers	Working Fluid	Temperature (°F)	$R_{56} \times 10^7$ (Hr-°F/BTU)
1	Water	70	358.8
2			362.4
3			365.9
4			370.0
1	Heptane	70	601.3
2			607.2
3			613.2
4			620.0
1	Water	100	162.7
2			164.3
3			165.9
4			167.8
1	Heptane	100	333.5
2			336.8
3			340.1
4			343.9
1	Water	200	22.73
2			22.96
3			23.18
4			23.44
1	Heptane	200	89.69
2			90.57
3			91.47
4			92.47
1	Water	300	6.422
2			6.485
3			6.549
4			6.621

Table 14a. (Continued)

Number of Layers	Working Fluid	Temperature (°F)	$R_{56} \times 10^7$ (Hr - °F/BTU)
1	Heptane	300	37.93
2			38.30
3			38.68
4			39.11
1	Water	400	2.878
2			2.906
3			2.935
4			2.967
1	Heptane	400	26.11
2			26.37
3			26.63
4			26.92
1	Water	500	1.842
2			1.861
3			1.879
4			1.900
1	Heptane	500	90.74
2			91.63
3			92.54
4			93.56

Table 14b. Interfacial Resistance at Condenser (R_{56}) (Condenser Capillary Structure: 200 Mesh Copper Screen)

Number of Layers	Working Fluid	Temperature (°F)	$R_{56} \times 10^7$ (Hr - °F/BTU)
1	Water	70	356.4
2			358.1
3			359.1
4			361.3
1	Heptane	70	597.3
2			600.2
3			602.5
4			605.4
1	Water	100	161.6
2			162.4
3			163.0
4			163.8
1	Heptane	100	331.3
2			332.9
3			334.2
4			335.8
1	Water	200	22.58
2			22.69
3			22.78
4			22.89
1	Heptane	200	89.09
2			89.52
3			89.87
4			90.31
1	Water	300	6.379
2			6.410
3			6.435
4			6.466

Table 14b. (Continued)

Number of Layers	Working Fluid	Temperature (^{o}F)	$R_{56^{o}}$ x 10^{7} (Hr-^{o}F/BTU)
1	Heptane	300	37.68
2			37.86
3			38.01
4			38.19
1	Water	400	2.859
2			2.873
3			2.884
4			2.898
1	Heptane	400	25.93
2			26.06
3			26.16
4			26.29
1	Water	500	1.830
2			1.839
3			1.846
4			1.855
1	Heptane	500	90.13
2			90.50
3			90.92
4			91.36

Table 14c. Interfacial Resistance at Evaporator (R_{56}) (Condenser Capillary Structure: 400 Mesh Copper Screen)

Number of Layers	Working Fluid	Temperature (^{o}F)	R_{56} (Hr-^{o}F/BTU)
1	Water	70	355.7
2			356.8
3			357.5
4			358.5
1	Heptane	70	596.1
2			597.9
3			599.0
4			600.8
1	Water	100	161.3
2			161.8
3			162.1
4			162.6
1	Heptane	100	330.7
2			331.6
3			332.3
4			333.2
1	Water	200	22.54
2			22.60
3			22.64
4			22.71
1	Heptane	200	88.92
2			89.17
3			89.35
4			89.61
1	Water	300	6.367
2			6.385
3			6.397
4			6.416

Table 14c. (Continued)

Number of Layers	Working Fluid	Temperature (^{o}F)	R_{56} ($Hr-^{o}F/BTU$)
1	Heptane	300	37.60
2			37.71
3			37.79
4			37.90
1	Water	400	2.853
2			2.861
3			2.867
4			2.875
1	Heptane	400	25.88
2			25.96
3			26.01
4			26.08
1	Water	500	1.827
2			1.832
3			1.835
4			1.841
1	Heptane	500	89.96
2			90.22
3			90.39
4			90.66

$$R_{67} = 1.961 \times 10^{-4} \frac{Hr-^{\circ}F}{BTU}$$

Table 15 summarizes the values of R_{67} for several combinations of capillary structures and working fluids.

Waveguide Thermal Resistance (R_{78})

The waveguide thermal resistance is found to be from equation (4.33)

$$R_{78} = \frac{\ln \frac{.1094}{.1042}}{\pi(228.39)(.6)}$$

$$R_{78} = 1.131 \times 10^{-4} \frac{Hr-^{\circ}F}{BTU}$$

Table 15. Wick-Liquid Thermal Resistance in Condenser (R_{67})

Capillary Structure	Number of Layers	Working Fluid	$R_{67} \times 10^6$ (Hr-°F/BTU)
100 mesh copper screen	1	Water	50.58
	2	Water	97.03
	3	Water	143.9
	4	Water	196.1
	1	Heptane	50.27
	2	Heptane	96.43
	3	Heptane	143.0
	4	Heptane	194.9
200 mesh copper screen	1	Water	17.86
	2	Water	40.29
	3	Water	58.31
	4	Water	80.93
	1	Heptane	17.98
	2	Heptane	40.56
	3	Heptane	58.70
	4	Heptane	81.48

Table 15. (Continued)

Capillary Structure	Number of Layers	Working Fluid	$R_{67} \times 10^6$ (Hr.-°F/BTU)
400 mesh copper screen	1	Water	8.950
	2	Water	22.41
	3	Water	31.40
	4	Water	44.92
	1	Heptane	9.005
	2	Heptane	22.54
	3	Heptane	31.59
	4	Heptane	45.20

APPENDIX L

EXPERIMENTAL DATA

The experimental data is presented in two tables. Table 16 lists the temperature distribution in the test heat pipe and Table 17 presents the heat pipe operating data. The following nomenclature is used in Table 17.

$\dot{Q}_{in}$ = Power delivered to the heat pipe

V_{wf} = Working fluid volume

T_{cw} = Inlet cooling water temperature

ΔT_{cw} = Cooling water temperature increase from inlet to outlet of the cooling water jacket.

P_i = Pressure inside the heat pipe at the beginning of test

P_f = Pressure inside the heat pipe at the end of the test

$\dot{m}_{cw}$ = Cooling water mass flow rate

It should also be noted that water was used as working fluid in tests 1 through 49, while heptane was used in the remaining tests.

Table 16. Test Heat Pipe Temperature Distribution (°F)

Test Number	Thermocouple Number 1	2	3	4	5	6	7	8
1	80	80	80	80	80	80	80	80
2	92.7	92.7	92.7	92.7	92.7	92.7	92.7	92.7
3	107	107	107	107	107	107	107	107
4	127.7	127.7	127.7	127.7	127.7	127.7	127.7	127.7
5	148	148	148	148	148	148	148	148
6	178	178	178	178	178	178	178	178
7	76.7	76.7	76.7	76.7	76.7	76.7	76.7	76.7
8	92.7	92.7	92.7	92.7	92.7	92.7	92.7	92.7
9	99	99	99	99	99	99	99	99
10	124.7	124.7	124.7	124.7	124.7	124.7	124.7	124.7
11	149	149	149	149	149	149	149	149
12	173.3	173.3	173.3	173.3	173.3	173.3	173.3	173.3
13	80.3	80.3	80.3	80.3	80.3	80.3	80.3	80.3
14	91	91	91	91	91	91	91	91
15	104.5	104.5	104.5	104.5	104.5	104.5	104.5	104.5
16	126.5	126.5	126.5	126.5	126.5	126.5	126.5	126.5
17	151.5	151.5	151.5	151.5	151.5	151.5	151.5	151.5
18	182.7	182.7	182.7	182.7	182.7	182.7	182.7	182.7
19	192.7	192.7	192.7	192.7	192.7	192.7	192.7	192.7
20	210	210	210	210	210	210	210	210
21	195.3	195.3	195.3	195.3	195.3	195.3	195.3	195.3
22	75	75	75	75	75	75	75	75
23	87	87	87	87	87	87	87	87
24	100.5	100.5	100.5	100.5	100.5	100.5	100.5	100.5
25	121.5	121.5	121.5	121.5	121.5	121.5	121.5	121.5

Table 16. (Continued)

Test Number	Thermocouple Number 9	10	11	12	13	14	15
1	80	80	110.7	103.3	115	101.5	32
2	92.7	92.7	156	134	166	125.5	32
3	107	107	192.7	170	223.7	154	32
4	127.7	127.7	290.5	223.7	312.7	197.5	32
5	148	148	366	278.5	388.7	238.5	32
6	178	178	391	306.7	>431	261.5	32
7	76.7	76.7	106.7	96.5	120.7	99	32
8	92.7	92.7	153.5	122.7	183.5	128.5	32
9	99	99	203	169.5	219	153	32
10	124.7	124.7	284	216.5	306	192.7	32
11	149	149	356.5	270.5	380.5	227.7	32
12	173.3	173.3	428	311	>431	267	32
13	80.3	80.3	131	101.5	120.3	100.5	32
14	91	91	190.5	126.5	175	124.3	32
15	104.5	104.5	283.5	171	249	163.5	32
16	126.5	126.5	370.5	217.7	325.5	325.5	32
17	151.5	151.5	421	267.3	406.5	235.5	32
18	182.7	182.7	>431	313.5	>431	275.3	32
19	192.7	192.7	>431	342	>431	297.3	32
20	210	210	>431	380.5	>431	324	32
21	195.3	195.3	>431	340.5	>431	293.3	32
22	75	75	131.5	97	124	96	32
23	87	87	200.5	126.5	186.3	124.7	32
24	100.5	100.5	271	161	249	157.7	32
25	121.5	121.5	379.7	207	347	199.5	32

Table 16. (Continued)

Test Number	Thermocouple Number 1	2	3	4	5	6	7	8
26	140.7	140.7	140.7	140.7	140.7	140.7	140.7	140.7
27	175	175	175	175	175	175	175	175
28	186.7	186.7	186.7	186.7	186.7	190.5	190.5	190.5
29	210	210	210	210	210	210	210	210
30	64.5	67	67	67	67	67	67	67
31	76.6	76.6	76.6	76.6	76.6	76.6	76.6	76.6
32	89.5	88.6	88.6	88.6	88.6	88.6	88.6	88.6
33	100.5	99	99	99	99	99	99	99
34	146	144.3	144.3	144.3	144.3	144.3	146	146
35	165.5	161.5	160.6	161.5	161.5	161.5	164.6	164.6
36	176	173.3	173.3	176	176	176	173.3	173.3
37	195.3	194.5	194.5	194.5	194.5	190	195.3	195.3
38	58.6	61	61	61	61	61	61	61
39	72.6	73	73	73	73	73	73	73
40	95	92.6	92.6	92.6	92.6	92.6	95	95
41	120.6	118.5	118.5	118.5	118.5	116.5	118.5	118.5
42	154	153.5	153.5	153.5	153.5	150	154	154
43	55.5	58.6	58.6	58.6	58.6	58.6	58.6	58.6
44	62.5	64.5	64.5	64.5	64.5	62.5	62.5	62.5
45	75.5	72.6	72.6	72.6	72.6	72.6	72.6	72.6
46	86.5	85.5	85.5	85.5	85.5	82.5	85.5	85.5
47	102	99	99	99	99	95.3	99	99
48	150	147.6	147.6	147.6	147.6	145.5	150	150
49	146	144	138.5	138.5	137	138.5	138.5	138.5
50	54.3	56.5	56.5	56.5	56.5	56.5	56.5	56.5
51	59	61.5	61.5	61.5	61.5	61.5	61.5	61.5
52	63.3	63.3	63.3	63.3	63.3	63.3	63.3	63.3
53	67.7	67.7	67.7	70	70	70	70	70
54	74.5	75	75	75	75	75	75	75
55	84.7	80	74	74	80	74	74	74
56	150.7	147.7	147.7	147.7	147.7	147	150.7	144
57	150.3	143.5	142	142	143.5	142	143.5	138

Table 16. (Continued)

Test Number	Thermocouple Number 9	10	11	12	13	14	15
26	140.7	140.7	>431	261	>431	251.3	32
27	175	175	>431	313.5	>431	279.7	32
28	190.5	190.5	>431	348.5	>431	311.7	32
29	210	210	551.5	392	614	348.3	32
30	69	69	108.5	96.5	108.5	88.3	32
31	77	77	179.3	136	173	113.3	32
32	88.6	88.6	235.5	183	235.5	152.5	32
33	99	99	297.6	233.6	275.3	175	32
34	148.5	148.5	385	285	396.5	242.5	32
35	165.5	165.5	459	334.3	473	279	32
36	179	179	519	375.3	522	306	32
37	198.3	198.3	574	410	576	341	32
38	61	61	97	84.6	94	78.5	32
39	73	73	223	147.6	221	129	32
40	95	95	391.5	237.3	387.5	201.3	32
41	120.6	120.6	525	332	539	283.5	32
42	155.5	155.5	602.6	421	614.5	372.5	32
43	58.6	58.6	89	77.5	92.6	76.6	32
44	62.5	62.5	217.3	143.5	217.3	134.3	32
45	75.5	75.5	364.5	218	364.5	187.5	32
46	85.5	86.5	487.5	310.5	507.3	261.5	32
47	102	102	582.3	391	582.3	336	32
48	153.5	153.5	508.5	336	496.6	303.5	32
49	144	146	649.3	402.5	649.6	352.5	32
50	56.5	56.5	88.7	84.7	95.0	80.7	32
51	61.5	61.5	133	120.7	159.5	110	32
52	63.3	63.3	168	154	208.5	133.5	32
53	70	70	189	191	290.5	173	32
54	75	75	234	236.5	378.5	212	32
55	80	84.7	490.5	374.5	587	314.5	32
56	154	154	533	388.3	584	336	32
57	149.5	150.3	647	417	653	358	32

Table 17. Test Heat Pipe Operating Data

Test Number	Q_{in} (BTU/Hr)	V_{wF} (mℓ)	T_{cw} (°F)	ΔT_{cw} (°F)	P_i (psia)	P_f (psia)	$\dot{m}_{cw}$ (psia)
1	53.94	20	71.7	9.32	.13	.18	2.64
2	122.90	20	74.8	20.8	.24	.49	2.90
3	214.40	20	74.8	36.7	.47	.79	2.83
4	341.40	20	75.7	54.7	.22	1.62	3.17
5	491.62	20	75.7	75.4	1.62	2.99	3.30
6	576.97	20	75.7	84.7	2.99	4.05	3.17
7	54.62	30	70.8	9.3	.14	.19	2.90
8	122.90	30	70.8	22.7	.24	.42	2.64
9	214.40	30	70.8	32.0	.16	.61	3.17
10	349.94	30	73.9	52.5	.61	1.42	3.22
11	491.62	30	73.9	79.0	1.46	3.05	3.17
12	669.14	30	75.3	102.8	3.05	6.07	3.17
13	53.26	40	71.3	10.8	.15	.22	3.17
14	117.78	40	71.3	19.9	.22	.38	2.96
15	218.50	40	71.3	36.6	.38	.75	2.90
16	348.23	40	71.3	55.6	.75	1.52	2.96
17	508.00	40	71.3	82.2	.18	3.34	2.77
18	705.42	40	72.6	111.4	3.30	7.18	3.04
19	860.33	40	69.9	123.6	.12	9.30	2.90
20	1121.50	40	70.4	143.7	9.41	13.96	2.90
21	871.25	50	70.4	129.7	13.75	10.42	3.17
22	55.99	50	68.6	9.32	.18	.24	3.11
23	122.90	50	68.6	19.9	.26	.42	2.93
24	214.40	50	70.4	32.5	.42	.73	2.95
25	349.94	50	68.6	27.6	.18	.71	2.90
26	508.00	50	68.6	74.1	.14	2.51	3.43
27	673.92	50	70.8	108.5	.40	6.47	2.72
28	890.44	50	68.6	121.6	.12	9.30	3.22
29	1118.43	50	70.8	141.7	9.10	14.77	2.17
30	54.28	30	64.1	7.24	.12	.15	4.87

Table 17. (Continued)

Test Number	Q_{in} (BTU/Hr)	V_{wF} (mℓ)	T_{cw} (°F)	ΔT_{cw} (°F)	P_i (psia)	P_f (psia)	$\dot{m}_{cw}$ (psia)
31	133.15	30	64.1	14.8	.15	.18	4.48
32	238.98	30	64.1	27.9	.18	.38	4.48
33	375.54	30	64.1	39.3	.38	.63	4.74
34	728.89	30	66.3	84.3	.17	3.03	4.45
35	942.26	30	66.3	99.0	2.53	4.65	4.74
36	1167.59	30	64.1	111.4	4.65	6.67	5.40
37	1450.95	30	66.3	131.4	6.63	11.23	5.27
38	52.58	30	60.5	4.4	.10	.12	10.53
39	232.15	30	60.5	14.1	.12	.16	10.53
40	542.83	30	61.8	32.3	.16	.51	10.14
41	955.92	30	61.8	57.3	.52	1.44	9.88
42	1468.02	30	61.8	89.8	1.44	4.05	9.69
43	52.58	30	57.3	2.4	.06	.06	23.44
44	232.15	30	57.3	7.5	.13	.12	23.05
45	542.83	30	57.3	16.2	.24	.24	22.12
46	955.92	30	57.3	26.7	.47	.47	23.44
47	1485.09	30	57.8	41.0	.89	.93	23.05
48	955.92	30	59.6	105.2	3.24	.89	5.82
49	955.92	30	59.6	79.2	3.24	-	5.82
50	52.98	30	59.6	2.4	.56	.58	23.97
51	135.19	30	59.6	5.4	.58	.65	23.70
52	232.15	30	59.6	6.5	.65	.75	23.65
53	392.61	30	59.6	11.6	.75	1.01	23.18
54	553.07	30	59.6	16.7	1.01	1.21	23.04
55	955.92	30	59.1	26.7	1.21	1.21	22.39
56	955.92	30	65.9	86.4	.73	6.67	5.79
57	955.92	30	65.9	82.2	6.67	-	5.74

BIBLIOGRAPHY

1. Skrabek, E. A. and Bienert, W. B., Heat Pipe Design Handbook - Part I, NASA-CR-134264, August, 1972.

2. Gaugler, R. S., "Heat Transfer Device", U. S. Patent 2,350,348, June 6, 1944.

3. Grover, G. M., Cotter, T. P. and Erickson, G. F., "Structures of Very High Thermal Conductance", Journal of Applied Physics, Vol. 35, pp. 1990-1991, 1964.

4. Cotter, T. P., Theory of Heat Pipes, Los Alamos Scientific Laboratory, Report LA-3246-MS, March 1965.

5. Cosgrove, J. H., Engineering Design of the Heat Pipe, Ph.D. Thesis, North Carolina State University, 1967.

6. Winter, E. R. F. and Barsch, W. O., "The Heat Pipe", Advances in Heat Transfer, Vol. 7, 1971.

7. Marcus, B. D., Theory and Design of Variable Conductance Heat Pipes, NASA CR-2018, July 1971.

8. Williams, C. L., Correlation of Heat Pipe Parameters, Ph.D. Thesis, Georgia Institute of Technology, 1973.

9. Knuz, H. R., Wyde, S. S., Nashick, G. H., and Baines, J. F., Vapor-Chamber Fin Studies, Operating Characteristics of Fin Models, NASA CR-1139, August, 1968.

10. Gray, V. H., "The Rotating Heat Pipe - A Wickless Hollow Shaft for Transferring High Heat Fluxes", ASME Publication 69-HT-19.

11. Katzoff, S., "Heat Pipes and Vapor Chambers for Thermal Control of Spacecraft", Thermophysics of Spacecraft and Planetary Bodies, Progress, in Astronautics and Aeronautics, Vol. 20, pp. 761-818, 1968.

12. Conway, E. C., and Kelley, M. J., "A Continuous Heat Pipe for Spacecraft Thermal Control", Aviation and Space: Progress and Prospects - Annual Aviation and Space Conference, pp. 655-8, June, 1968.

13. Feldman, K. T. and Whiting, G. H., "Applications of the Heat Pipe", Mechanical Engineering, pp. 48-53, November, 1968.

14. Bliss, Jr., F. E., Clark, Jr., E. G., and Stein, B., "Construction and Test of a Flexible Heat Pipe", ASME Publication 70-HT/SpT-13.

15. Talcott, R. C., Thrasher, B. H., and Colwell, G. T., Thermal Control and Heat Pipe Investigation Report, Report prepared by Radiation, a division of Harris-Intertype under contract No. N00014-73-C-0446 for Office of Naval Research, Department of Navy, Arlington, Virginia, February, 1974.

16. Neal, L. G., An Analytical and Experimental Study of Heat Pipes, Research Report, TRW Systems, Redondo Beach, California, January 1967.

17. Schwartz, J., "Performance Map of an Ammonia (NH_3) Heat Pipe", ASME Publication 70-HT/SpT-5.

18. Deverall, J. E., "Mercury as a Heat-Pipe Fluid", ASME Publication 70-HT/SpT-8.

19. Kunz, H. R., Langton, L. S., Hilton, B. H., Wyde, S. S., and Nashick, G. H., Vapor-Chamber Fin Studies, Transport Properties and Boiling Characteristics of Wicks, NASA CR-812, June 1967.

20. Ferrell, J. K., Winston, H., and Davis, R., "Heat Pipe Wick Properties and Performance", NSF Heat Pipe Conference, University of Maryland, November 1973.

21. Armour, J. C. and Cannon, J. N., "Fluid Flow Through Woven Screens", AIChE Journal, Vol. 14, No. 3, May 1968.

22. Corman, J. C., Trefethen, L., and Walmet, G. E., "Characterization of Parameters for Liquid Flow in Rigid Porous Media", ASME Publication 73-WA/HT-3.

23. Phillips, E. C. and Hinderman, J. D., "Determination of Properties of Capillary Media Useful in Heat Pipe Design", ASME Publication 69-HT-18.

24. Cosgrove, J. H., Ferrell, J. K., and Carnesale, A.,"Operating Characteristics of Capillary Limited Heat Pipes", Journal of Nuclear Energy, Vol. 21, pp. 547-558, 1967.

25. Busse, C. A., "Theory of the Ultimate Heat Transfer Limit of Cylindrical Heat Pipes", International Journal of Heat and Mass Transfer, Vol. 16-1, pp. 169-186, January 1973.

26. Lyman, F. A., and Huang, Y. S., "Analysis of Temperature Distributions in Heat Pipe Wicks", ASME Publication 73-HT-P.

27. Fox, R. D., Carothers, K. G., and Thomson, W. I., Internal Temperature Distributions in an Operational Heat Pipe, University of Idaho, Moscow, Idaho, March 1972.

28. Bankston, C. A. and Smith, H. J., "Vapor Flow in Cylindrical Heat Pipes," ASME Publication 73-HT-P.

29. Colwell, G. T., Williams, C. L., Hsu, J. C., and Zevallos, G. E., "A Study of Noncondensable Effects in a Heat Pipe", Nuclear Technology, Vol. 10, pp. 293-300, March 1971.

30. Corman, J. C. and McLaughlin, M. H., Thermal Development of Heat Pipe Cooled IC Packages, General Electric, Report No. 72CRD181, June 1972.

31. Corman, J. C. and McLaughlin, M. H., Thermal Design - Heat Pipe Cooled A-C Motor, General Electric, Report No. 71-C-140, May, 1971.

32. Sparrow, E. M., Ramsey, J. W., and Wehner, G. K., Research Applied to Solar-Thermal Power Systems, University of Minnesota and Honeywell, Report NSF/RANN/SE/GI-34871/PR/73/4, January 1974.

33. Kirkpatrick, J. P., Variable Conductance Heat Pipes from the Laboratory to Space, NASA-TM-X-62290, July 1973.

34. Bassett, H. L. and Colwell, G. T., "Heat Pipe Cooled Microwave Window", Georgia Institute of Technology Projects A-1434 and E25-627, January 1973.

35. Colwell, G. T., Bassett, H. L., and Schuchardt, M., "Heat Pipe Cooled Microwave Window", Georgia Institute of Technology Projects E25-635 and A-1532, February 1974.

36. Moreno, T., Microwave Transmission Design Data, Dover Publications, New York, 1958.

37. Davis, W. R., Evaporative Heat Transfer of Liquid Potassium in Porous Media, Ph.D. Thesis, North Carolina State University at Raleigh, 1974.

38. Silverstein, C. C., "Surface Flux for Incipient Boiling in Liquid Metal Heat Pipes", Nuclear Technology, Vol. 12, No. 1, pp. 56-62, 1971.

39. Chisholm, D., The Heat Pipe, Mills and Boom Limited, London, 1971.

40. Kreith, F., Principles of Heat Transfer, International Textbook Company, Scranton, Pennsylvania, 1966.

41. Wilcox, S. and Rohsenow, W., "Film Condensation of Potassium Using Copper Condensing Block for Precise Wall Temperature Measurement", ASME Transactions, Journal of Heat Transfer, Vol. 92, No. 3, p. 359, August 1970.

42. Williams, C. L. and Colwell, G. T., "Heat Pipe Model Accounting for Variable Evaporator and Condenser Lengths", AIAA Journal, Vol. 12, No. 9, pp. 1261-67, September 1974.

43. Maxwell, J. B., Data Book on Hydrocarbons, Application to Process Engineering, D. Van Nostrand Company, Inc., New York, 1950.

44. Scheidegger, A. E., The Physics of Flow Through Porous Media, Macmillan, New York, 1960.